1. Report No.	2. Government Accession No.	3. Recipient's Catalog No.
TX-00/2937-1		

4. Title and Subtitle	5. Report Date
SRICOS: PREDICTION OF SCOUR RATE AT BRIDGE PIERS	December 1999
	6. Performing Organization Code

7. Author(s)	8. Performing Organization Report No.
Jean-Louis Briaud, Francis Ting, H. C. Chen, Rao Gudavilli, Kiseok Kwak, Bertrand Philogene, Seung-Woon Han, Suresh Perugu, Gengsheng Wei, Prahoro Nurtjahyo, Yiwen Cao, and Ya Li	Report 2937-1

9. Performing Organization Name and Address	10. Work Unit No. (TRAIS)
Texas Transportation Institute The Texas A&M University System College Station, Texas 77843-3135	11. Contract or Grant No. Project No. 7-2937

12. Sponsoring Agency Name and Address	13. Type of Report and Period Covered
Texas Department of Transportation Construction Division Research and Technology Transfer Section P. O. Box 5080 Austin, Texas 78763-5080	Research Oct. 7, 1994 - Aug. 31, 1999
	14. Sponsoring Agency Code

15. Supplementary Notes

Research performed in cooperation with the Texas Department of Transportation.
Research Project Title: Scour Rate of Cohesive Soils

16. Abstract

A new method called SRICOS is proposed to predict the scour depth z versus time t around a cylindrical bridge pier of diameter D founded in clay. The steps involved are: 1. taking samples at the bridge pier site; 2. testing them in an erosion function apparatus (EFA) to obtain the scour rate $\dot{z}$ versus the hydraulic shear stress applied τ; 3. predicting the maximum shear stress τ_{max} that will be induced around the pier by the water flowing at v_o before the scour hole starts to develop; 4. using the measured $\dot{z}$ versus τ curve to obtain the initial scour rate $\dot{z}_i$ corresponding to τ_{max}; 5. predicting the maximum depth of scour z_{max} for the pier; 6. using $\dot{z}_i$ and z_{max} to develop the hyperbolic function describing the scour depth z versus time t curve; and 7. reading the z versus t curve at a time corresponding to the duration of the flood to find the scour depth that will develop around that pier.

A new apparatus is developed to measure the $\dot{z}$ versus t curve of step 2, a series of advanced numerical simulations are performed to develop an equation for the τ_{max} value of step 3, and a series of flume tests are performed to develop an equation for the z_{max} value of step 5. The method is evaluated by comparing predictions and measurements in 42 flume experiments.

The method is extended to include a random velocity-time history and a multilayer soil stratigraphy; it is called the extended SRICOS or E-SRICOS. The algorithms to accumulate the effects of different velocities and to sequence through a series of soil layers are described. The procedure followed by the computer program to step into time is outlined. A simplified version of E-SRICOS called S-SRICOS is also presented; calculations for the S-SRICOS method can easily be done by hand. Eight bridges in Texas are used as case histories to compare predictions by the two new methods (E-SRICOS and S-SRICOS) with measurements at the bridge sites.

17. Key Words	18. Distribution Statement
Scour, Bridges, Bridge Piers, Cohesive Soils, Foundations, Erosion Rate	No restrictions. This document is available to the public through NTIS: National Technical Information Service 5285 Port Royal Road Springfield, Virginia 22161

19. Security Classif.(of this report)	20. Security Classif.(of this page)	21. No. of Pages	22. Price
Unclassified	Unclassified	138	

SRICOS: PREDICTION OF SCOUR RATE AT BRIDGE PIERS

by

Jean-Louis Briaud
Research Engineer
Texas A&M University

Francis Ting
Assistant Professor
South Dakota State University

H. C. Chen
Associate Professor
Texas A&M University

Rao Gudavalli, Kiseok Kwak, Bertrand Philogene, Seung-Woon Han, Suresh Perugu,
Gengsheng Wei, Prahoro Nurtjahyo, Yiwen Cao, and Ya Li
Graduate Students
Texas A&M University

Report 2937-1
Project Number 7-2937
Research Project Title: Scour Rate of Cohesive Soils

Sponsored by the
Texas Department of Transportation

December 1999

TEXAS TRANSPORTATION INSTITUTE
The Texas A&M University System
College Station, Texas 77843-3135

DISCLAIMER

The contents of this report reflect the views of the authors, who are responsible for the facts and accuracy of the data presented herein. The contents do not necessarily reflect the official views of policies of the Texas Department of Transportation (TxDOT). This report does not constitute a standard, specification, or regulation. In addition, the above assumes no liability for its contents or use thereof. The engineer in charge of the project was Dr. Jean-Louis Briaud, P.E. # 48690.

ACKNOWLEDGMENTS

This project was sponsored by the Texas Department of Transportation, where Tony Schneider, Melinda Luna, Kim Culp, Peter Smith, and Jay Vose were very helpful and supportive.

TABLE OF CONTENTS

TABLE OF CONTENTS (CONTINUED)

LIST OF FIGURES

LIST OF FIGURES (CONTINUED)

LIST OF FIGURES (CONTINUED)

LIST OF TABLES

IMPLEMENTATION RECOMMENDATIONS

The following steps need to be taken in order to implement the results of this project:

1. TxDOT purchases three EFA (Erosion Function Apparatus) at cost from TTI and places them in selected district laboratories.
2. TTI trains the district laboratory engineers on how to use the EFA including data reduction.
3. TTI transforms the SRICOS program into a user friendly program (Windows environment).
4. TTI teaches the district laboratory engineers how to use the SRICOS program.

CHAPTER 1. THE ORIGINAL SRICOS METHOD

1.1 INTRODUCTION

There are approximately 600,000 bridges in the United States and 500,000 of them are over water (National Bridge Inventory, 1997). During the last 30 years over 1,000 of the 600,000 bridges have failed and 60 percent of those failures are due to scour, with earthquake accounting for only 2 percent (Shirole and Holt, 1991). The average cost for flood damage repair of highways on the federal aid system is 50 million dollars per year (Lagasse et al., 1995).

On April 5, 1987, a 32-year-old bridge over Schoharie Creek in the state of New York collapsed when the spread footing foundation became undermined by pier scour. This collapse and the associated deaths prompted the Federal Highway Administration (FHWA) to ask the state departments of transportation for an evaluation of their over-water bridges for scour susceptibility. The result of this 10-year effort shows that 62.4 percent of these bridges have a low risk of scour failure, 13.5 percent are scour susceptible, 20.0 percent have unknown foundations, 0.6 percent are left to be screened and 3.5 percent or about 17,000 bridges are scour critical, which means that they are likely to fail if they are subjected to a 100-year flood (Pagan-Ortiz, 1998). These numbers indicate the importance of the bridge scour problem.

Research on bridge scour has been active since at least the late fifties. The Schoharie bridge failure prompted an increase in sponsored research with about 11 million dollars spent over the last six years (Parola, 1997). Most of this research has been dedicated to bridge scour in sand. The topic of this article is bridge scour in clay, more specifically the prediction of the scour depth versus time curve for circular piers founded in clay. Does clay scour to the same final depth of scour as sand? How fast does clay scour? These are some of the questions addressed.

1.2 CURRENT PRACTICE

Scour can be divided into general scour (general erosion of the streambed without obstacles), local scour (scour generated by the presence of obstacles such as piers and abutments, (Fig. 1), and channel migration (lateral movement of the main stream channel). Current practice is heavily influenced by two FHWA hydraulic engineering circulars called HEC-18 and HEC-20 (Richardson and Davis, 1995; Lagasse et al., 1995). For pier scour, the topic of this study, HEC-18

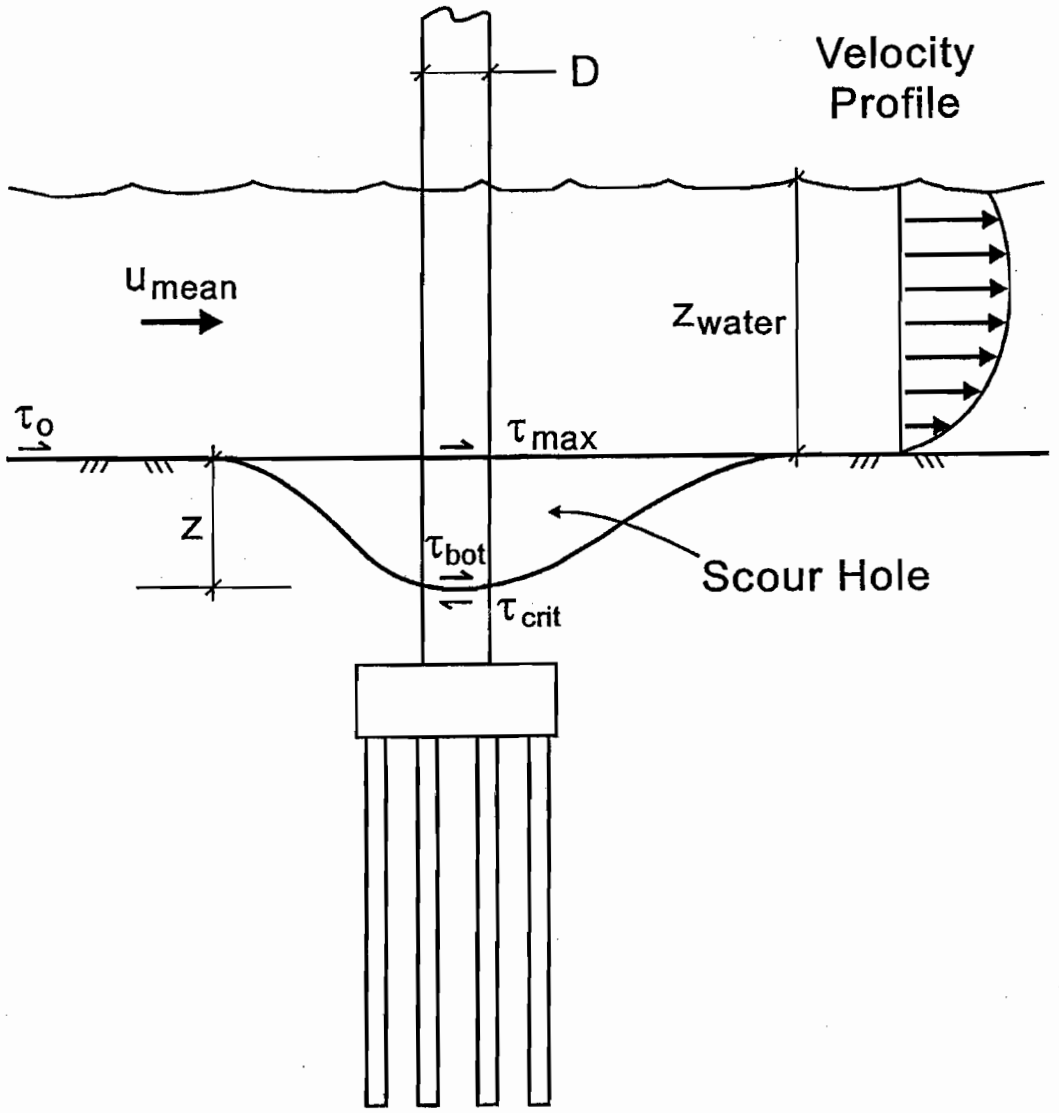

Figure 1. Scour around a Bridge Pier.

recommends the use of the following equation to predict the maximum depth of scour z_{max} above which all soil resistance must be discounted:

$$z_{max} = 2z_o K_1 K_2 K_3 K_4 \left(\frac{D}{z_0}\right)^{0.65} F_o^{0.43} \quad (1)$$

where z_0 is the depth of flow just upstream of the bridge pier excluding local scour, K_1, K_2, K_3, K_4 are coefficients to take into account the shape of the pier, the angle between the direction of the flow and the direction of the pier, the streambed topography, and the armoring effect; D is the pier diameter; and F_0 is the Froude number defined as $v/(gz_0)^{0.5}$ where v is the mean flow velocity and g is the acceleration due to gravity.

This equation is based on model scale experiments in sand and has recently been evaluated (Fig. 2) against full-scale observations for 56 bridges founded primarily on sand (Landers and Mueller, 1996). Nothing in HEC-18 gives guidance to calculate the rate of scour in clay, and it is implicit that (Eq. 1) should also be used for the final depth of scour for bridges on clay. Common sense tells us that clays scour much more slowly than sand and using Eq. 1 for clays, regardless of time, appears to be overly conservative and therefore expensive. The potential savings in this respect is what prompted sponsorship of this research.

1.3 SHEAR STRESS IMPOSED

The scour process is highly dependent on the shear stress developed by the flowing water at the soil-water interface. Indeed, at that interface the flow is tangential to the soil surface regardless of the flow condition above it; very little water, if any, flows perpendicular to the interface. The water velocity in the river is in the range of 0.1 m/s to 3 m/s while the bed shear stress is in the range of 1 to 50 N/m^2 and increases with the square of the water velocity. The magnitude of this shear stress is a very small fraction of the undrained shear strength of clays used in foundation engineering for example (Fig. 3). It is amazing to see that such small shear stresses are able to scour rocks to a depth of 1600 m as is the case for the Grand Canyon over the last 20 million years at an average scour rate of 9 x 10^{-6} mm/hr. This rate leads one to think that even small shear stresses, if applied cyclically by the turbulent nature of the flow and after a sufficient number of cycles, can overcome the crystalline bonds in a rock and the electromagnetic bonds in a clay. This phenomenon also leads one to think that there is no cyclic stress threshold but that any stress is

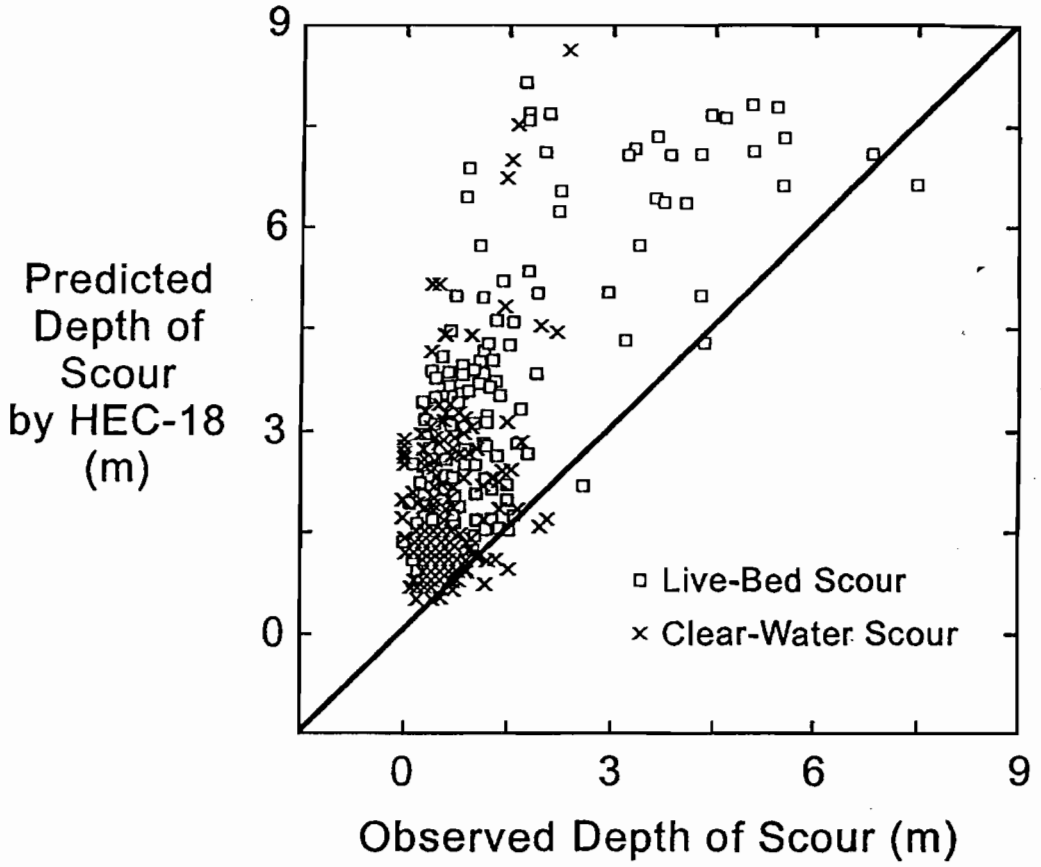

Figure 2. Precision of the HEC-18 Equation for Maximum Depth of Scour (after Landers and Mueller, 1996).

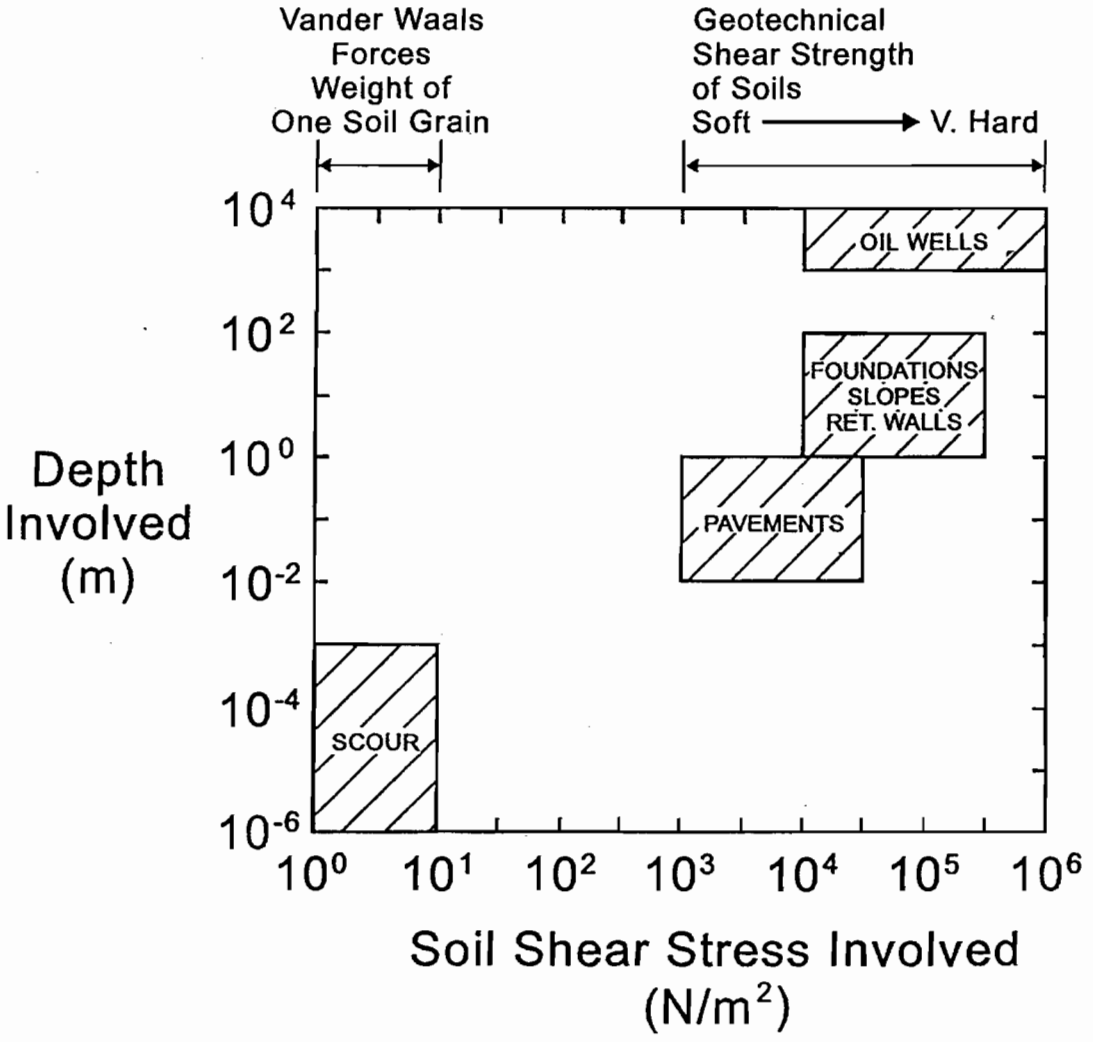

Figure 3. Difference between Shear Stresses for Scour Problems and Foundation Problems.

associated with a number of cycles to failure. Gravity bonds seem to be an exception to this postulate as it appears that gravity bonds cannot be weakened by cyclic loading. This postulate contradicts the critical shear stress concept discussed later.

The shear stress τ imposed by the water at a boundary can be evaluated in a number of ways. The first one is for open channels without obstructions and is based on equilibrium considerations (Munson et al., 1990):

$$\tau = r_h S_{EGL} \gamma_w \tag{2}$$

where r_h is the hydraulic radius defined as the cross section area of the flow divided by the wetted perimeter, S_{EGL} the slope of the Energy Grade Line (slope of the riverbed generally); and γ_w the unit weight of water. The second one is for circular pipes without obstructions and is also based on equilibrium considerations (Munson et al., 1990):

$$\tau = \frac{R}{2} \times \Delta p / \ell \tag{3}$$

where R is the pipe radius and $\Delta p / \ell$ is the pressure drop Δp per length ℓ of pipe. The pressure drop can either be measured or calculated by using the Moody chart (Munson et al., 1990, p. 501).

When a cylinder obstructs the flow in an open channel with a flat bottom, the maximum shear stress τ_{max} is located as shown on Fig. 4 and is many times larger than the value given when there is no obstruction (Eq. 2). In this study a detailed numerical simulation, described later, was performed (Wei et al., 1997) to obtain τ_{max}. It was found (Fig. 5) that, for large water depth $(Z_0 / D > 2)$, τ_{max} was dependent on the Reynolds number R_e, the mean flow velocity V, and the mass density of water ρ:

$$\tau_{max} = 0.094 \, \rho \, V^2 \left(\frac{1}{\log R_e} - \frac{1}{10} \right) \tag{4}$$

where the Reynolds number R_e is defined as VD/υ where V is the mean flow velocity, D is the pier diameter, and υ is the kinematic viscosity of water (10^{-6} m^2/s at 20° C). If this value of τ_{max} is larger than the critical shear stress τ_c that the soil can resist, scour is initiated. As the scour hole deepens around the cylinder, the shear stress at the bottom of the hole decreases. A profile of the shear stress at the bottom of the scour hole τ_{bot} as a function of the depth of the scour hole, using the same numerical analysis, is shown in Fig. 6. Once the scour hole becomes deep enough, τ_{bot}

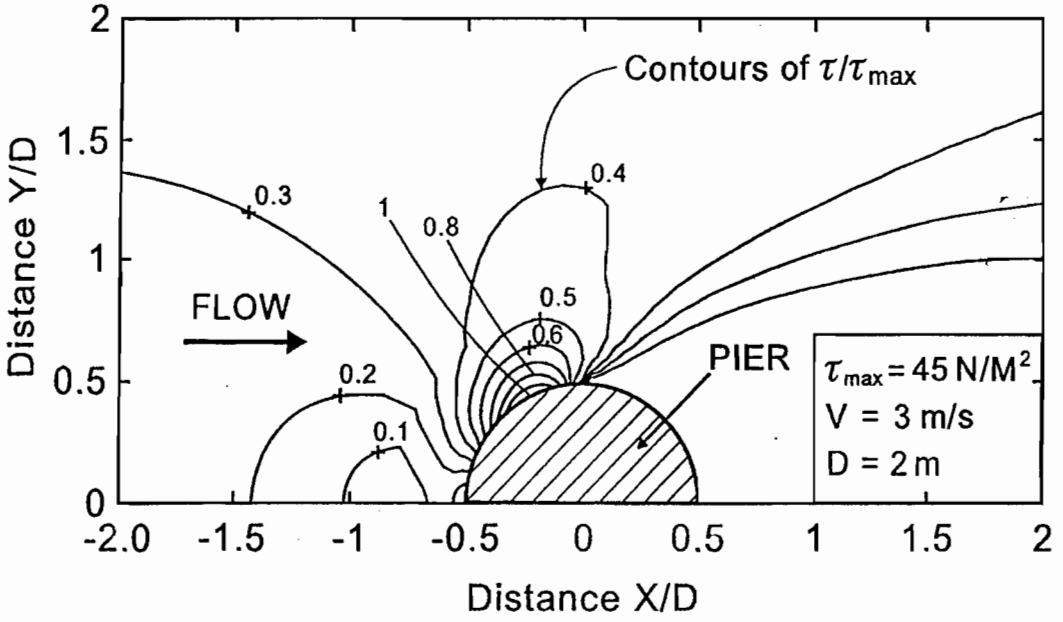

Figure 4. Maximum Shear Stress around a Cylindrical Pier.

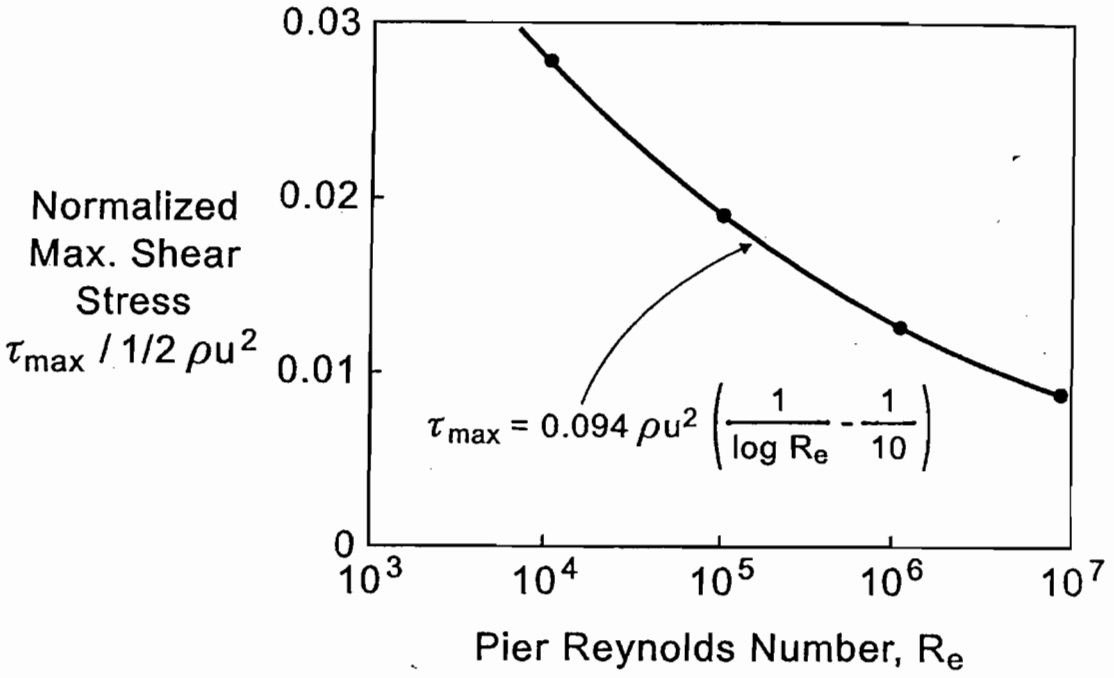

Figure 5. Maximum Shear Stress as a Function of Reynolds Number.

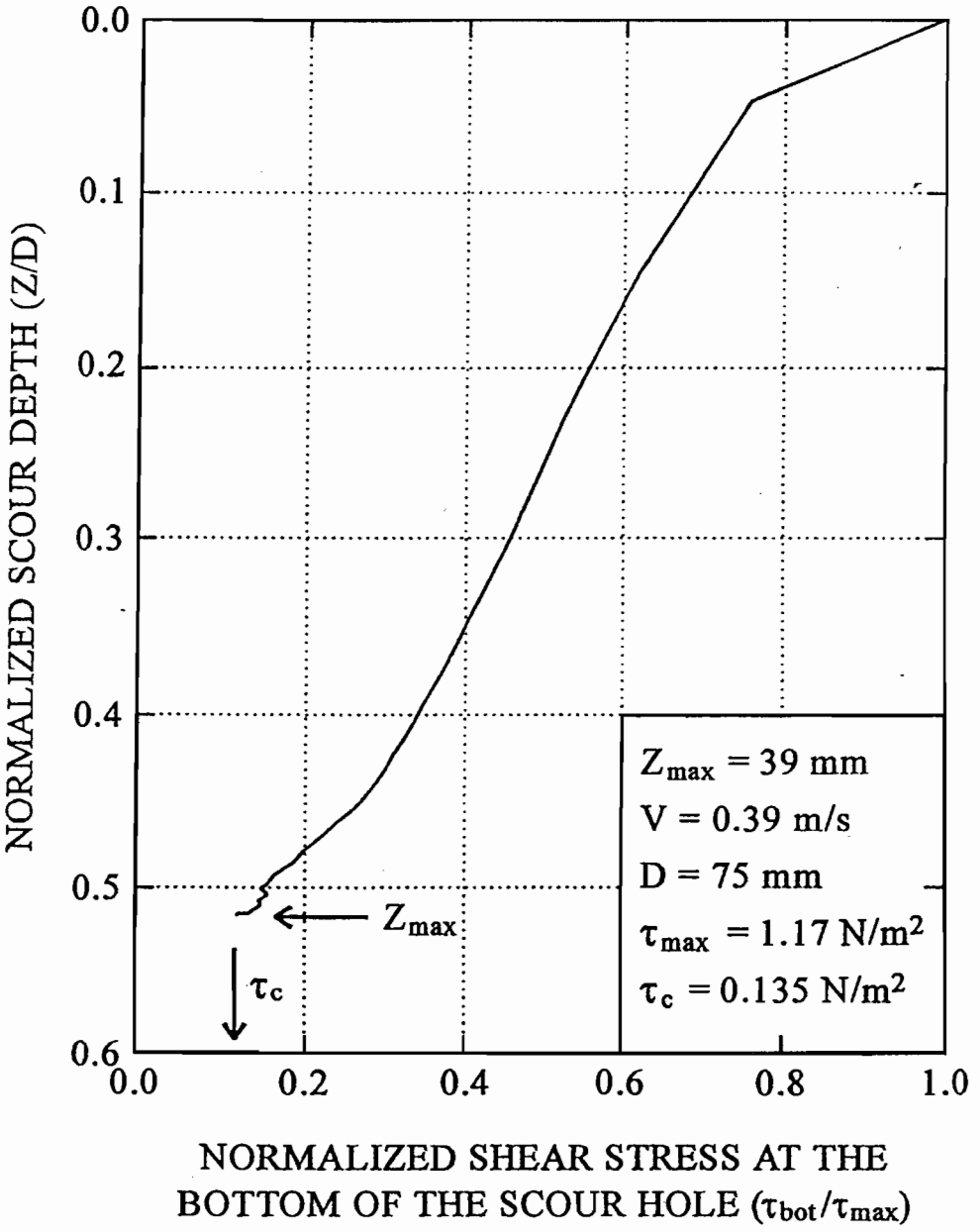

Figure 6. Variation of the Shear Stress at the Bottom of the Scour Hole as a Function of the Depth of the Scour Hole.

becomes equal to τ_c (the critical shear stress for the soil), the soil stops scouring, and the final depth of scour z_{max} is reached.

1.4 CRITICAL SHEAR STRESS

The critical shear stress τ_c is the shear stress imposed by the water on the soil when scour is initiated. Below this shear stress, the soil particles are not displaced; above this shear stress, the soil particles are transported away and a certain scour rate is established. As discussed earlier, this concept may not be theoretically correct; however, it is practically useful. It may be that a more acceptable definition of τ_c is the shear stress corresponding to a standardized small erosion rate. For the experiments in this study, this threshold erosion rate was taken as 1 mm/hr Erosion Function Apparatus (EFA) as an arbitrary limit that would create only 168 mm of scour for a week-long flood.

In the case of sand and gravel, the scour process is controlled by the weight of the particles, and one way to estimate τ_c is to calculate the shear force T necessary for the water to overcome the friction between two stacked particles:

$$T = W \tan\phi = (\rho_s - \rho_w) g \frac{\pi d^3}{6} \tan\phi \tag{5}$$

where W is the weight of the particle, ϕ is the friction angle, ρ_s and ρ_w the mass density of the sand particle and water respectively, g is the acceleration due to gravity, and d the diameter of the sand particle, which is assumed to be spherical. The drag force F applied by the water on the particle is

$$F = \tau A_e \tag{6}$$

where A_e is the effective area of the sand particle over which the hydraulic shear stress τ is applied. If A_e is expressed as a fraction α of the particle maximum cross section $\left(\pi \frac{d^2}{4}\right)$, the expression for τ_c comes from equating Eqs. 5 and 6.

$$\tau_c = \frac{2(\rho_s - \rho_w) g d \tan\phi}{3\alpha} \tag{7}$$

Table 1. Measured Critical Shear Stress.

	SAND	GRAVEL
Mean Diameter d_{50} *(mm)*	3.375	7.90
Coefficient of Uniformity C_u	1.54	1.20
Coefficient of Curvature C_c	0.835	0.969
Dry Unit Weight $\gamma_d \left(kN/m^3\right)$	13.77	11.30
Critical Shear Stress $\tau_c \left(N/m^2\right)$	4.0	7.0
τ_c / d_{50} $\left(N/m^2/mm\right)$	1.18	0.88
Coefficient α (Eq. 7)	5.25	7.03

Experiments were performed to evaluate the coefficient α. A uniform sand and a uniform gravel were tested in the EFA developed for this research and described later. (Table 1) shows the results obtained. The values of α in Table 1 were obtained by assuming the following values of the other parameters in Eq. 7: $\rho_s = 2650 kg/m^3$, $\rho_w = 1000 kg/m^3$, $g = 9.81 m/s^2$, $d = d_{50}$, $\phi = 30°$. The mean α value was 6.14.

The value of α is surprisingly high because one would expect α to be less than one. This value shows that the assumed scour process by sliding is at best incomplete. Close observations on slow-motion videotapes show that the scour process is a combination of rolling, sliding, and plucking of the particle. It also shows that the turbulence in the water at the soil-water interface induces cyclic loading on the particles.

The average ratio between the measured values of τ_c in N/m^2 and d_{50} in mm is 1.03 and leads to the equation

$$\tau_c\left(N/m^2\right) = d_{50}\ (mm) \tag{8}$$

while the data is very limited (Table 1); the equation proposed by Laursen (1962) is similar to Eq. 8 and consistent with earlier data by Shields:

$$\tau_c\left(N/m^2\right) = 0.63\, d_{50}\ (mm) \tag{9}$$

In the case of silts and clays, other forces come into play besides the weight of the particles; these are the electrostatic and Van der Waals forces. Electrostatic forces are likely to be repulsive because clay particles are negatively charged. Van der Waals forces are relatively weak electromagnetic forces that attract molecules to each other (Mitchell, 1993); although electrically neutral, the molecules form dipoles that attract each other like magnets. The Van der Waals forces are the forces that keep H_2O molecules together in water. The magnitude of these Van der Waals forces can be estimated by (Black et al., 1960):

$$f\left(N/m^2\right) = \frac{10^{-28}}{d(m)^4} \tag{10}$$

where *d(m)* is the distance in *m* between soil particles and *f* is the attraction force in N/m^2. By multiplying f by the particle surface area, one can obtain the interparticle force. Table 2 shows the value of these forces for a sand and a clay particle. In both cases, the soil particle was assumed to be spherical, and the distance between particles was taken equal to the particle diameter. While such an evaluation of the Van der Waals force can only be considered as a crude estimate, the

Table 2. Gravity and Van der Waals Forces for a Sand and a Clay Particle.

	SAND PARTICLE	CLAY PARTICLE
Diameter d (m)	2×10^{-3}	1×10^{-6}
Weight W (N)	1.1×10^{-3}	1.36×10^{-13}
Van der Waals Attraction F_{VDW} (N)	7.85×10^{-23}	3.14×10^{-16}
F_{VDW} / W	7.1×10^{-20}	2.3×10^{-3}

following observations regarding the numbers in (Table 2) are interesting. First, the ratio between the weight of the sand particle and of the clay particle is similar to the ratio between the weight of a Boeing 747 and of a postage stamp. Therefore, if the critical shear stress is proportional to the particle weight, the critical shear stress for clays is practically zero. Second, the ratio between the Van der Waals force and the weight of the sand particle indicates that the Van der Waals force is truly negligible for sands. Third, the same ratio for the clay particle, while many times larger than for sand, also indicates that the Van der Waals forces are negligible compared to the weight of the clay particle. This fact would lead one to think that the critical shear stress τ_c is essentially zero for clays. Note that the electrostatic forces have not been calculated here but, since they are predominantly repulsive, they would decrease, if anything, the attraction due to the Van der Waals forces. Other phenomena give cohesion to clays. They include water meniscus forces such as those developing when a clay dries and diagenetic bonds due to aging such as those developing when a clay turns into rock under pressure and over geologic time. Because of the number and complexity of these bonds, it is very difficult to predict τ_c for clays empirically on the basis of a few index properties. Several researchers, however, have proposed empirical equations for τ_c in clays such as Dunn (1959) and Lyle and Smerdon (1965). In the approach described in this paper, it is preferred to measure τ_c directly for each clay in the new EFA test as described later.

One problem associated with measuring τ_c is determining the initiation of scour. When the particles are visible with the naked eyes, it is simple to detect when the first particle is scoured away. For clays, this is not the case, and various investigators define the initiation of scour through different means. These vary from "when the water becomes muddy" to extrapolation of the scour rate versus shear stress curve back to zero scour rate. Table 3 shows a wide variety of measured τ_c; the lack of precise definition for the initiation of scour may be in part responsible for the wide range of values.

1.5 SCOUR RATE

Beyond the critical shear stress, a certain scour rate $\dot{z}$ (mm/hr) is established. This scour rate is rapid in sand, slow in clay, and extremely slow in rocks. The example of the Grand Canyon rocks cited earlier leads to a value of $\dot{z}$ equal to 9×10^{-6} mm/hr while fine sands erode at rates of 10^4 mm/hr as measured in the EFA. Clays scour at intermediate rates with common values in the

Table 3. Measured Critical Shear Stress in Clays.

AUTHORS	RANGE OF T_c (N/m^2)
Dunn, 1959	2 - 25
Enger et al., 1968	15 - 100
Hydrotechnical Construction, Moscow, 1936	1 - 20
Lyle and Smerdon, 1965	0.35 - 2.25
Smerdon and Beasley, 1959	0.75 - 5
Arulanandan et al., 1975	0.1 - 4
Arulanandan, 1975	0.2 - 2.7
Kelly and Gularte, 1981	0.02 - 0.4

Table 4. Measured Erosion Rates in Clay.

AUTHORS	RESULTS	INFERRED SCOUR RATE* (mm/hr)
Richardson & Davis, 1995	Maximum Scour Depth Reached in Days	10 - 100
Arulanandan et al., 1975	1-4 $g/cm^2/min$	300-1200
Shaikh et al., 1988	0.3-0.8 $N/m^2/min$	9-24
Ariathurai and Arulanandan, 1978	0.005-0.09 $g/cm^2/min$	1.5-27
Kelly and Gularte, 1981	0.0057-0.01 $gm/cm^2/s$	100-180

*Scour Rate $\frac{dz}{dt} = \left(\text{weight loss rate per unit area } \frac{dw}{adt} \right) \times \frac{1}{unit\ weight\ \gamma}$

range of 1 to 1000 mm/hr (Table 4). The high scour rate in sand exists because, once gravity is overcome, no other force slows the scour process down. The very low scour rate in rock exists probably because it takes a large number of shear stress cycles imposed by the turbulent nature of the flow to overcome the very strong crystalline bonds binding the rock together. The low scour rate in clays is probably also associated with the fact that it takes a large number of shear stress cycles to overcome the electromagnetic bonds created by the Van der Waals forces between clay particles. Even though these bonds are relatively weak, as discussed previously, they are sufficient to slow the scour process significantly.

The scour rate $\dot{z}$ versus shear stress τ curve (Fig. 7) is used to quantify the scour rate of a soil as a function of the flow velocity in a stream. Several researchers have measured the rate of erosion in cohesive soils; most have proposed a straight line variation (DE on Fig. 7) (Ariathurai and Arulanandan, 1978) while some have found S-shape curves (OABC on Fig. 7) (Christensen, 1965). This S shape would indicate that different physical phenomena take place as the water velocity increases (Fig. 7).

1.6 THE SRICOS METHOD

SRICOS stands for Scour Rate In COhesive Soils. It is a method to predict the scour depth versus time curve around a cylindrical bridge pier standing in the way of a constant velocity flow and founded in a uniform cohesive soil. The method consists of the following steps, which are explained in the next sections. It is important for any engineer to understand the limitations of this proposed method before using it. These limitations are discussed later.

1. Obtain standard 76.2 mm diameter Shelby tube samples as close to the pier as possible.
2. Perform EFA tests on the samples from the site to obtain the curve linking the erosion rate $\dot{z}$ and the hydraulic shear stress imposed τ.
3. Determine the maximum shear stress τ_{max}, which will exist on the river bottom around the pier at the beginning of the scour process.
4. Obtain the initial scour rate $\dot{z}_i$ corresponding to τ_{max}.
5. Calculate the maximum depth of scour z_{max}.
6. Develop the complete scour depth z versus time t.

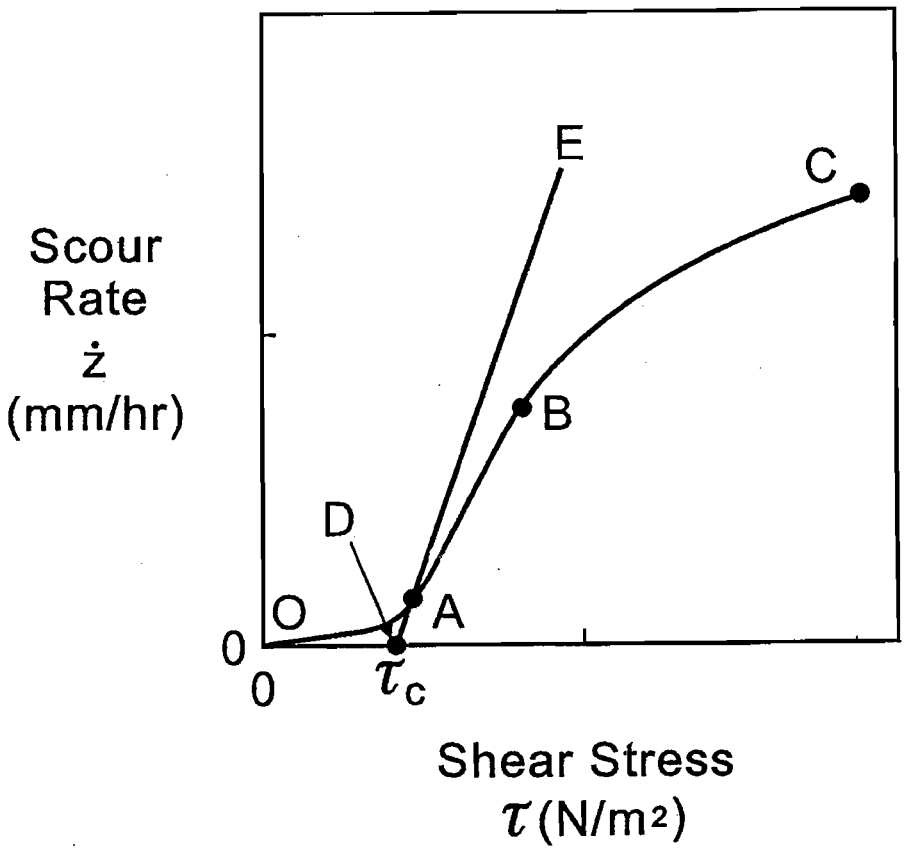

Figure 7. Scour Rate versus Shear Stress Curve.

7. Predict the depth of scour by reading the z versus t curve at the time corresponding to the duration of the flood.

1.7 OBTAIN SAMPLES AND PERFORM EFA TESTS

SRICOS is a site specific scour prediction method because samples from the bridge site are collected and tested. The samples should be 76.2 mm diameter Shelby tube samples (ASTM-D1587) obtained close to the bridge pier. The samples are brought back to the laboratory where they are tested in the EFA.

The EFA (Figs. 8 and 9) is an apparatus which was developed for this study. The sample is pushed out of the Shelby tube by a piston only as fast as it takes to erode the soil by water flowing over it. The sample is pushed vertically upward into a test section which is made of a pipe with a rectangular cross-section; the Plexiglas^{TM} pipe is 50.8 mm high and 101.6 mm wide to accommodate the 76.2 mm diameter sample. In a standard test, the sample is pushed so that it protrudes 1 mm into the test section. The protrusion distance was varied from 0.1 mm to 2 mm. There was little difference between a protrusion of 0.1 mm, 0.5 mm, and 1 mm. The 2 mm protrusion led to a higher scour rate; the protrusion distance was standardized to 1 mm. The water flows over the sample at a chosen velocity v and the sample is advanced another 1 mm as soon as it is eroded back to be flush with the bottom of the Plexiglas test section. This process is repeated for at least one hour and leads to an average erosion rate $\dot{z}$ for the velocity v. An electronic eye system was used at first to automate this process but the unevenness of the scoured sample surface, often due to soil heterogeneity, created some erroneous scour rate readings. Pressure ports just before and just after the sample location give the differential pressure Δp necessary to calculate the shear stress τ applied by the water (Eq. 3). The detail of these calculations is in Perugu et al. (1999).

One test leads to one $\dot{z}$ and one corresponding τ value. Several tests are performed for a range of velocities varying between 0.1 m/s to 6 m/s. The corresponding range of τ values is approximately 0.1 N/m^2 to 100 N/m^2. A series of points $(\dot{z}, \tau)$ is obtained for the soil. A typical result on porcelain clay is shown in (Fig. 10). For comparison purposes, the $\dot{z}$ versus τ curve for sand is also shown on Fig. 10. The properties of the clay are shown in Table 5. The $\dot{z}$ versus τ curve is not linear, as often found in the literature, but has a shape more similar to the results presented by Christensen (1965). In the EFA test, it was considered that $\dot{z}$ was zero if $\dot{z}$ was less than 1 mm/hr.

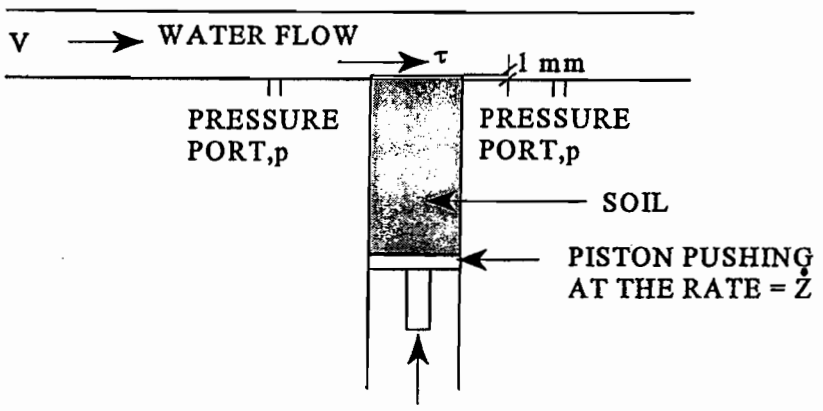

Figure 8. The Concept of the Erosion Function Apparatus.

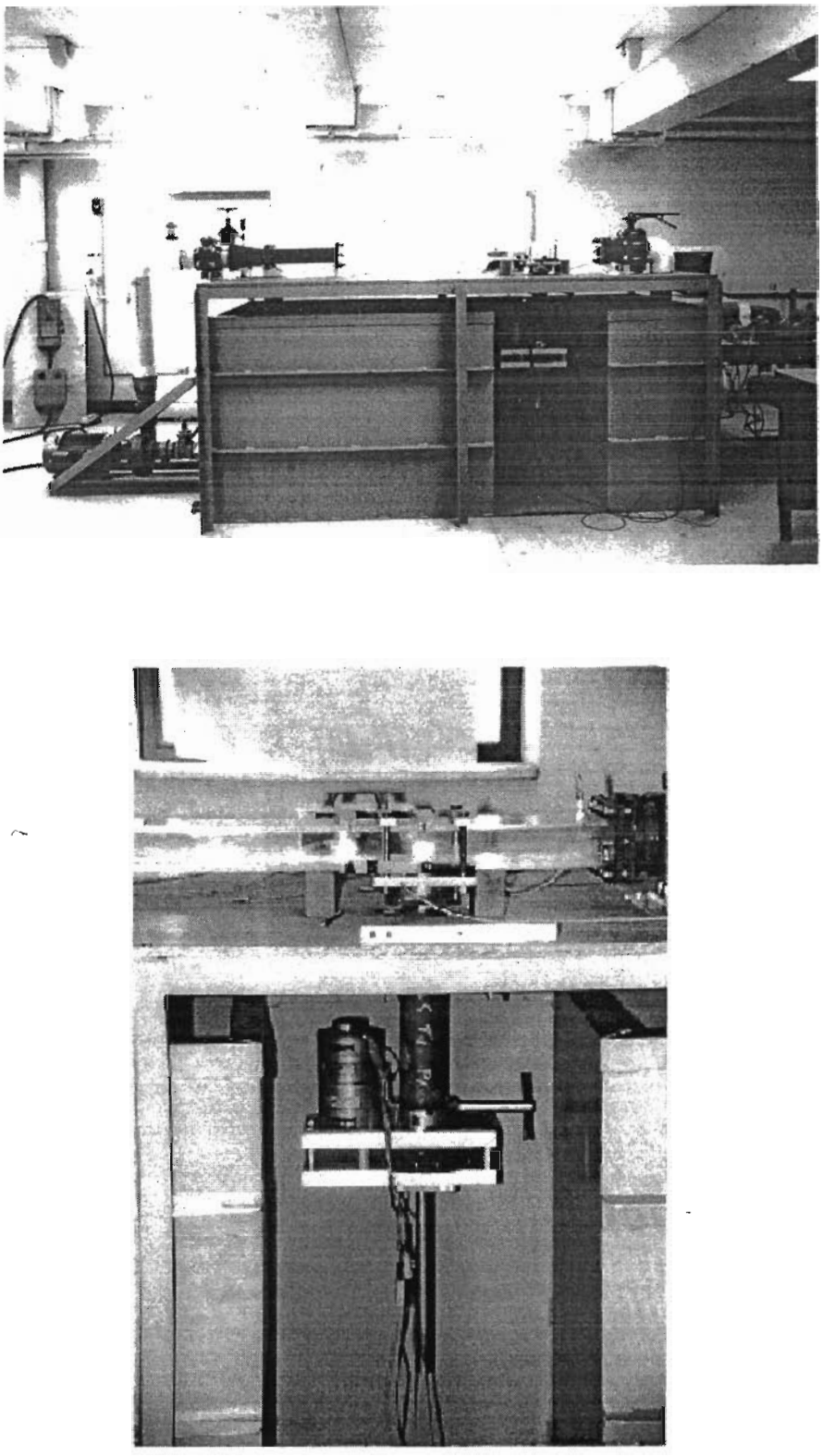

Figure 9. The Erosion Function Apparatus.

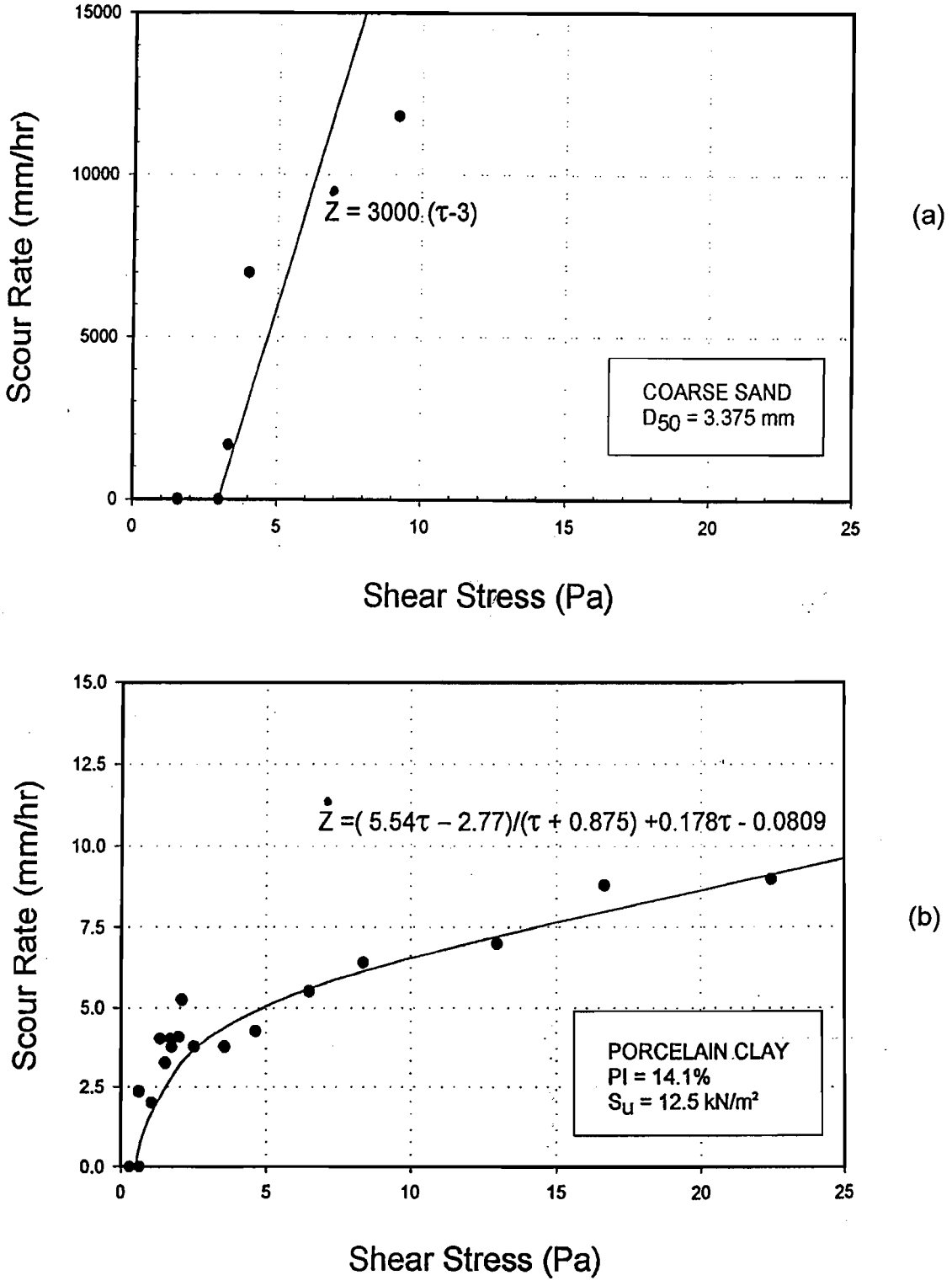

Figure 10. Example of EFA Results: (a) Sand, (b) Clay.

Table 5. Properties of the Porcelain Clay.

Mean Diameter d_{50} (mm)	0.0062
Sand Content (%)	0
Silt Content (%)	75
Clay Content (%)	25
Natural Water Content (%)	28.5
Plastic Limit (%)	20.2
Liquid Limit (%)	34.4
Unit Weight (kN/m^3)	18.0
Specific Gravity	2.61
Undrained Shear Strength by Mini Vane (kN/m^2)	12.5
Cation Exchange Capacity (meq/100 g)	8.3
Sodium Adsorption Ratio	5
pH	6
Electrical Conductivity (mmhos/cm)	1.2

Therefore, the critical shear stress τ_c was defined as the shear stress that would generate a scour rate of 1 mm/hr (24 mm/day). This arbitrary number was used because, in a week-long flood event, the scour depth would still be very small for 1 mm/hr.

1.8 MAXIMUM SHEAR STRESS AND INITIAL SCOUR RATE

In order to evaluate the maximum shear stress occurring around a cylindrical pier, a numerical simulation of the water flow was performed (Wei et al., 1997). The CHIMERA - RANS method was used (Chen et al., 1996). Chimera is a dragon with the head of a lion, the body of a goat, and the tail of a snake. This word is used to illustrate the fact that the total mesh representing the water is divided into several blocks of three-dimensional elements later assembled to make a whole. This division is necessary to make the problem more mathematically manageable considering the very large number of elements involved. These often very different blocks of elements are assembled by mass and momentum conservation laws at the boundaries reminding one of the Chimera dragon. RANS stands for Reynolds-Averaged Navier Stokes equations. The Navier-Stokes equations and the continuity equation are four partial differential equations where the unknowns are the flow velocities (u, v, w) and the pressure p to be solved as a function of the position and time coordinates x, y, z, and t. These equations come from three equations of motion linking the stresses, one continuity equation linking the velocities, and six constitutive equations linking the stresses to the velocities by using the fact that water is a linear Newtonian viscous fluid. In laminar steady state flow, u, v, w, and p do not fluctuate at a given point, and the Navier-Stokes equations plus the continuity equation are sufficient to solve the complete problem.

In turbulent steady state flow, u, v, and w fluctuate (Fig. 11) around mean values in a random cyclic fashion. This state is where the term Reynolds average comes from. The mean cyclic amplitude of the velocity fluctuations $\sqrt{\overline{u^2}}$ divided by the mean velocity $\bar{u}$ is the turbulence intensity of the water flow with typical values for pier scour between 0.1 and 0.2. The mean frequency of the cycles can vary drastically and is likely in the 10 to 100 Hz range for pier scour. In modeling the turbulent flow, the equations of motion and the continuity equation remain the same but the mean amplitude of the velocity fluctuations introduces additional variables which require additional modeling equations. The energy level in the water flow is used to characterize these additional velocity components. The layer eddy viscosity model is one of the models used to describe these additional velocity components (Chen and Patel, 1988).

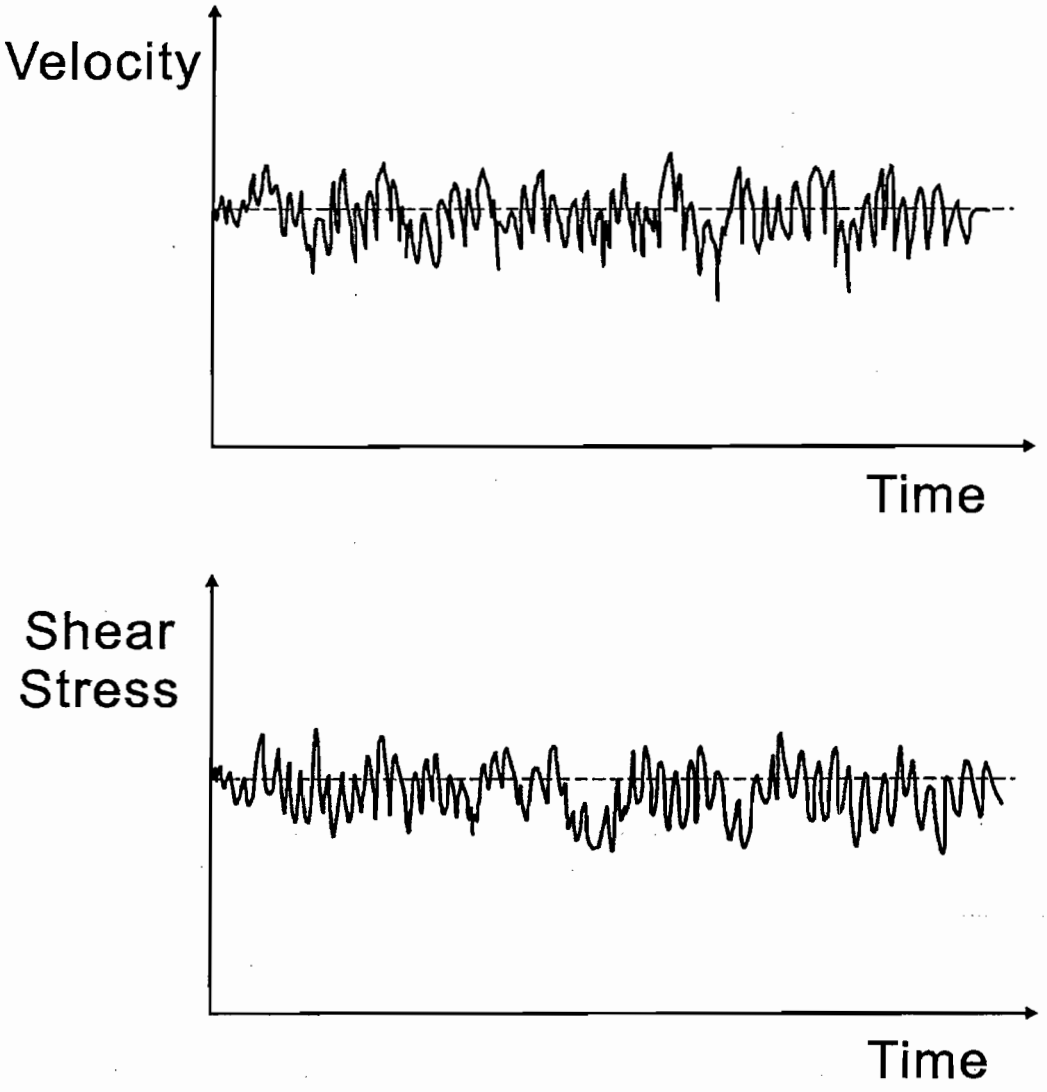

Figure 11. Qualitative Variation of Velocity and Shear Stress in Turbulent Flow.

One output of the computer simulation is the shear stress variation on the riverbed around the pier (Fig. 4). This figure corresponds to the first step in the CHIMERA-RANS solution—the one for a flat river bottom. A series of analyses of this flat river bottom or initial condition case was performed by varying the water velocity and the pier diameter. The results were used to prepare Fig. 5 and the associated Eq. 4, which give the maximum shear stress τ_{max} around the pier for a flat river bottom condition. If τ_{max} is larger than the critical shear stress for the soil τ_c, scour will be initiated in regions where $\tau > \tau_c$. The initial scour rate $\dot{z}_i$ is then read on the $\dot{z}$ versus τ curve, obtained from the EFA tests on the soil sample, at the value of τ_{max} .

1.9 MAXIMUM DEPTH OF SCOUR

In order to evaluate the maximum depth of scour z_{max} for clay, a series of flume experiments was performed. The detailed description of those experiments can be found in Gudavalli et al. (1997). Two flumes were used; the first flume was 457 mm wide and the second 1525 mm wide. The diameter of the cylindrical piers varied from 25 mm to 76 mm for the smaller flume and from 76 mm to 229 mm for the larger flume. Four different soils were used: three clays and one sand. The water depth varied from 160 mm to 400 mm in the smaller flume and 250 mm to 400 mm in the larger flume while the velocity ranged from 0.204 m/s to 0.83 m/s in the smaller flume and 0.3 m/s to 0.404 m/s in the larger flume. A total of 42 experiments was performed. An example of the results obtained for each experiment is shown in Fig. 12 for a 75 mm diameter pier in the porcelain clay (Table 5).

Note on Fig. 12 that the scour hole is developing mostly behind the pier after starting near the location of τ_{max} on Fig. 4. This is quite different from what has been observed for scour in sand where the hole develops all around the pier. Therefore, it would be more desirable for piles in clay to place any monitoring instrument behind the pier than in front of the pier.

As can also be seen on Fig. 12, the experiments were carried out for several days in order to approach the final depth of scour z_{max}; however, z_{max} was not reached. In order to get a better estimate of z_{max}, several models were used to curve fit the experimental scour depths versus time curve. The best fitting model was a hyperbola with the following equation:

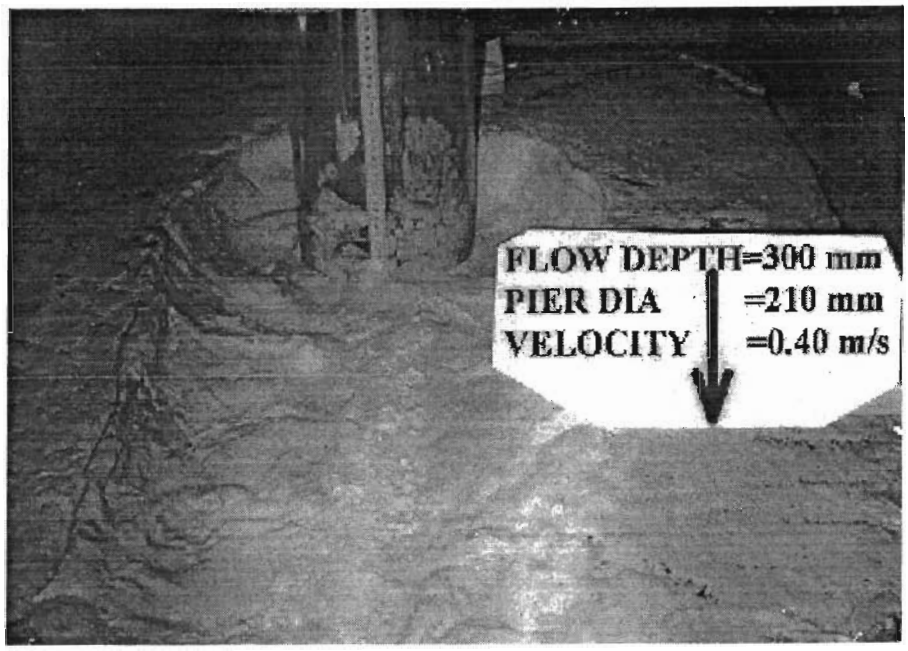

(a)

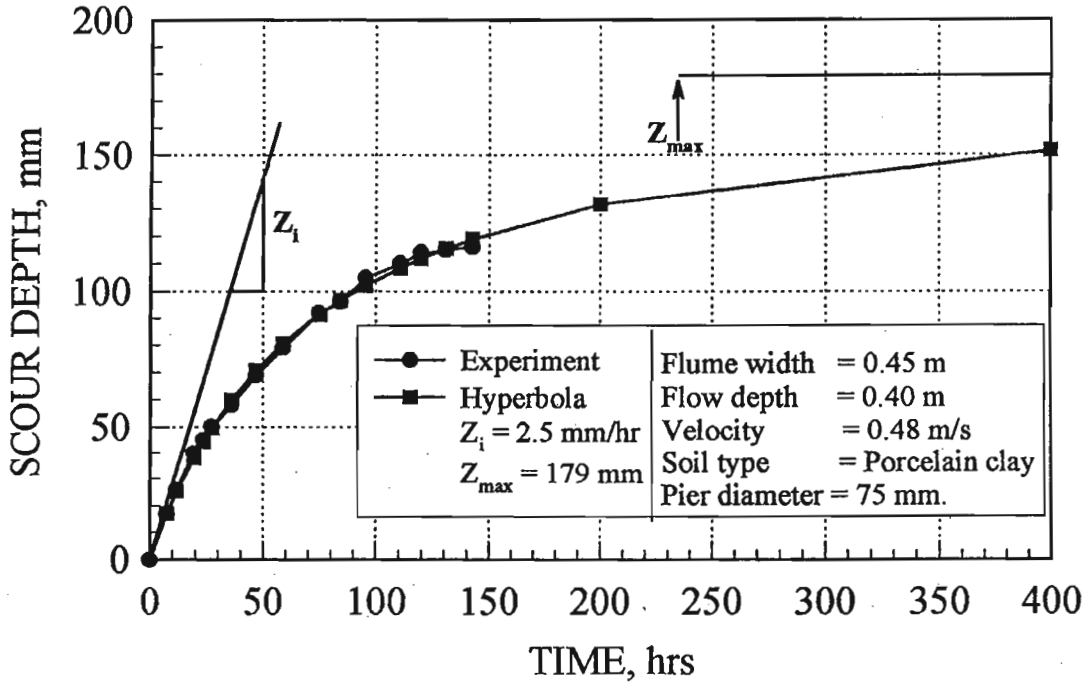

(b)

Figure 12. Example of Flume Test Results:
(a) Photo of Scour Hole, (b) Scour Depth versus Time Curve.

$$z = \frac{t}{\frac{1}{\dot{z}_i} + \frac{t}{z_{max}}} \tag{11}$$

where $\dot{z}_i$ is the initial slope of the z versus t curve, and z_{max} is the ordinate of the asymptote. The parameter z_{max} represents the final depth of scour at $t = \infty$. The curve-fitted hyperbola is shown on Fig. 12. The definition of z_{max} as the asymptotic value of the hyperbola can be argued with; however, it has the advantage to be a consistent definition for all experiments. The real proof of the model will be achieved if the predictions match the observed behavior on full-scale bridges over long periods of time. This observation is an ongoing process.

The z_{max} values for all the experiments were obtained and were plotted against various parameters. It was found (Fig. 13) that the most well behaved relationship was obtained when plotting z_{max} versus the pier Reynolds number R_e:

$$R_e = \frac{VD}{\upsilon} \tag{12}$$

where V is the mean flow velocity, D the pier diameter, and υ the kinematic viscosity of the water (10^{-6} m^2/s at 20°C). The proposed relationship is:

$$z_{max}(mm) = 0.18\ R_e^{0.635} \tag{13}$$

The simplicity of this relationship is most attractive. Shen at al. (1969) developed a very similar one. This relationship and Fig. 13 lead to the following observations. First, the maximum depth of scour in sand and in clay appears to be the same. This is confirmed by the fact that the HEC-18 equation developed from sand experiments fits this data on clay quite well. Second, the Reynolds number, which characterizes the ratio of inertia force over viscous force, was found to be a better indicator of z_{max} than the Froude number, which characterizes the ratio of inertia force to gravity force. This seems logical since, from the hydraulics point of view, the viscous force has more to do with the hydraulic shear stress and, therefore, the scour problem than the gravity force. Third, the water depth was varied in the experiments but was found to have very little influence on the results; hence, it does not appear in Eq. 13. This is confirmed to some extent by the fact that the power exponent on the water depth in the HEC-18 equation is very low (0.135). Fourth, the most important factors are the mean flow velocity V and the pier diameter D. For most common full-

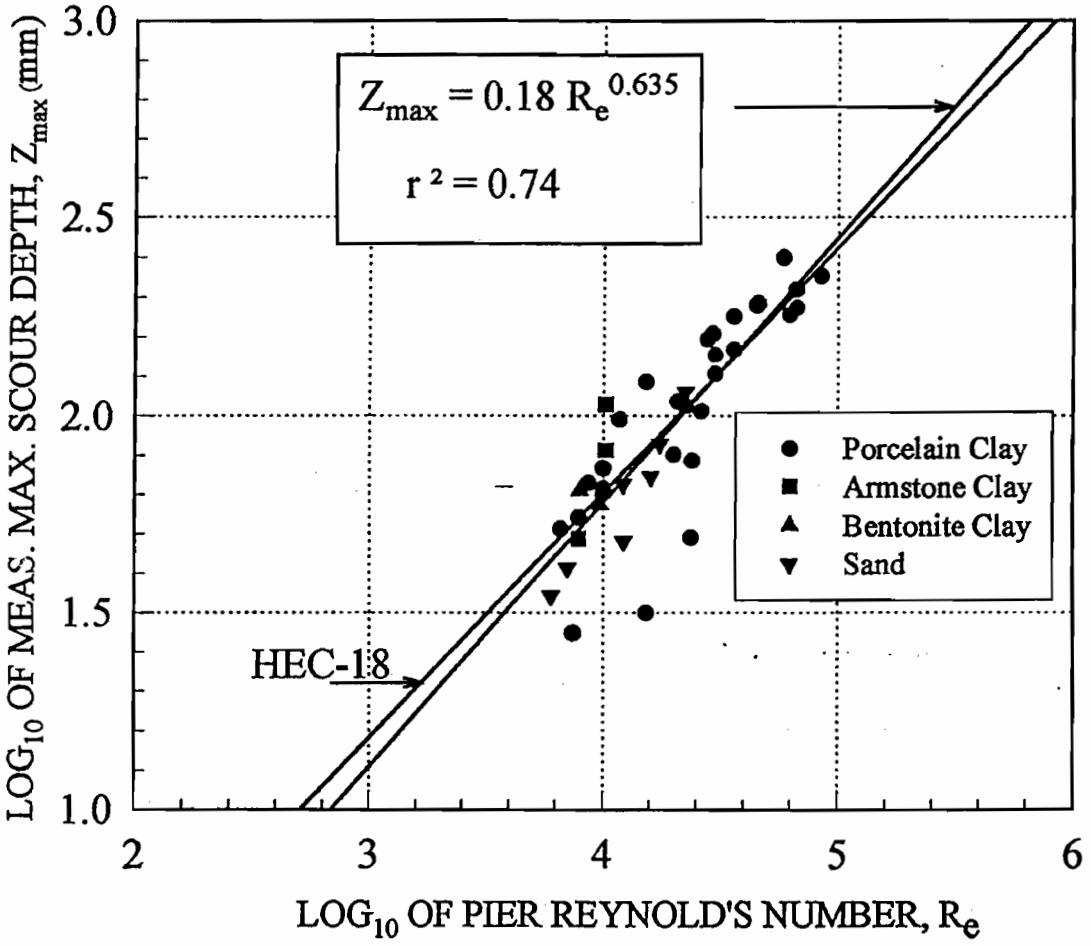

Figure 13. Measured Maximum Depth of Scour versus Pier Reynolds Number for Flume Experiments.

scale flood situations (D between 1 m and 3 m and V between 2 m/s and 4 m/s), the ratio z_{max} / D varies between 2 and 4.

1.10 SCOUR DEPTH VERSUS TIME CURVE AND PREDICTION

The hyperbolic model of Eq. 11 can be used since $\dot{z}_i$ and z_{max} are now known. The initial rate of scour $\dot{z}_i$ is obtained from the erosion curve $\dot{z}$ versus τ generated with the EFA on samples from the site; $\dot{z}_i$ is found on that curve at the maximum shear stress τ_{max}, which will occur around the pier to initiate scour; τ_{max} is obtained from Eq. 4, which is based on numerical modeling results. The value of z_{max} is obtained from Eq. 13, which is based on flume tests results. Therefore, SRICOS requires the knowledge of the mean flow velocity of the stream, the diameter of the pier D, and the erosion curve $\dot{z}$ versus τ from the EFA.

With $\dot{z}_i$ and z_{max} the complete scour depth z versus time t curve Eq. 11 is generated for the bridge pier (Fig. 14). Then the duration t_{design} of the design flood event is evaluated and the anticipated depth of scour z_{design} is read on the z, t curve at t_{design}.

In order to evaluate the precision of SRICOS, one can compare z_{max} predicted with z_{max} measured (Fig. 15). The measured values of z_{max} on Fig. 15 come from the flume tests performed in this study while the predicted values come from Eq. 13. The scatter in Fig. 15 is reasonably small; however, this comparison between predicted and measured values is not a true evaluation of the precision of the z_{max} Eq. 13 since that equation was generated by using the same database. In that sense, Fig. 15 is likely to represent the most favorable comparison.

Another way to evaluate SRICOS is to compare predicted with $\dot{z}_i$ measured (Fig. 16). The measured values of $\dot{z}_i$ on Fig. 16 come from the flume tests; the predicted values come from using Eq. 4 to get τ_{max} and then reading $\dot{z}_i$ on the EFA generated $\dot{z}$ versus τ curve at τ_{max}. There is more scatter for $\dot{z}_i$ than for z_{max}, which confirms that predicting small deformations is more erratic than predicting large deformations. The scatter for $\dot{z}_i$, however, is similar to the one on Fig. 2. The best fit regression through the origin of Fig. 16 gives:

$$\dot{z}_{im} = 1.05\, \dot{z}_{ip} \tag{14}$$

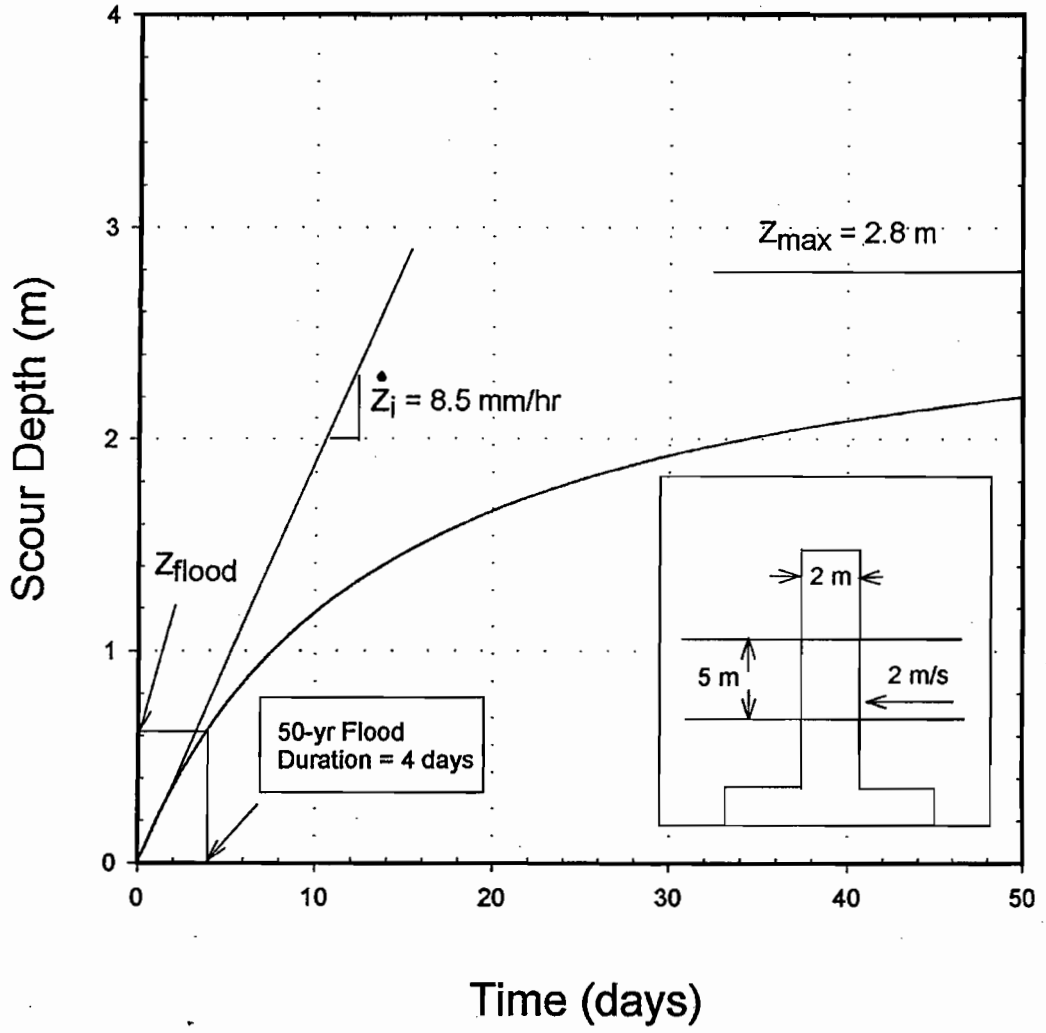

Figure 14. Example of a Scour Depth versus Time Curve for a Full-Scale Pier.

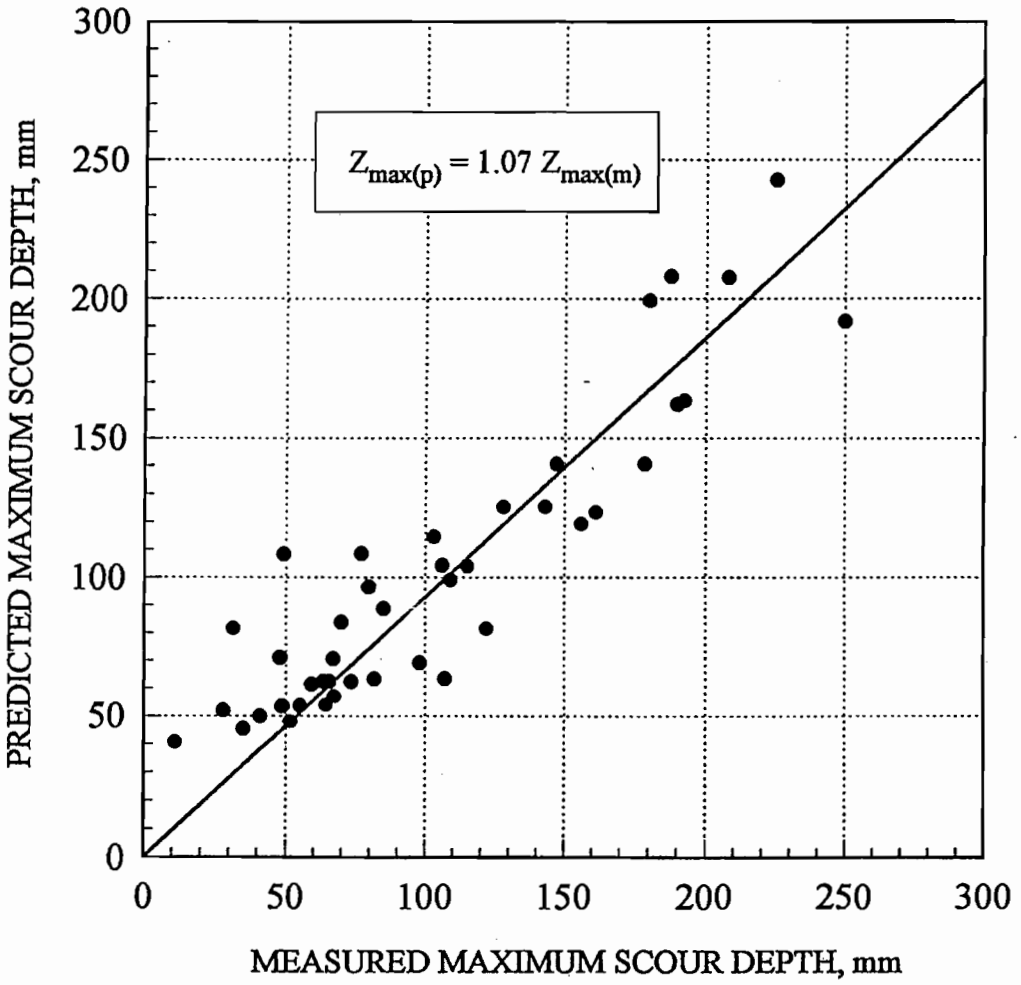

Figure 15. Comparison of Predicted and Measured Maximum Depth of Scour.

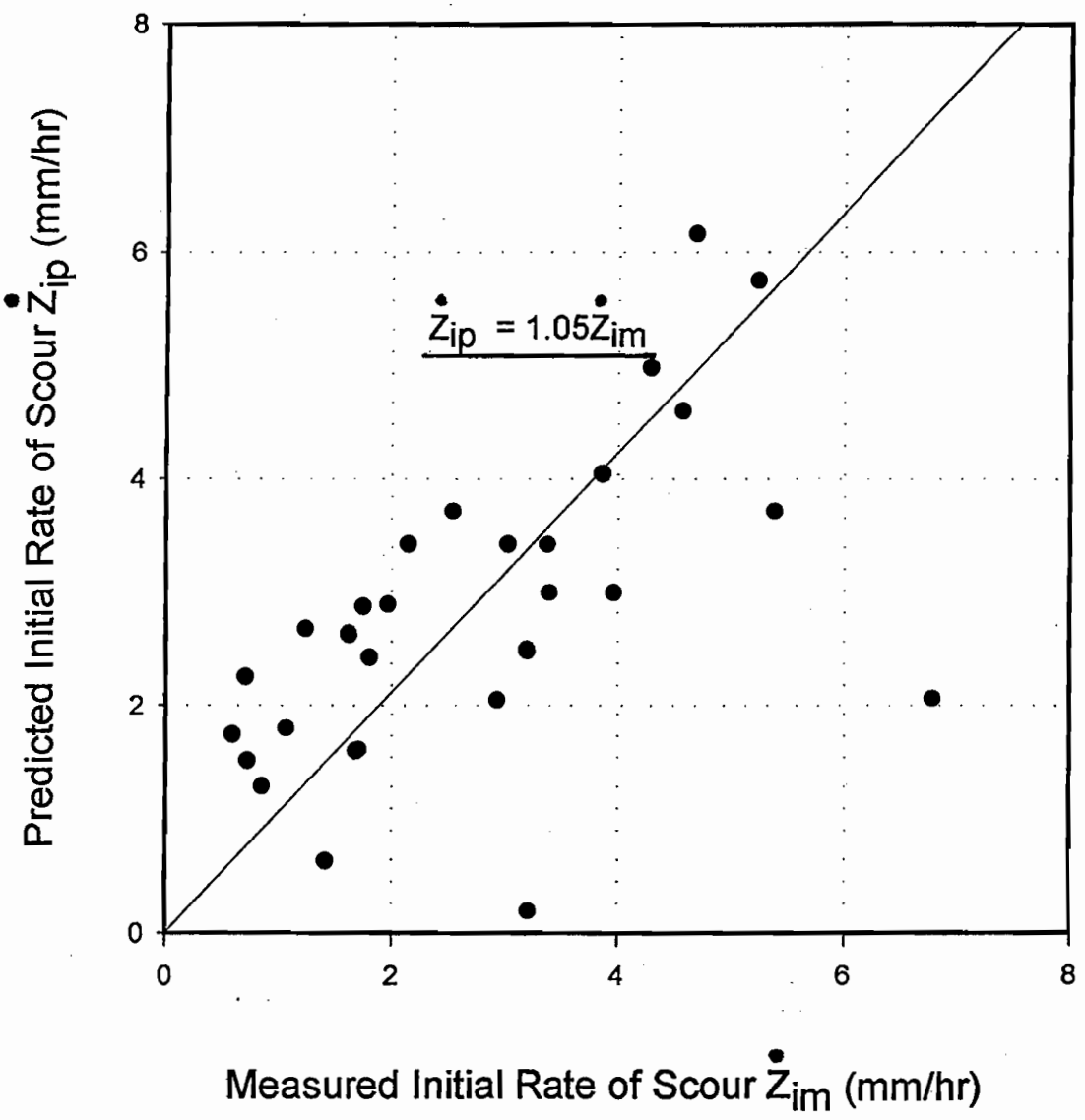

Figure 16. Comparison of Predicted and Measured Initial Rate of Scour.

1.11 EXAMPLE

A bridge pier is 2 m in diameter in a river that will experience a flood velocity of 2 m/s for a duration of four days. Shelby tube samples of the clay were recovered at the site, tested in the EFA, and led to the scour rate $\dot{z}$ versus shear stress τ curve of Fig. 10b. The maximum shear stress τ_{max} around the pier before scour begins is given by Eq. 4.

$$\tau_{max} = 0.094 \times 1000 \times 2^2 \left(\frac{1}{\log \frac{2 \times 2}{10^{-6}}} - \frac{1}{10} \right) = 19.4 \frac{N}{m^2}$$

For this τ_{max} value, the initial rate of scour $\dot{z}_i$ is found on Fig. 10b:

$$\dot{z}_i = 8.5 \; mm/hr$$

The maximum depth of scour z_{max} is calculated according to Eq. 13:

$$z_{max}(mm) = 0.18 \times \left(\frac{2 \times 2}{10^{-6}} \right)^{0.635} = 2803 \; mm$$

Then the complete depth of scour z versus time t curve is generated according to Eq. 11 (Fig. 14):

$$z(mm) = \frac{t\,(hrs)}{\frac{1}{8.5} + \frac{t\,(hrs)}{2803}} = 632 \; mm$$

After four days or 96 hours, the scour depth z is:

$$z(mm) = \frac{96}{\frac{1}{8.5} + \frac{96}{2803}} = 632 \; mm$$

In this case the scour depth is only 22.5% of the maximum scour depth.

1.12 FUTURE IMPROVEMENTS OF THE SRICOS METHOD

In the quest for continuous improvement, one should at least demonstrate that any new method is better than all currently used methods. Since, at present, there is essentially no commonly used method to predict the scour depth versus time curve for a pier in clay, SRICOS represents an improvement corresponding to an initial step filling up a void. At the same time SRICOS has limitations that need to be discussed so that the engineer can make more educated decisions.

The method needs to be compared with full-scale scour measurements. The biggest pier that SRICOS has been evaluated against is 230 mm in diameter at a velocity of 0.4 m/s. Comparisons

with a number of piers with diameters of the order of 2000 mm and velocities of about 3 m/s are desirable. Some confidence comes from the fact that the HEC-18 equation fits the z_{max} data well and that the HEC-18 equation has been checked at full-scale.

SRICOS has been developed for the simplest case of a circular pier. Bridge piers with different shapes will likely lead to somewhat different scour depth versus time curves. In first approximation, one might use the shape correction factor proposed for sand in Eq. 1. For that matter the other coefficients in Eq. 1, which are for the difference in direction between the pier and the flow, for the streambed topography, and for the armoring effect, could also be used while waiting for the same data to be developed for clays.

The data indicate that the maximum depth of scour z_{max} may be the same for clay and for sand. This would imply that the scour hole stops becoming deeper at the same shear stress whether in clay or in sand. This would then imply that the critical shear stress τ_c is the same for sand and clay, which is not what current data indicate. The premise that z_{max} is the same for sands and clays, and yet that τ_c is different for sands and clays, is a puzzle that needs to be addressed.

The site specific aspect of SRICOS through sampling at the site is an advantage, yet the volume of soil sampled represents a very small fraction of the volume to be scoured around the pier (e.g., 0.05%). This will induce scatter because of the natural heterogeneity of the soil. One way to remedy this situation is to use geophysical methods, which can give a complete scan of the area with depth at a reasonable cost, and use the scan to extend the result obtained on the samples.

Two aspects of the EFA can be improved. First, the pressure in the test section is not controlled; it is whatever is generated by the water velocity. A valve on the downstream side of the test section can be used to run tests at different pressures but at the same velocity. This would indicate the influence of the water pressure or normal stress on the $\dot{z}$ versus τ curve. Second, the turbulence intensity in the test section is not controlled; it is whatever is generated by the water velocity and the roughness of the wall. Placing adjustable obstacles on the walls could be used to vary the turbulence intensity while measuring it qualitatively with the pressure versus time signal. This would indicate the influence of the turbulence intensity on the $\dot{z}$ versus τ curve.

1.13 ALTERNATIVE METHOD

The CHIMERA-RANS numerical simulation method can be used to predict the complete scour history in three dimensions (Wei et al., 1997). This prediction is achieved by attaching a soil erosion model to the current CHIMERA-RANS hydraulic model. The procedure steps into time and, at each time step, the shear stresses τ at the water-soil interface are calculated, the scour rate $\dot{z}$ is determined at each location by reading the $\dot{z}$ versus τ curve at the proper τ. For the following time step, the water-soil interface is lowered in the simulation mesh by an amount equal to $\dot{z}\Delta t$ at each location. With this new profile of the interface, CHIMERA-RANS predicts a new set of hydraulic shear stresses τ, which leads to a new set of soil scour rate values $\dot{z}$, which scours the river bottom by $\dot{z}\Delta t$, and the process goes on until τ becomes smaller or equal to the critical shear stress t_c at all locations along the water-soil interface.

Such a process with the CHIMERA-RANS program will tie up an average work station for at least 24 hours. A comparison between predicted and measured results is shown in Fig. 17. The favorable comparison is proof that this method is able to reproduce existing data, but it needs to be checked against full-scale data in a series of true prediction events much like SRICOS.

1.14 CONCLUSIONS

A new method called SRICOS is proposed to predict the scour depth z versus time t curve around a cylindrical bridge pier of diameter D founded in clay. The steps involved are: 1. taking samples at the bridge pier site, 2. testing them in an Erosion Function Apparatus (EFA) to obtain the scour rate $\dot{z}$ versus the hydraulic shear stress applied τ, 3. predicting the maximum shear stress τ_{max} that will be induced around the pier by the water flowing at v_o before the scour hole starts to develop, 4. using the measured $\dot{z}$ versus t curve to obtain the initial scour rate $\dot{z}_i$ corresponding to τ_{max}, 5. predicting the maximum depth of scour z_{max} for the pier, 6. using $\dot{z}_i$ and z_{max} to develop the hyperbolic function describing the scour depth z versus time t curve, and 7. reading the z versus t curve at the time t_o to find the scour depth z_o that will develop around that pier.

A new apparatus is developed to measure the $\dot{z}$ versus t curve of step 2, a series of advanced numerical simulations is performed to develop an equation for the τ_{max} value of step 3,

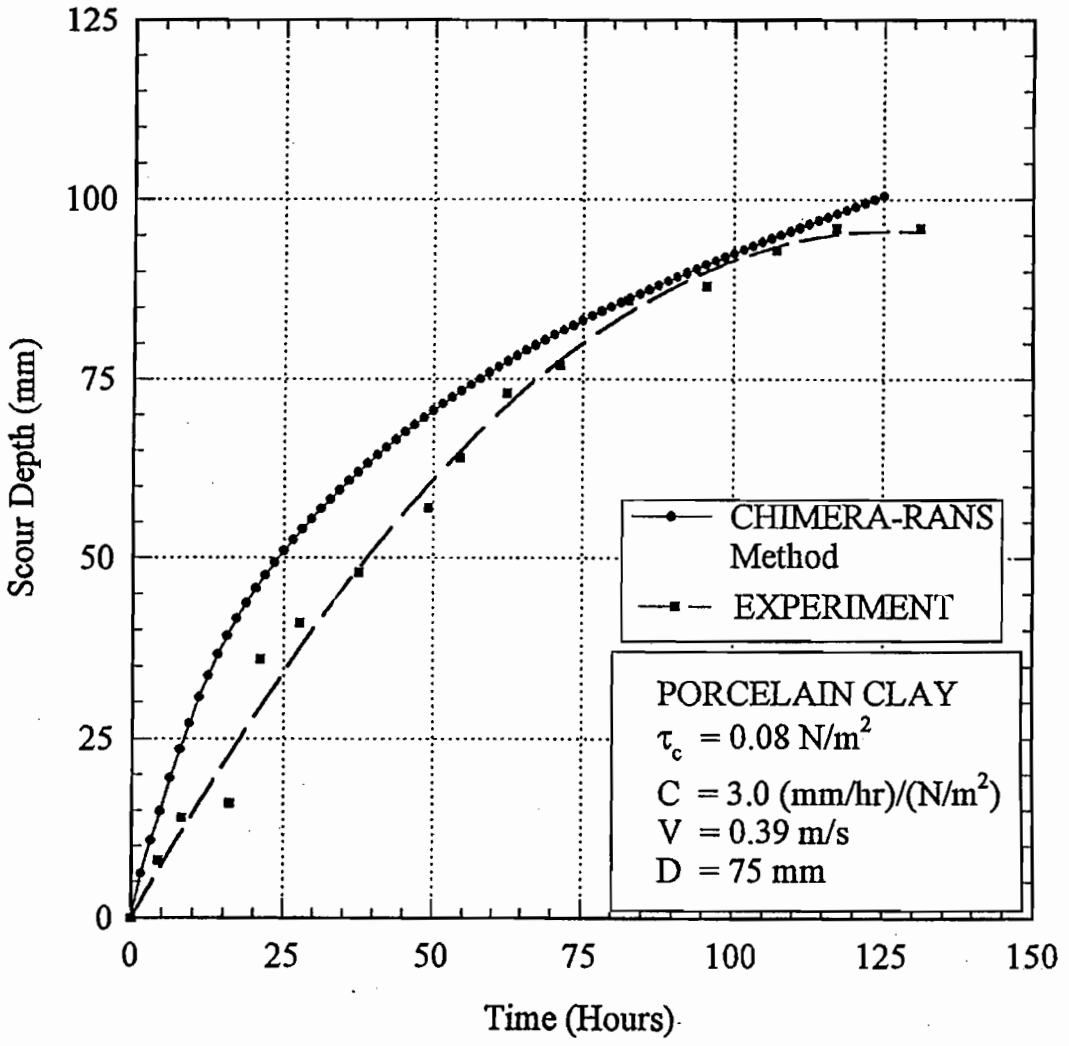

Figure 17. Example Comparison between CHIMERA-RANS Prediction and Flume Test.

and a series of flume tests is performed to develop an equation for the z_{max} value of step 5. The method is evaluated by comparing predictions and measurements in 42 flume experiments. Future developments of SRICOS are discussed, and the more general CHIMERA-RANS method is presented.

CHAPTER 2. THE EROSION FUNCTION APPARATUS FOR SCOUR RATE PREDICTIONS

2.1 HOW DO SOILS ERODE?

Clean sands and gravels erode particle by particle. This has been observed on slow-motion videotapes. Two mechanisms seem to be possible: sliding and rolling. In sliding, the shear stress τ imposed by the water on the particle becomes large enough to overcome the friction between two particles staked on top of each other. The critical shear stress τ_c is the threshold shear stress at which erosion is initiated. Referring to Fig. 18(a), horizontal equilibrium leads to (White, 1940):

$$\tau_c A_e = W \tan \phi \tag{14}$$

where A_e is the effective friction area of the water on the particle, W is the submerged weight of the particle, and ϕ is the friction angle of the interface between two particles. If the particle is considered to be a sphere, Eq. 14 can be rewritten.

$$\tau_c \alpha \frac{\pi D_{50}^{\ 2}}{4} = (\rho_s - \rho_w) g \frac{\pi D_{50}^{\ 3}}{6} \tan \phi \tag{15}$$

or

$$\tau_c = 2 \frac{(\rho_s - \rho_w) g \tan \phi}{3\alpha} D_{50} \tag{16}$$

where α is the ratio of the effective friction area over the maximum cross section of the spherical particle, D_{50} is the mean diameter representative of the soil particle size distribution, ρ_s and ρ_w are the mass density of the particles and of water, respectively, and g is the acceleration due to gravity. Eq. 15 shows that the critical shear stress is linearly related to the particle diameter. Briaud et al. (1999(b)) showed experimentally for sand and gravel tested in the EFA that:

$$\tau_c (N/m^2) \simeq D_{50} (mm) \tag{17}$$

Using Eqs. 16 and 17 and assuming reasonable values for ρ_s, ρ_w, g, and ϕ leads to a value of α equal to about 6. This value is many times higher than would be expected and shows that the sliding mechanism is not the eroding mechanism or at least not the only one involved.

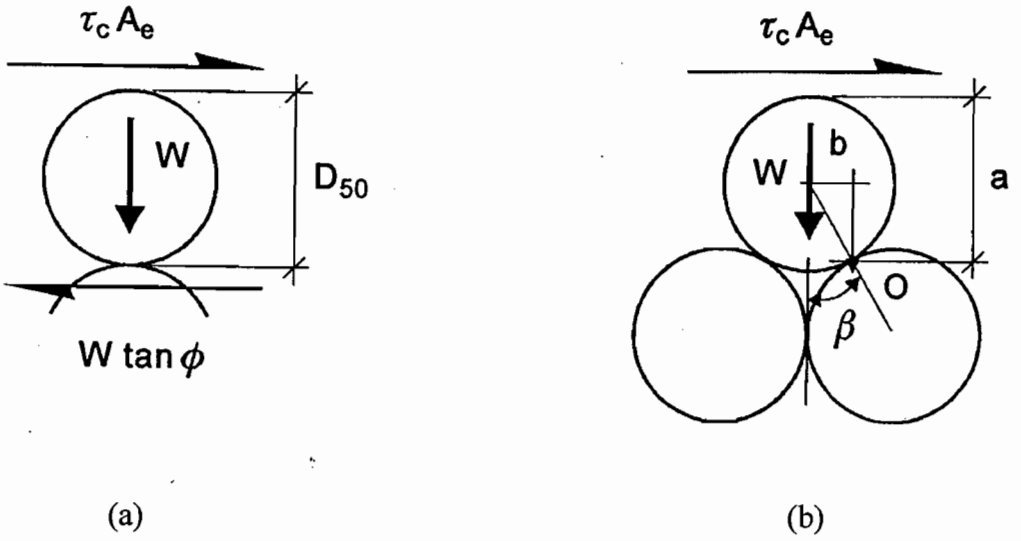

(a) (b)

Figure 18. Forces Applied to Soil Grain during Scour.

For rolling and referring to (Fig. 18(b)), moment equilibrium around the contact point O leads to (White, 1940):

$$\tau_c A_e a = Wb \tag{18}$$

or

$$\tau_c \times \frac{\alpha \pi D_{50}^{\ 2}}{4}\left(\frac{D_{50}}{2}+\frac{D_{50}\cos\beta}{2}\right)=(\rho_s-\rho_w)g\,\frac{\pi D_{50}^{\ 3}}{6}\times\frac{D_{50}}{2}\sin\beta \tag{19}$$

or

$$\tau_c \frac{2(\rho_s-\rho_w)g\sin\beta}{3\alpha(1+\cos\beta)}D_{50} \tag{20}$$

Eq. 20 confirms that τ_c is linearly proportional to D_{50}. For reasonable values of ρ_s, ρ_w, and g, for $\alpha = 1$ and using Eqs. 17 and 20 leads to β values equal to about 10 to 12 degrees, which is indicative of a loose arrangement; indeed the sand and the gravel tested were placed in a very loose condition in the EFA. Eq. 20 tends to indicate that while τ_c is linearly proportional to D_{50}, the proportionality factor may depend on the relative density. The dominant value of the angle β can be obtained from a contact angle distribution diagram such as the ones shown in Fig. 19.

These simplistic analyses of the sliding and rolling mechanisms help the researchers (or us) understand the important factors affecting the incipient motion of coarse grained soils. However they are not reliable for prediction purposes, and experiments are favored over theoretical expressions to determine τ_c. Shields (1936) ran a series of flume experiments with water flowing over flat beds of sands. He plotted the results of his experiments in a dimensionless form on what is now known as the Shields diagram. These data as well as other data on sand and the data for this study are plotted on Fig. 20 as critical shear stress τ_c versus mean grain size D_{50}. Eq. 17 is shown on Fig. 20 and seems to fit well for sands. Shields did not perform any experiments on silts and clays. The data developed for silts and clays in this study show that Eq. 17 is not applicable to fine-grained soils and that D_{50} is not a good predictor of τ_c for those types of soils. Parameters influencing the erodibility of fine-grained soils are discussed later.

Fine-grained soils may erode particle by particle as observed in the EFA. When this process takes place it is invisible to the naked eye, and the only evidence is that the water becomes less clear. The soil surface erodes over time periods that are typically measured in hours. Even though

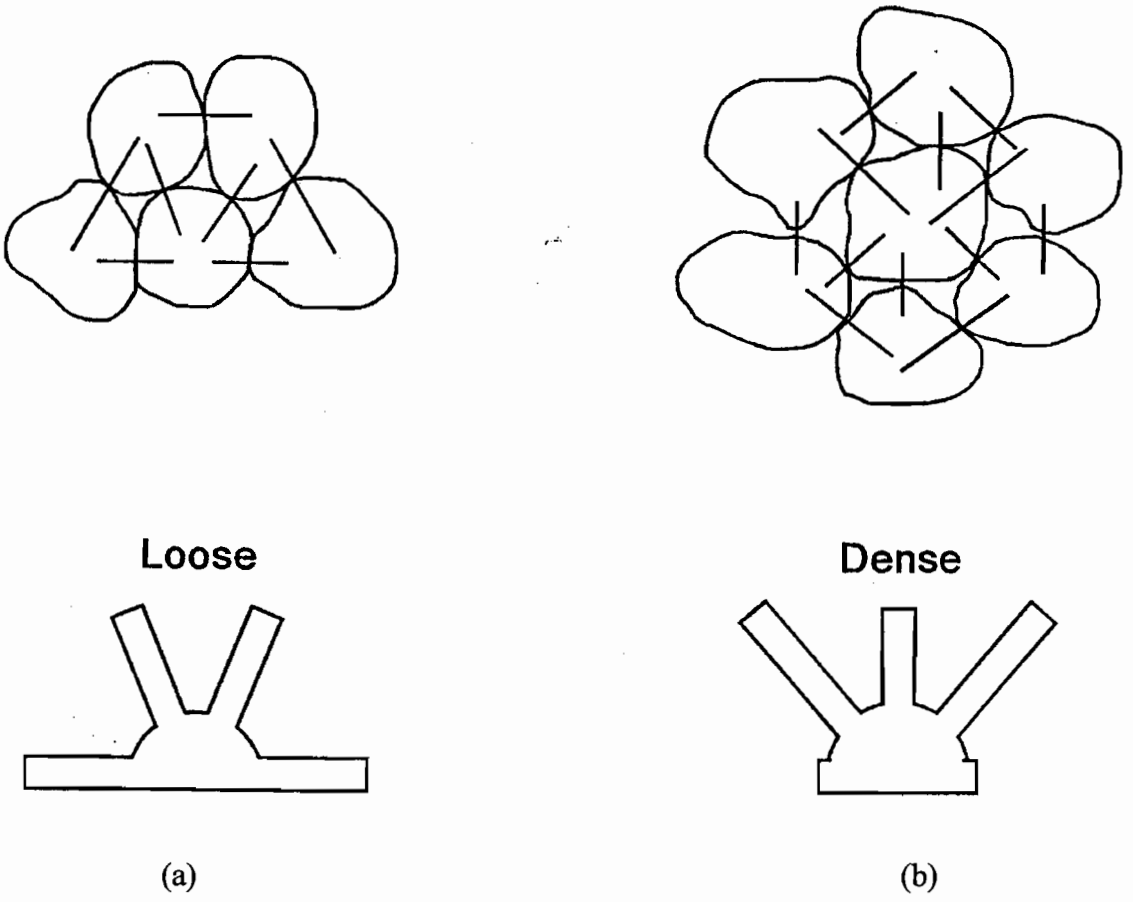

Figure 19. Rosettes Representing the Distribution of Contact Angles between Grains.

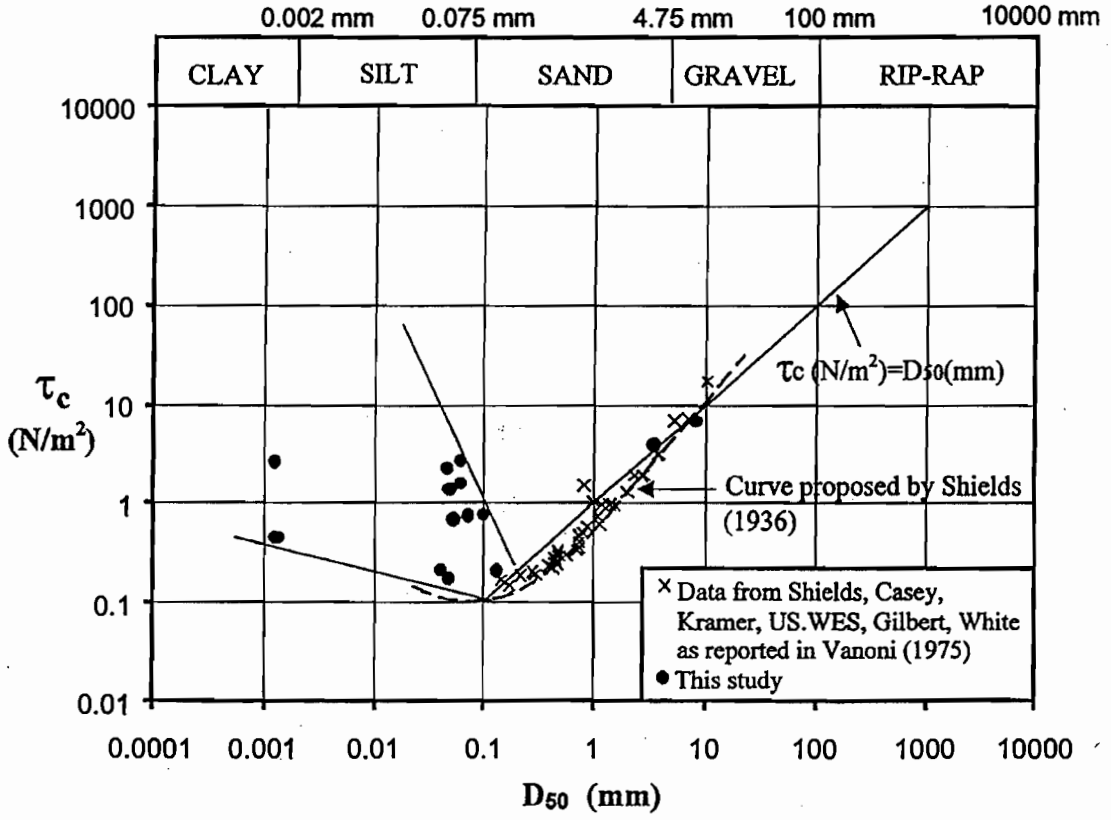

Figure 20. Critical Shear Stress versus Mean Soil Grain Diameter.

the fine-grained soil erodes particle by particle, Eq. 17 is not applicable because the electromagnetic interparticle forces increase the scour resistance (Briaud et al., 1999(b)). If the fine-grained soil has fissures that create weak blocks, the soil may erode block by block. These blocks can be one cubic centimeter in size, and the process is easily identified.

There seems to be a general consensus on the use of the shear stress τ applied by the water to the soil at the soil water interface as the major parameter causing erosion. It is likely that the hydraulic normal stress or pressure σ created by the water at that interface also contributes to the process. This contribution would come from a dynamic differential water pressure in excess of differential hydrostatic water pressure $(\Delta p - \Delta p_o)$ between the bottom and the top of the soil particle. This problem has been addressed by Einstein and El-Samni (1949) and Apperley (1968). Nevertheless, the use of the shear stress only has remained common practice and the role of the normal stress, which generates bursts of uplift forces during turbulent flow has yet to be included in common approaches to scour.

2.2 PREVIOUS EROSION APPARATUS

The erosion function is the relationship between the erosion rate $\dot{z}$ of the soil and the hydraulic shear stress τ. The erosion function is a measure of the erodibility of the soil. A few laboratory apparatus have been developed to measure the erodibility of fine-grained soils. The rotating cylinder apparatus was proposed by Moore and Masch (1962). It consists of an outer cylinder rotating around a stationary inner cylinder. The inner cylinder is made of a soil sample wrapped around a center rod. The gap between the two cylinders is filled with the eroding fluid. The rotating outer cylinder imparts motion to the eroding fluid, which in turn applies a shear stress to the toric soil sample. This shear stress generates a torque that is measured on the center rod. The critical shear stress τ_c is calculated from the torque measured at the initiation of the erosion process. The erosion rate e_r is measured by weighing the sample at regular time intervals; e_r is quoted in weight per unit area and per unit of time $(\mathrm{N}/m^2 \cdot hr)$.

The drill hole apparatus was proposed by Rohan et al. (1986) in order to improve upon the rotating cylinder test. The test consists of drilling a 6.35 mm diameter hole through a sample, fitting the sample in a tube, and circulating water through the 6.35 mm hole. This test is a more sophisticated version of the pinhole tests (ASTM-D4647). The shear stress applied at the water-soil

interface is calculated from the head loss in the drill hole, and the erosion rate is obtained by weighing at regular time intervals the soil collected in a sedimentation tank. Other apparatus have been developed and are described in Lee and Mehta (1994) and Philogene and Briaud (1996). They include the vertical grid oscillator, the EROMES System, the rotating disk device, and the submerged jet. In addition, several flume systems have been used: straight flumes, annular flumes, racetrack flumes, and rocking flumes.

The Erosion Function Apparatus described in this article was developed with the following specific goals in mind: be able to perform site specific scour studies, minimize sample disturbance, measure erosion rate versus shear stress for the soil tested, measure the critical shear stress for the soil tested, and incorporate the test results in a scour prediction method.

2.3 THE EROSION FUNCTION APPARATUS (EFA)

The EFA (Figs. 21 and 22) was conceived in 1991, designed in 1992, and built in 1993. The sample of soil, fine-grained or not, is taken in the field by pushing an ASTM standard Shelby tube with a 76.2 mm outside diameter (ASTM-D1587). One end of the Shelby tube full of soil is placed through a circular opening in the bottom of a rectangular cross section pipe. A snug fit and an O-ring establish a leakproof connection. The cross section of the rectangular pipe is 101.6 mm by 50.8 mm. The pipe is 1.22 m long and has flow straighteners at one end. The water is driven through the pipe by a pump. A valve regulates the flow and a flow meter is used to measure the flow rate. The range of mean flow velocities is 0.1 m/s to 6 m/s. The end of the Shelby tube is held flush with the bottom of the rectangular pipe. A piston at the bottom end of the sampling tube pushes the soil until it protrudes 1 mm into the rectangular pipe at the other end. This 1 mm protrusion of soil is eroded by the water flowing over it.

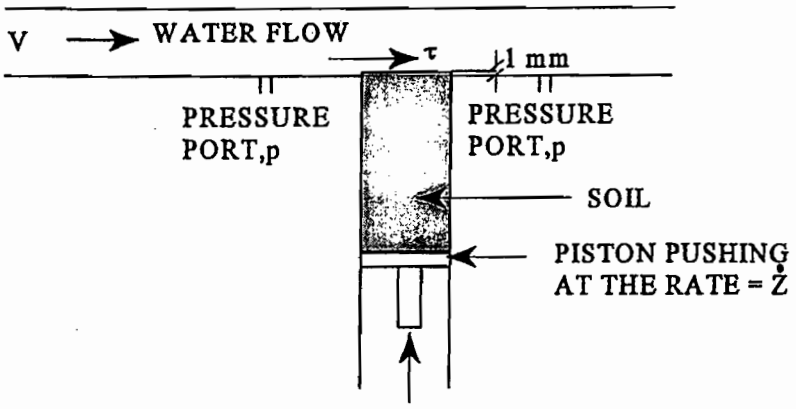

Figure 21. Conceptual Diagram of the Erosion Function Apparatus.

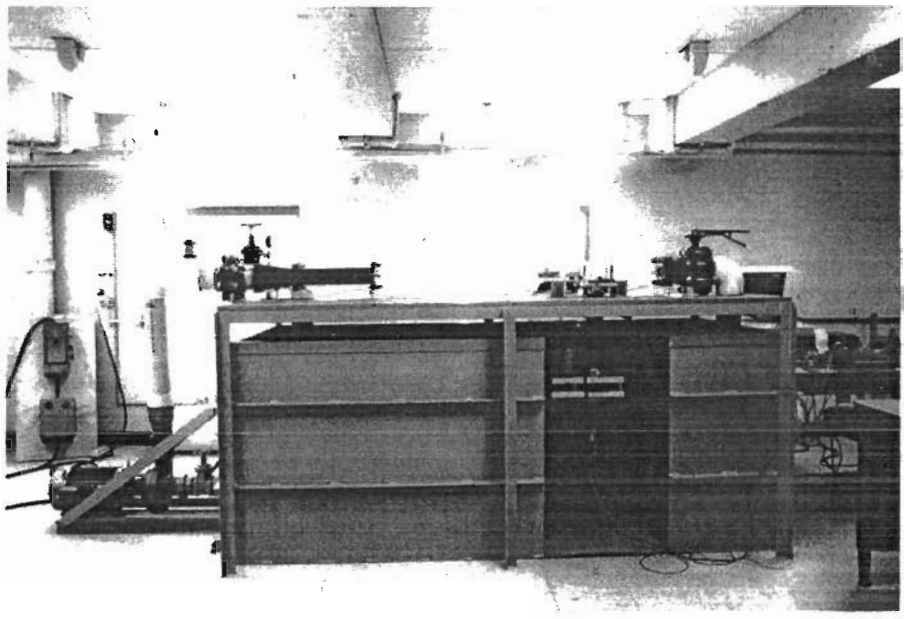

(a)

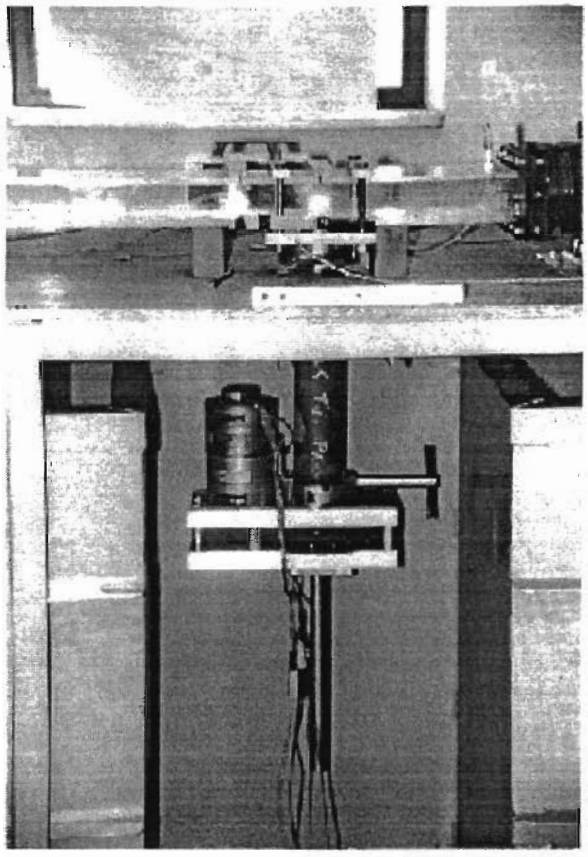

(b)

Figure 22. Photographs of the Erosion Function Apparatus (a) General View, (b) Close-up of the Test Section.

The procedure for the EFA test consists of:

1. Place the sample in the EFA, fill the pipe with water, and wait one hour.
2. Set the velocity to 0.3 m/s.
3. Push the soil 1 mm into the flow.
4. Record how much time it takes for the 1 mm soil to erode.
5. When the 1 mm of soil is eroded or after 1 hour of flow, whichever comes first, increase the velocity to 0.6 m/s and bring the soil back to a 1 mm protrusion.
6. Repeat step 4.
7. Then repeat steps 5 and 6 for velocities equal to 1 m/s, 1.5 m/s, 2 m/s, 3 m/s, 4.5 m/s, and 6 m/s.

The test result consists of the erosion rate $\dot{z}$ versus shear stress τ curve (Fig. 23). For each flow velocity, the erosion rate $\dot{z}$ (mm/hr) is simply obtained by dividing the length of sample eroded by the time required to do so. This linear erosion rate $\dot{z}$ is related to the weight erosion rate e_r measured in the rotating cylinder apparatus and the drill hole apparatus as follows:

$$e_r = \gamma \dot{z} \tag{21}$$

where γ is the total unit weight of the soil.

2.4 SHEAR STRESS AT SOIL-WATER INTERFACE

The first attempt at measuring the shear stress τ at the soil-water interface was to measure the pressure just before the sample (p_2 at position 2 on Fig. 24) and just after the sample (p_3 at position 3 on Fig. 24). These measurements were first made using standpipe manometers. However the difference in water level corresponding to $(p_2 - p_3)$ was small and fluctuated due to the turbulence in the flow. The manometer at positions 2 and 3 was replaced by a very sensitive differential transducer, which gave a more accurate measure of $(p_2 - p_3)$. Free body equilibrium of the water volume in the pipe between positions 2 and 3 gives the shear stress τ across the sample. The value of τ obtained in this fashion and when testing fine-grained soil was in error because the small 1 mm protrusion created a pressure difference not included in the calculations. This did not seem to be a problem for coarse grain soils where the size of the grains was of the order of the 1 mm protrusion. In other words the natural roughness of the soil was of the order of magnitude of the roughness created by the protrusion. For fine-grained soils, however, the protrusion induced a

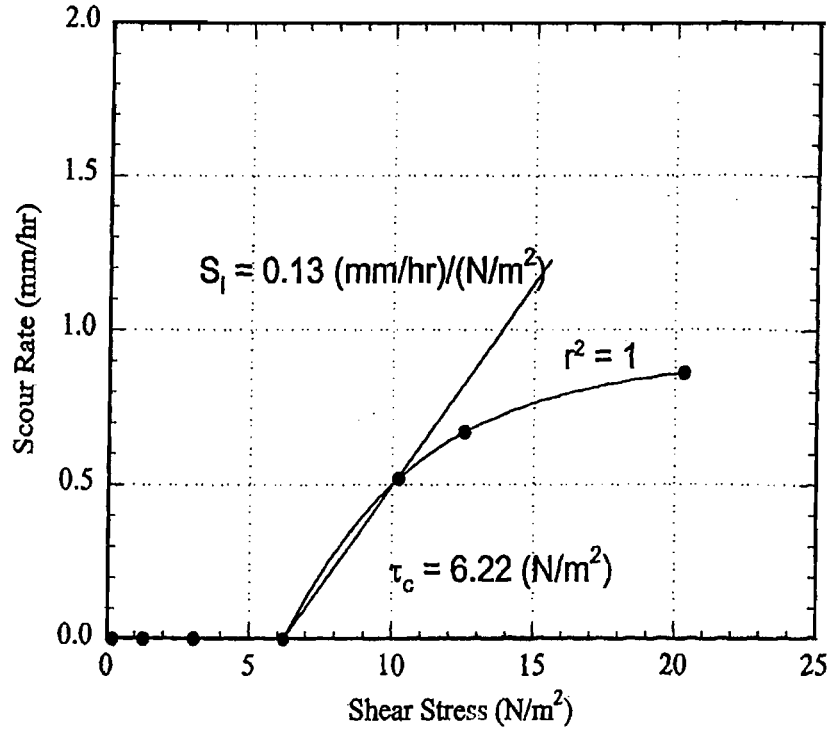

(a)

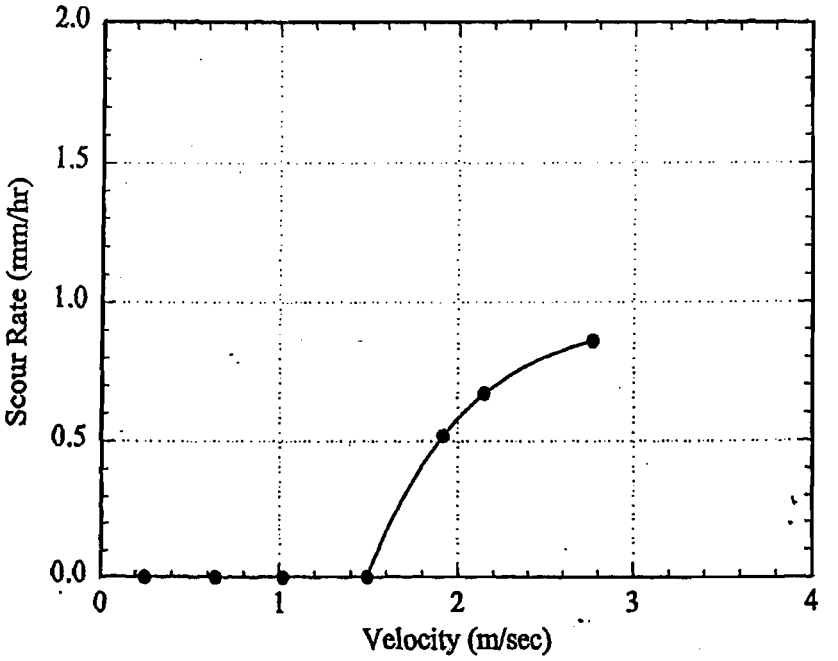

(b)

Figure 23. Erosion Rate versus Hydraulic Shear Stress Curve.

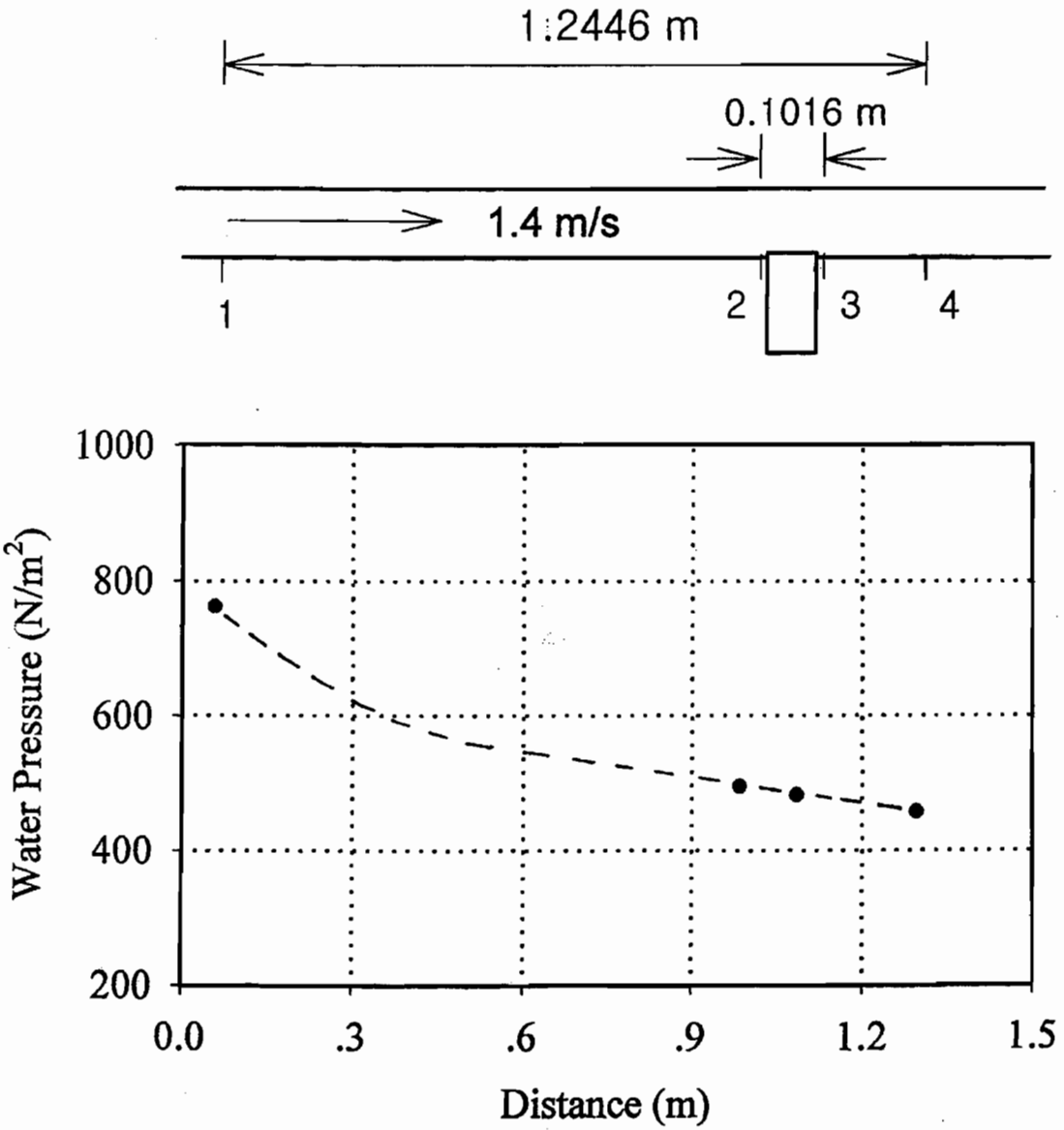

Figure 24. Pressure Losses along the Erosion Function Apparatus Pipe.

roughness much larger than the natural roughness of the soil; indeed for fine-grained soils the mean grain size D_{50} is measured in hundredths of a millimeter, if not thousandths of a millimeter.

In order to study the influence of the protrusion on the calculated shear stress values using either the manometer or the transducer readings, the following experiment was conducted. The soil sample in the Shelby tube was replaced by an aluminum cylinder having the same dimensions. EFA tests were then conducted with no protrusion of the aluminum cylinder and then with a protrusion equal to 1.2 mm. In both cases the velocity was varied from 0.2 m/s to 5.6 m/s and for each velocity the shear stress was calculated from the manometer and transducer readings. Fig. 25 shows the influence that the protrusion has on the calculated shear stress.

In order to solve the problem of the protrusion influence, pressure measurements were made at positions 1 and 4 in the pipe (Fig. 24). The average shear stress obtained by using $(p_1 - p_4)$ was a hydraulically smooth pipe shear stress much more consistent with the smoothness of fine-grained soils. Still, the head loss in the entrance region of the pipe was larger than in the rest of the pipe where the flow is fully developed (Fig. 24). As a result, the loss $p_1 - p_4$ is not a steady state smooth pipe pressure loss. It was found, after comparing the τ values obtained by various methods, that the best way to calculate τ for the EFA was by using the Moody chart (Moody, 1944) (Fig. 26)

$$\tau = \frac{1}{8} f \rho v^2 \tag{22}$$

where τ is the shear stress on the wall of the pipe, f is the friction factor obtained from the Moody chart (Fig. 26), ρ is the mass density of water (1000 kg/m^3), and v is the mean flow velocity in the pipe. The friction factor f is a function of the pipe Reynolds number R_e and the pipe roughness ε/D. The Reynolds number is $\frac{vD}{\upsilon}$ where D is the pipe diameter and υ is the kinematic viscocity of water $\left(10^{-6} m^2/s \; at \; 20^\circ C\right)$. The relative roughness ε/D is the ratio of the average height of the roughness elements on the pipe surface over the pipe diameter D. Since the pipe in the EFA has a rectangular cross section, D is taken as the hydraulic diameter $D=4A/P$ where A is the cross-sectional flow area, P is the wetted perimeter, and the factor 4 is used to ensure that the hydraulic diameter is equal to the diameter for a circular pipe. For a rectangular cross section pipe:

$$D = 2ab/(a+b) \tag{23}$$

where a and b are the dimensions of the sides of the rectangle.

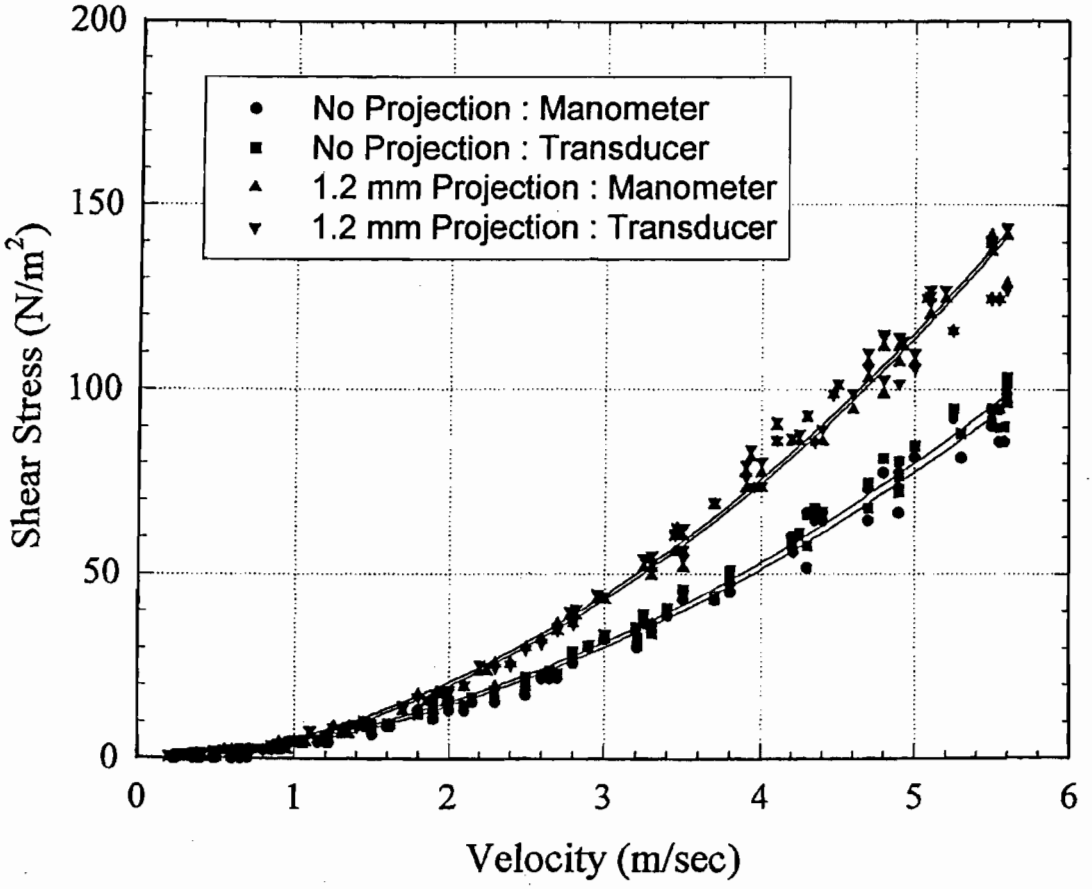

Figure 25. Influence of Sample Protrusion on Calculated Shear Stress.

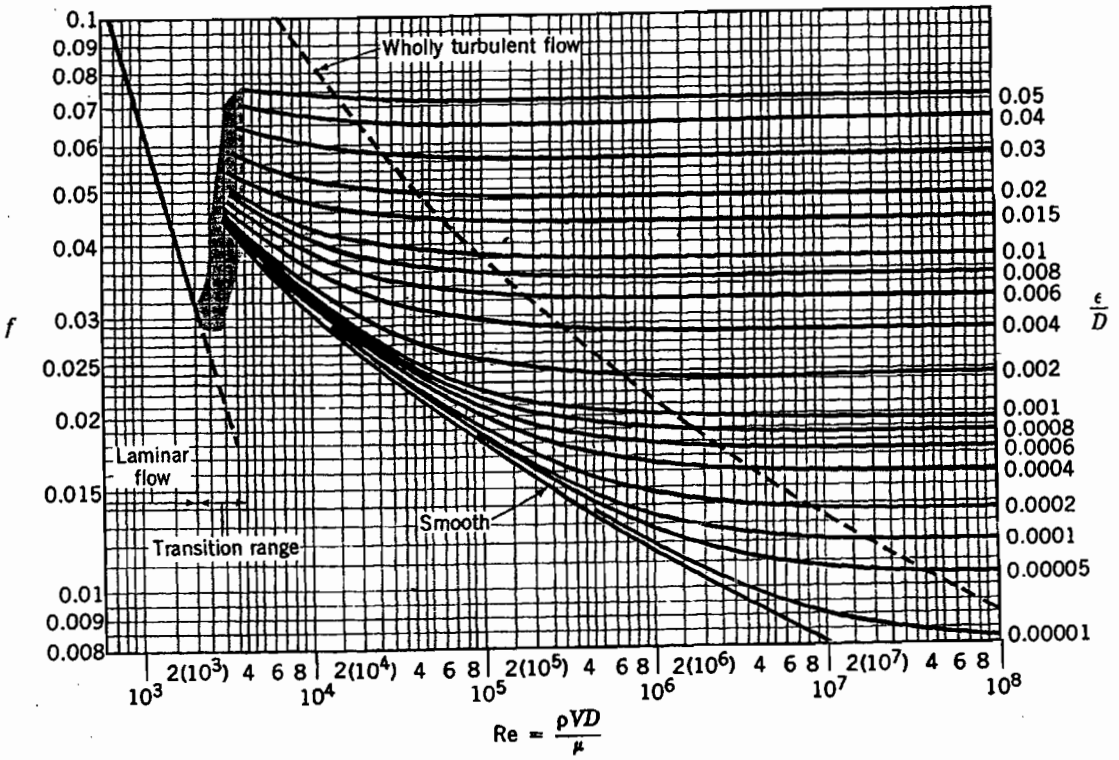

Figure 26. Moody Chart (Reprinted with Permission from Munson et al. 1990).

The Moody chart approach to calculating τ was selected because of the following verification. A porcelain clay (Table 6) was tested extensively in the EFA and τ_c was calculated by the Moody chart approach. That clay was also tested in an open channel flume where τ_c could be obtained independently by velocity profile measurements (Gudavalli et al., 1997). Fig. 27 shows the results of the $\dot{z}$ versus τ data from the EFA (using Moody chart to get τ) and the $\dot{z}$ versus τ data from the open flume tests. As can be seen, the Moody chart shear stress values from the EFA are consistent with the measured shear stress values from the flume.

2.5 DATA REDUCTION AND TYPICAL RESULTS

The erosion rate $\dot{z}$ at a given velocity v is:

$$\dot{z} = \frac{h}{t} \tag{24}$$

where h is the length of soil sample eroded in a time t. The length h is 1 mm, and the time t is the time required for the sample to be eroded flush with the bottom of the pipe (visual inspection through a Plexiglas window). The shear stress τ is:

$$\tau = \frac{1}{8} f \rho v^2 \tag{25}$$

where v is the mean flow velocity obtained from the flow meter, ρ is the mass density of water (1000 kg/m^3), and f is the friction coefficient. The value of f is read at the corresponding Reynolds number R_e and the soil surface roughness ε/D on Moody chart (Fig. 26). The Reynolds number is $\frac{vD}{\upsilon}$ where D is the hydraulic radius of the rectangular pipe (Eq. 23), and υ is the kinematic viscosity of water ($10^{-6} m^2/s \; at \; 20^\circ C$). The average height of the roughness elements ε is taken equal to $\frac{1}{2} D_{50}$ where D_{50} is the mean particle diameter for the soil. The factor of $\frac{1}{2}$ is used because it is assumed that the top half of the particle protrudes into the flow while the bottom half is buried into the soil mass.

If the erosion rate is slow (less than 10 mm/hr) the error on $\dot{z}$ is estimated at 0.5 mm/hr. If the erosion rate is fast (more than 100 mm/hr) the error on $\dot{z}$ is estimated at 2 mm/hr. Therefore, the relative error on $\dot{z}$ is estimated to be less than 10 percent. Comparison between the τ_c results for the sand and the gravel tested in this study and shown on Fig. 20 with Shields data indicates a

Table 6. Properties of the Porcelain Clay.

1	Liquid Limit, %	34.40
2	Plastic Limit, %	20.25
3	Plasticity Index, %	14.15
4	Specific Gravity	2.61
5	Water Content, %	28.51
6	Mean Diameter D_{50}, (mm)	0.0062
7	Sand Content, %	0.0
8	Silt Content, %	75.00
9	Clay Content, %	25.00

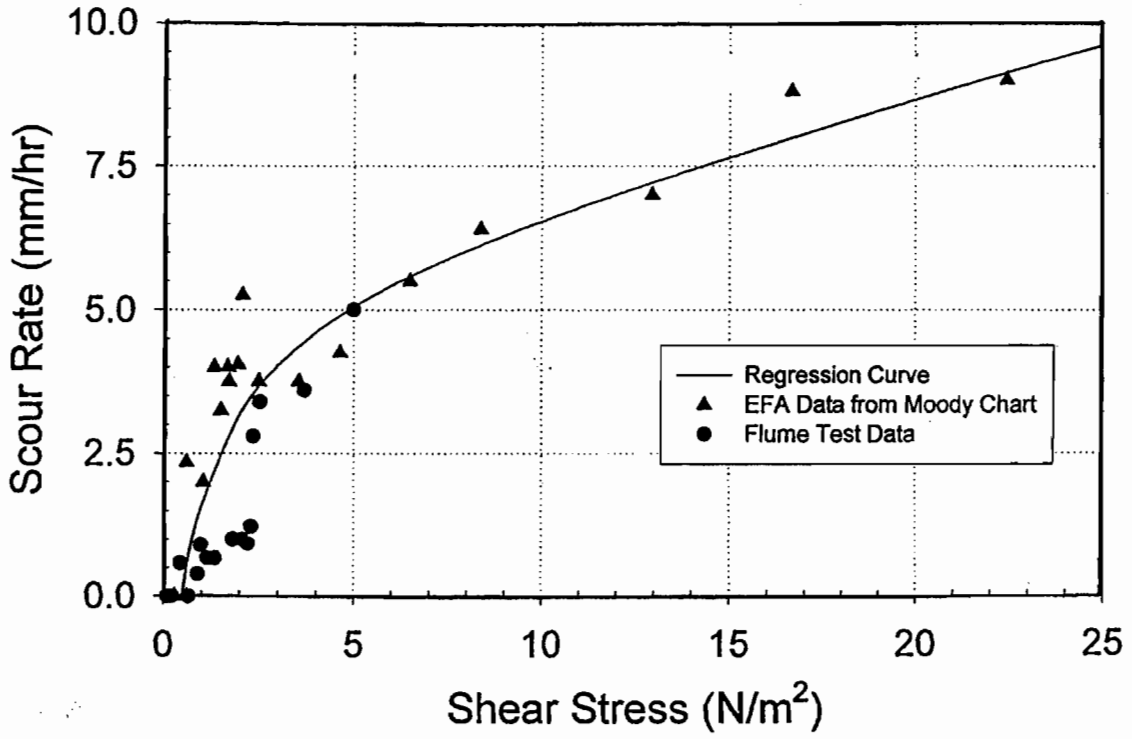

Figure 27. Erosion Rate versus Shear Stress Curve from EFA (Moody Chart) and from Flume Tests (Velocity Profiles).

difference of about 10 percent. Therefore it is estimated that both $\dot{z}$ and τ are measured with a relative error of about 10 percent.

The $\dot{z}$ versus τ curve is the result of a series of tests, each of which is performed at a constant velocity. A typical series of eight velocity tests lasts one working day. Fig. 28 is the result of a test in a clean coarse sand, Fig. 29 is for a very fine sand and silt, while Figs. 30 and 31 are for two clays. The soils corresponding to Figs. 29, 30, and 31 are natural soils; more details on those soils can be found in Table 7. The water used for the EFA tests had an alkalinity averaging 395 mg/1, a hardness of 20 mg/1, and pH of 8.8.

Fig. 28 shows a clear initial shear stress of 3 N/m^2 for this coarse sand $(D_{50} = 3.375\,mm)$. The erosion rate beyond τ_c is dramatic and measured in m/hr. By comparison Fig. 31 shows the results for the San Marcos River clay where the erosion rate beyond τ_c only reaches 2 mm/hr at 7 N/m^2. The San Marcos River clay was fissured and eroded particle by particle at lower velocities but block by block at 2.2 m/s with a dramatically higher erosion rate. The most common shape of the erosion function curve is concave (Figs. 23, 28, and 29), but it can be straight (Fig. 30) or even convex (Fig. 31). The convex shape is usually associated with a change of erosion process from particle by particle to block by block.

2.6 CORRELATION BETWEEN ERODIBILITY AND SOIL PROPERTIES

Is it really necessary to run erosion tests on site specific samples or is it possible to correlate erodibility to common soil properties? The data collected with the EFA and obtained from the literature were used to shed some light on this question. The erodibility of a soil is characterized by the erosion function, which is the $\dot{z}$ versus τ curve. This nonlinear relationship requires a number of curve-fitting parameters to describe it. In order to find a correlation between erodibility and soil parameters one would have to find correlations between each one of the curve-fitting parameters and soil parameters.

One of the curve-fitting parameters involved in the erodibility of a soil is the critical shear stress τ_c. In clean sands and gravels, the main soil parameter influencing τ_c is the size of the grains represented by D_{50}. Indeed in this case, gravity forces control the critical shear stress and a reasonable relationship exists between τ_c and D_{50} (Eq. 17, Fig. 20). In fine-grained soils, the size

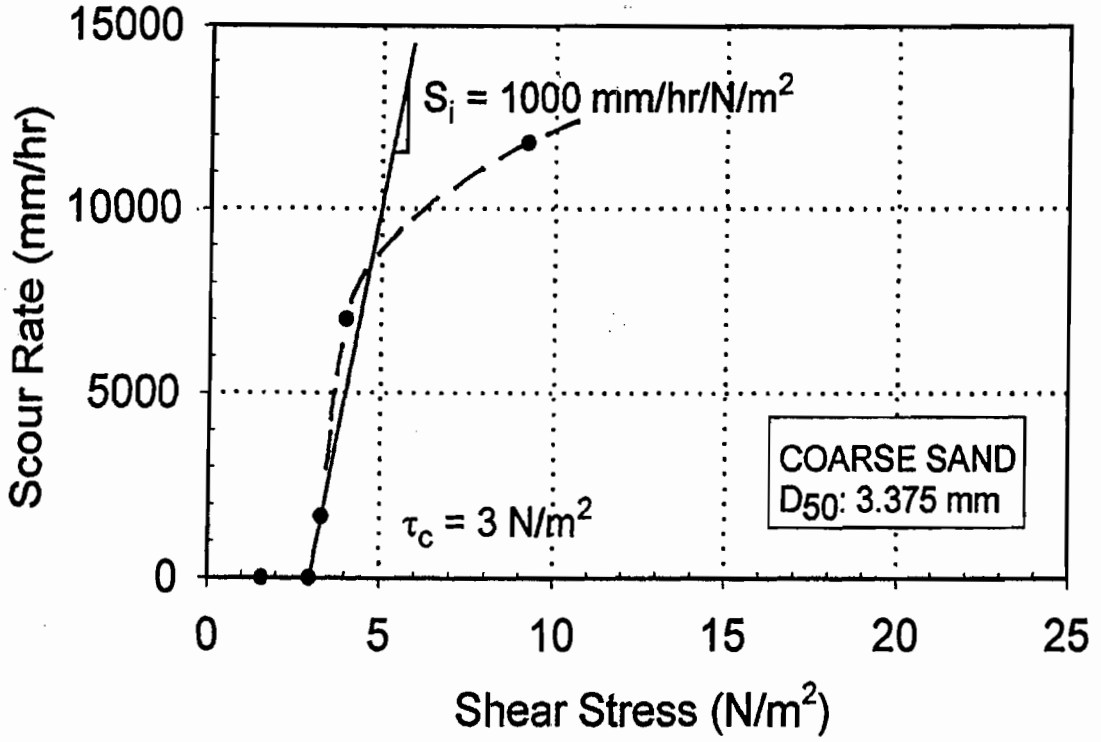

(a)

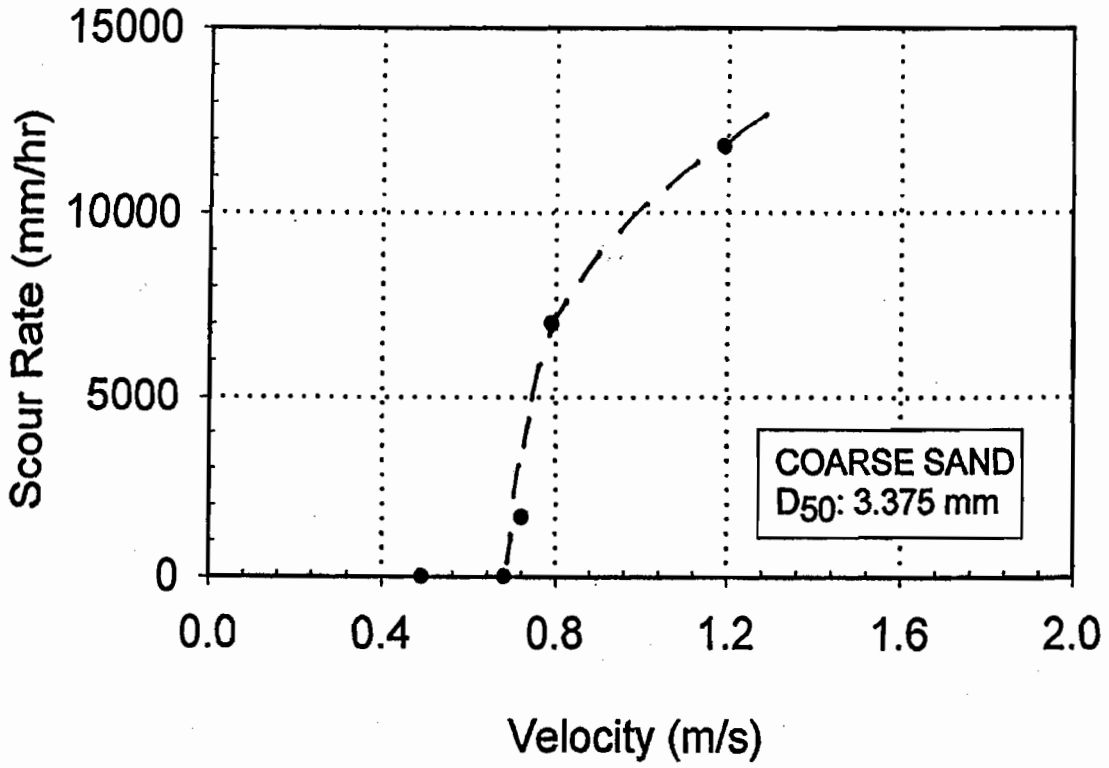

(b)

Figure 28. Erosion Curve for a Coarse Sand.

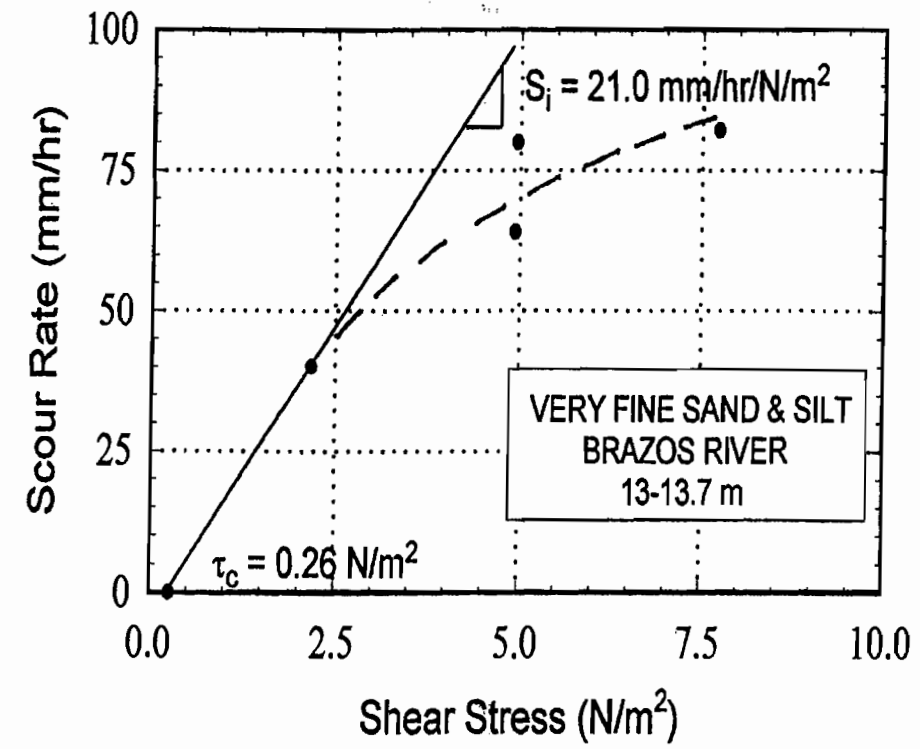

(a)

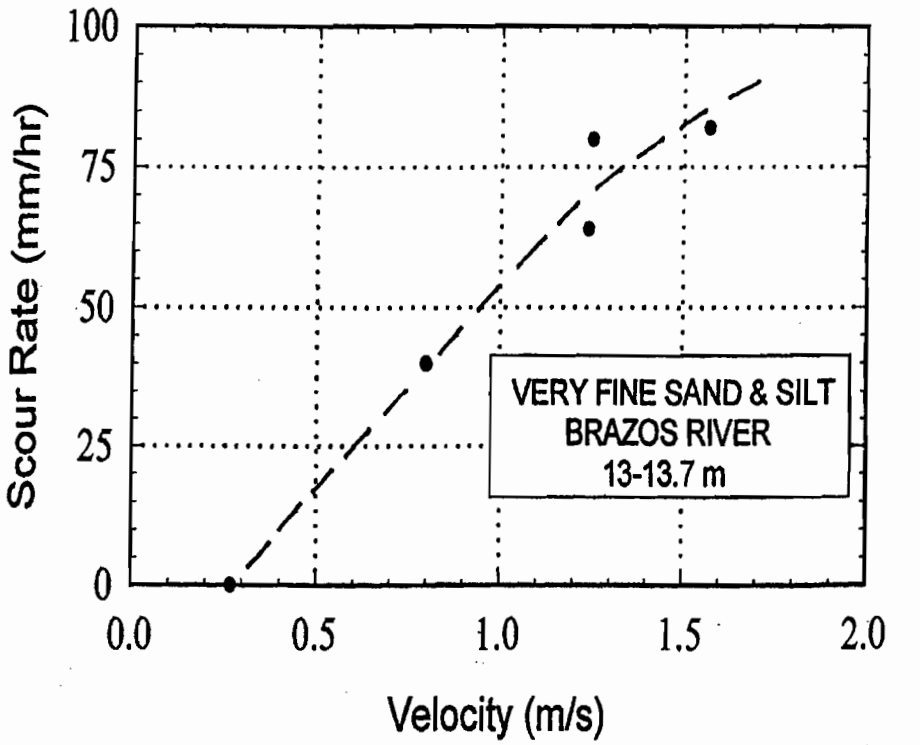

(b)

Figure 29. Erosion Curve for a Very Fine Sand and Silt (Brazos River).

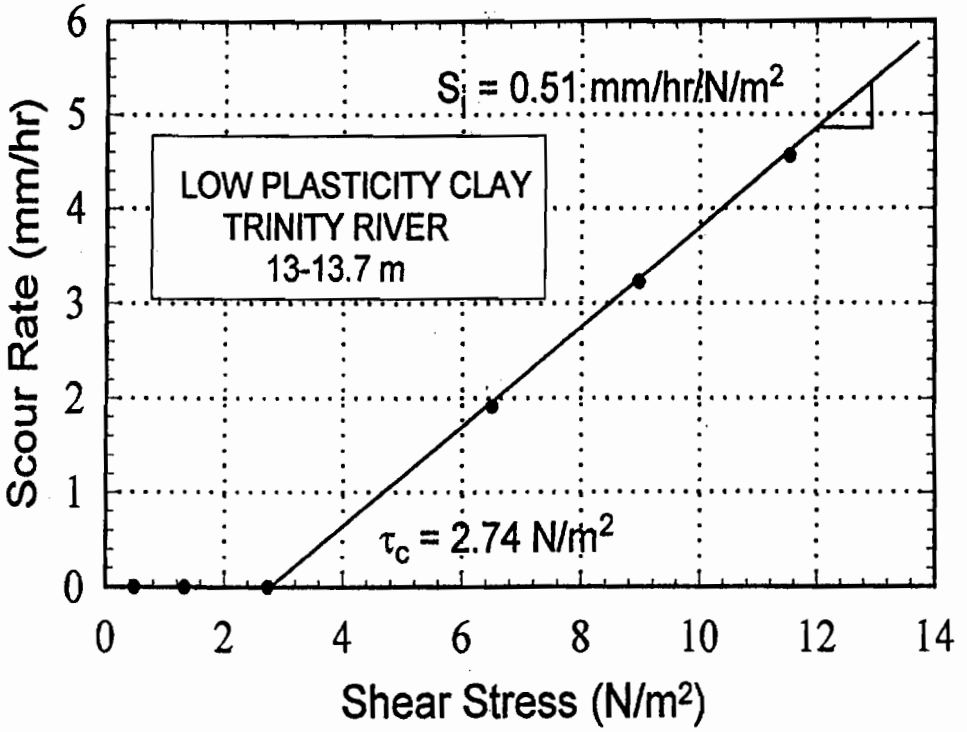

(a)

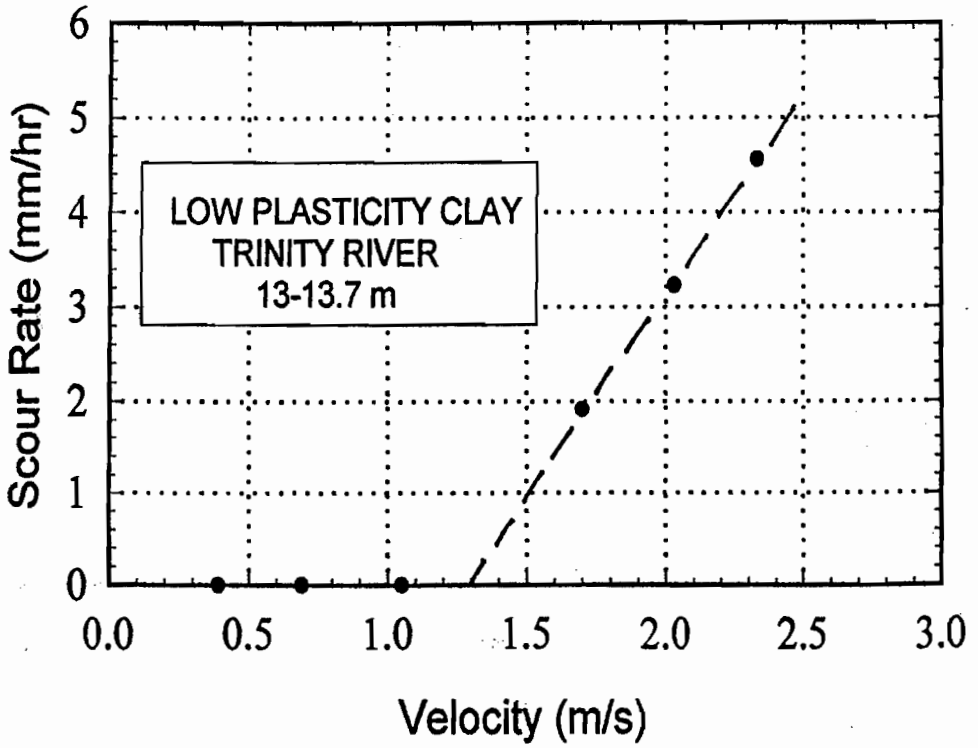

(b)

Figure 30. Erosion Curve for a Low Plasticity Clay (Trinity River).

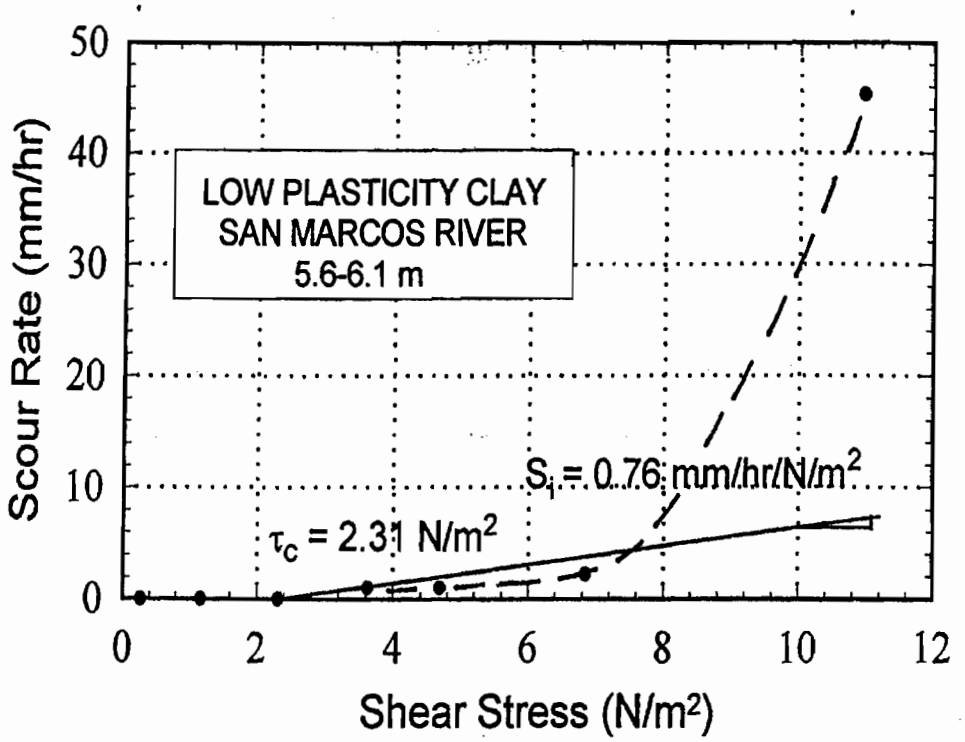

(a)

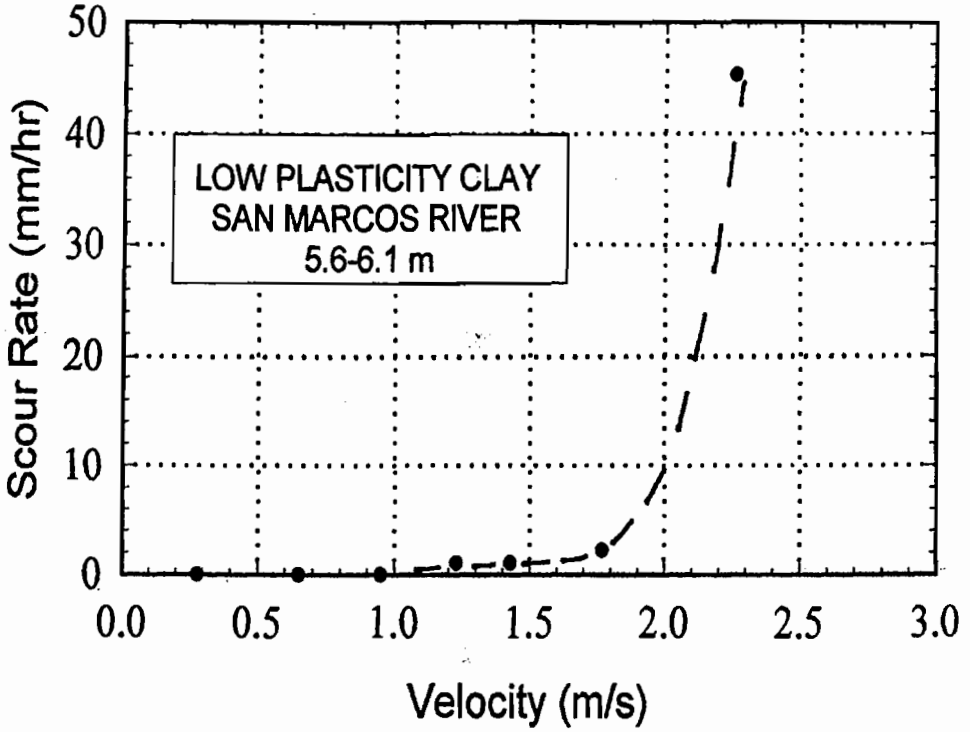

(b)

Figure 31. Erosion Curve for a Low Plasticity Clay (San Marcos River).

of the grains (D_{50}) alone is not a good predictor of τ_c (Fig. 20), and Eq. 17 is not applicable. The reason is that gravity forces no longer control the soil behavior and that other forces such as electromagnetic forces become significant; these forces are rooted in the chemistry of the particle and of the water and lead to many influencing factors for τ_c. In fine-grained soils, the influencing factors for τ_c, according to a literature review (Briaud et al., 1999(a)), include the soil water content (w), the soil unit weight (γ), the soil plasticity (PI), the soil shear strength (s_u), the soil void ratio (e), the soil swell, the soil mean grain size (D_{50}), the soil percent passing the no. 200 sieve (%200), the soil clay mineral, the soil dispersion ratio (DR), the soil cation exchange capacity (CEC), the soil sodium absorption ratio (SAR), the soil pH, the soil temperature (T_s), the water temperature (T_w), and the water chemical composition. Although there are sometimes contradictory findings in the literature, the general trends are as follows; the critical shear stress of fine-grained soils increases when γ increases, PI increases, s_u increases, e decreases, swell decreases, %200 increases, DR decreases, T_s decreases, or T_w decreases. The measured values of τ_c in fine-grained soils reported in the literature vary between 0 and 5 N/m^2. This range is similar to the range for clean sands and gravels.

Beyond the critical shear stress, erodibility is controlled by the erosion rate $\dot{\varepsilon}$. In clean sands and gravels, the value of $\dot{\varepsilon}$ is measured in tens of thousands of mm/hr. For fine-grained soils, the range of measured values with the EFA and with other apparatus as reported in the literature varies from 0.3 mm/hr to 30 mm/hr. Therefore the erosion rate of fine-grained soils is thousands of times slower than the erosion rate of clean coarse-grained soils. According to a literature review (Briaud et al., 1999(a)), the factors influencing the rate of erosion include the hydraulic shear stress applied (τ), the clay content (% clay), the soil temperature (T_s), the water temperature (T_w), the chemical composition of the water, the soil sodium absorption ratio (SAR), the extent of remolding of the soil sample, the soil water content (w), the PI, the unit weight (γ), the undrained shear strength (S_u), the percent passing sieve no. 200 (% 200), and the mean grain size (D_{50}). The same literature review indicates that $\dot{\varepsilon}$ for fine-grained soils increases when percent clay decreases, when τ increases, and when T_s and T_w increase.

In order to investigate the influence of fine-grained soil properties on the erosion function, two erodibility parameters were defined: the critical shear stress τ_c and the initial slope S_i of the $\dot{z}$ versus τ curve after τ_c. This slope S_i and the critical shear stress τ_c are shown on Figs. 28 to 31. A number of natural soils collected at bridge sites have been tested in the EFA to get τ_c and S_i and have also been tested with conventional soil tests. Table 7 shows the soil parameters accumulated. The erodibility parameters τ_c and S_i were plotted against the same soil parameters such as plasticity index (Fig. 32), undrained shear strength (Fig. 33), and percent passing sieve number 200 (Fig. 34). All correlations are very poor; furthermore, the low number of data points precludes any multiple regression attempt. Fig. 35 shows an encouraging relationship between τ_c and S_i. The validity of the correlations is severely limited by the very low number of data points; it is interesting to note however that soils with higher undrained shear strength eroded faster than soils with lower undrained shear strength. This is consistent with the first author's experience in drilling borehole in some strong fine-grained soils that eroded remarkably fast.

The previous discussion has shown that soil properties influence the erodibility of a soil. Therefore it appears logical to think that a correlation exists between erodibility and soil properties. For fine-grained soils, researchers have looked for such a correlation since the early sixties (Moore and Masch, 1962) without success. Indeed today (1999) no such correlation is widely accepted. If a correlation is likely to exist on one hand, and if it has not been found after 40 years of effort on the other hand, the correlation must be complex. It is likely that such a correlation would involve many parameters and that finding the proper multiple regression would involve significant research effort. Since the number of mechanical and chemical soil and water properties involved in the correlation would be large, the amount of testing required to use the correlation would also be large. Furthermore since clean coarse-grained soils and fine-grained soils exhibit such different responses to erosion, different correlations may be necessary with the problem of discontinuity of predictions at the boundary between the two soil types. Considering all the problems associated with correlations, a direct measurement with the EFA is favored.

2.7 EXAMPLE OF USE

The erosion function ($\dot{z}$ versus τ curve) measured in the EFA can be used to predict the evolution of the depth $\dot{z}$ of the scour hole at a bridge pier as a function of time τ. The method has

Table 7. Soil Properties and Scour Parameters for 11 Soils.

Soil Sample	Unit Weight (kN/m^3)	Passing #200 (%)	D_{50} (mm)	Water Content (%)	W_L (%)	PI (%)	US Class.	S_u (kPa)	τ_c (%)	S_I ($mm/hr/N/m^2$)
Navasota River 4.9-5.9 m	18.80	57.70	0.07	26.60	26.42	20.17	CL	32.10	0.78	2.35
Trinity River 13.0-13.7 m	22.10	68.40	0.06	22.22	42.24	33.54	CL	11.48	2.74	0.51
San Marcos River 5.6-6.1 m	18.62	85.00	0.045	21.14	46.43	26.96	CL	17.24	2.31	0.76
San Marcos River 6.1-6.6 m	19.60	78.30	0.052	22.00	41.34	24.67	CL	27.30	0.70	2.50
San Marcos River 7.2-7.6 m	20.20	73.40	0.06	24.40	40.31	21.13	CL	29.67	1.60	1.06
Sim Bayou River 2.3-3.0 m	19.90	99.46	0.0013	20.16	108.36	93.92	CH	120.00	0.46	2.16
Sim Bayou River 3.0-3.7 m	19.60	99.07	0.0012	25.25	84.16	68.11	CH	23.00	2.70	2.67
Sim Bayou River 3.7-4.6 m	19.20	98.77	0.0012	40.11	105.51	89.48	CH	40.00	0.46	3.33
Bedias 756.1-6.9 m	20.04	86.81	0.048	18.07	47.86	34.30	CL	10.00	1.42	4.73
Bedias 90 0.8-1.5 m	19.10	86.77	0.047	17.53	31.55	16.00	CL	44.00	0.18	3.15
Bedias 90 1.5-2.3 m	19.60	91.31	0.04	23.63	55.08	39.29	CH	62.00	0.22	7.59

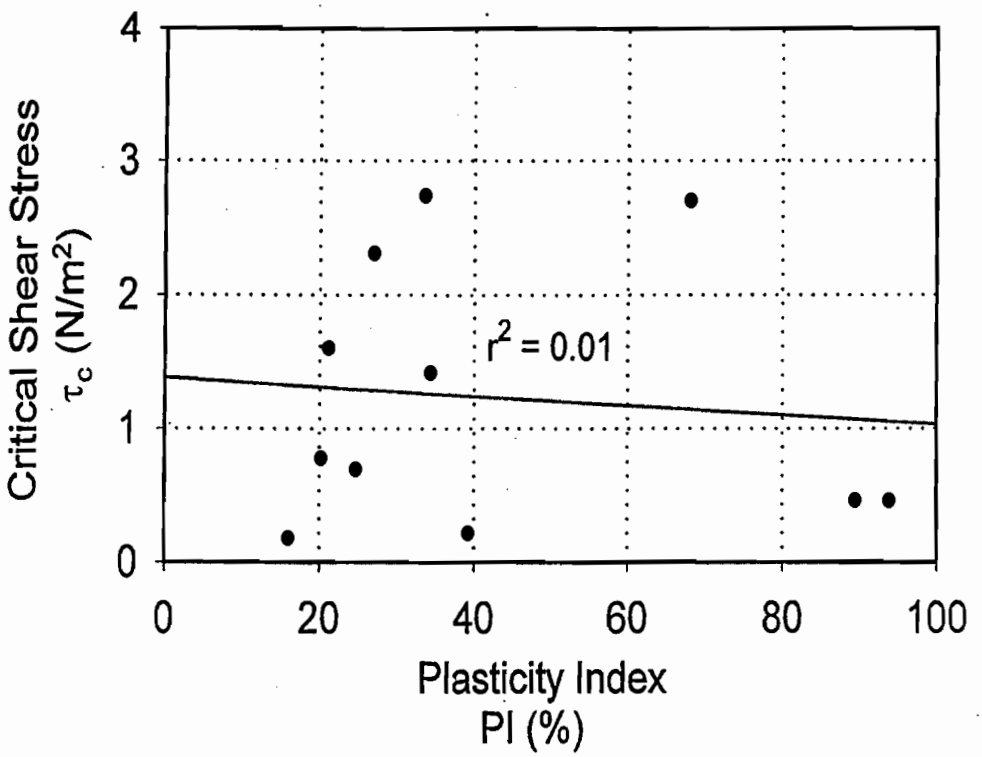

(a)

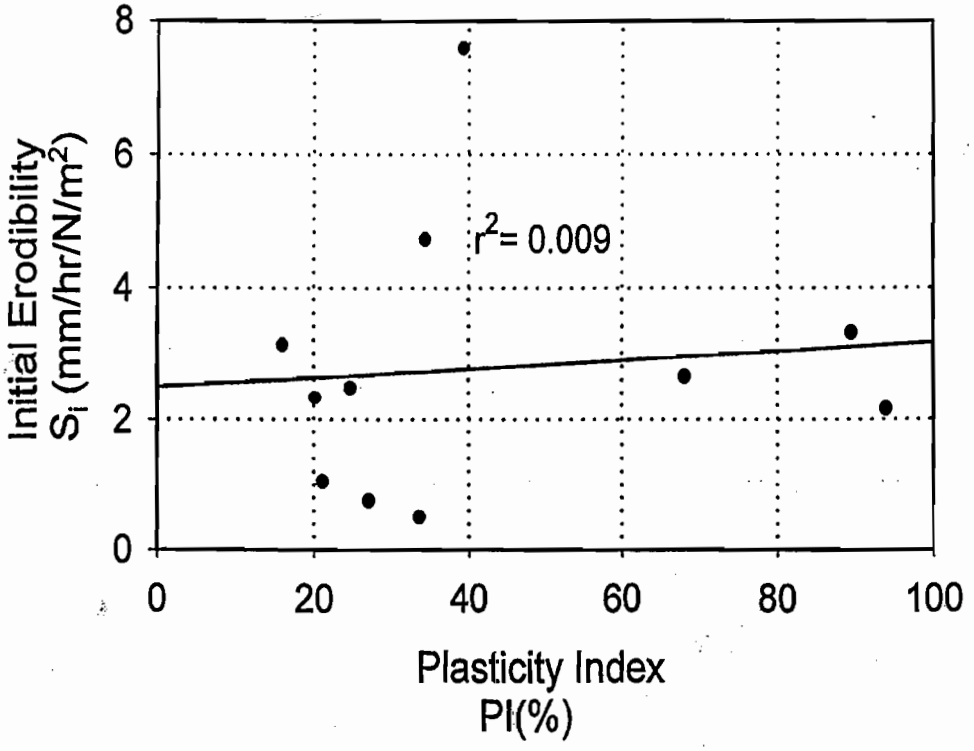

(b)

Figure 32. Correlation between Critical Shear Stress, Initial Erodibility, and Plasticity Index.

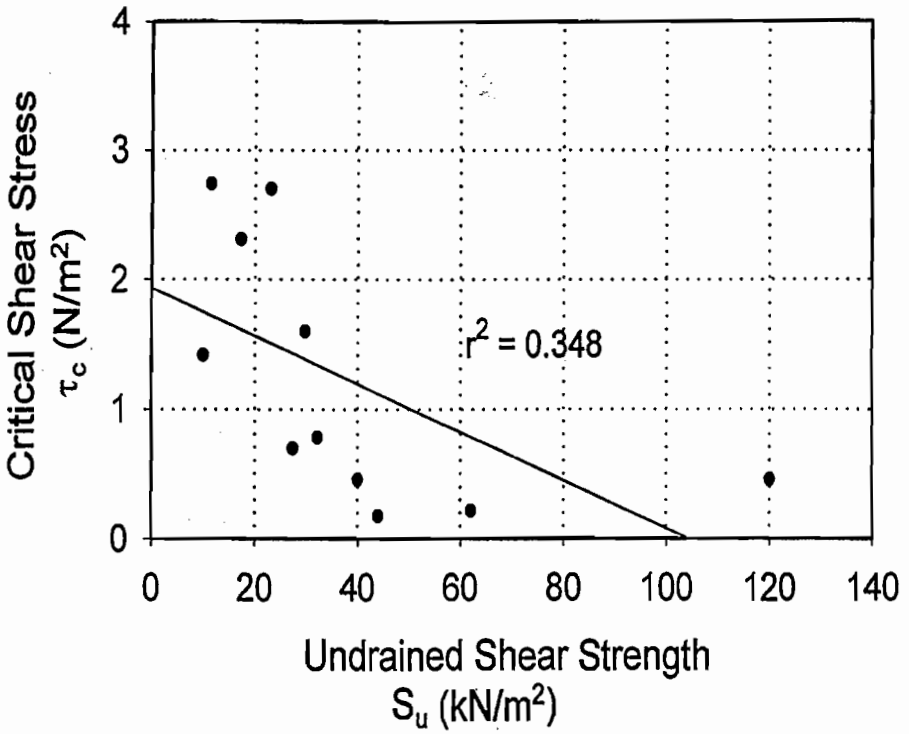

(a)

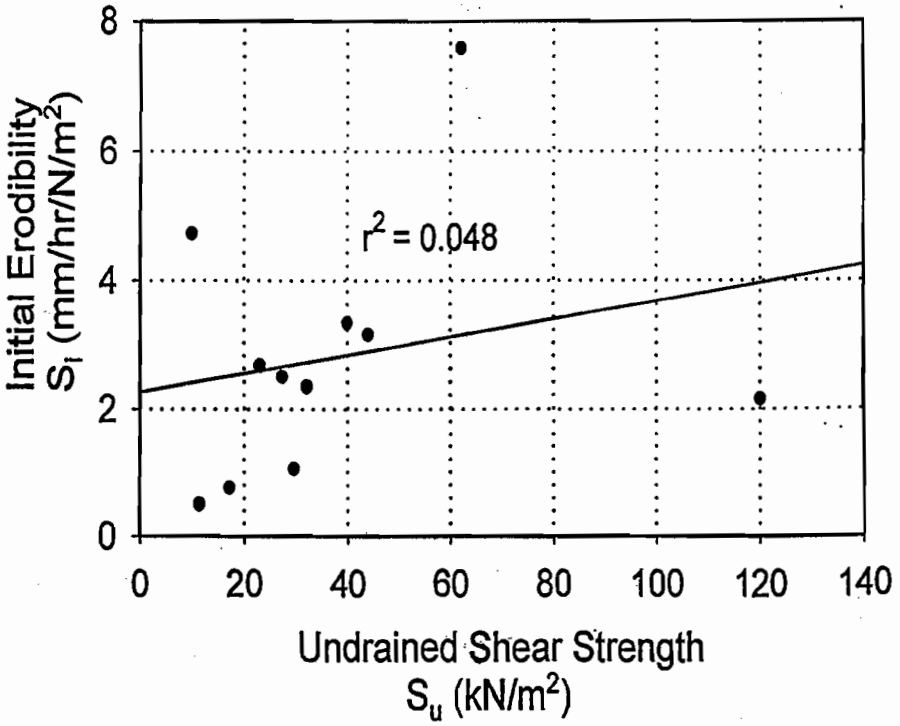

(b)

Figure 33. Correlation between Critical Shear Stress, Initial Erodibility, and Undrained Shear Strength.

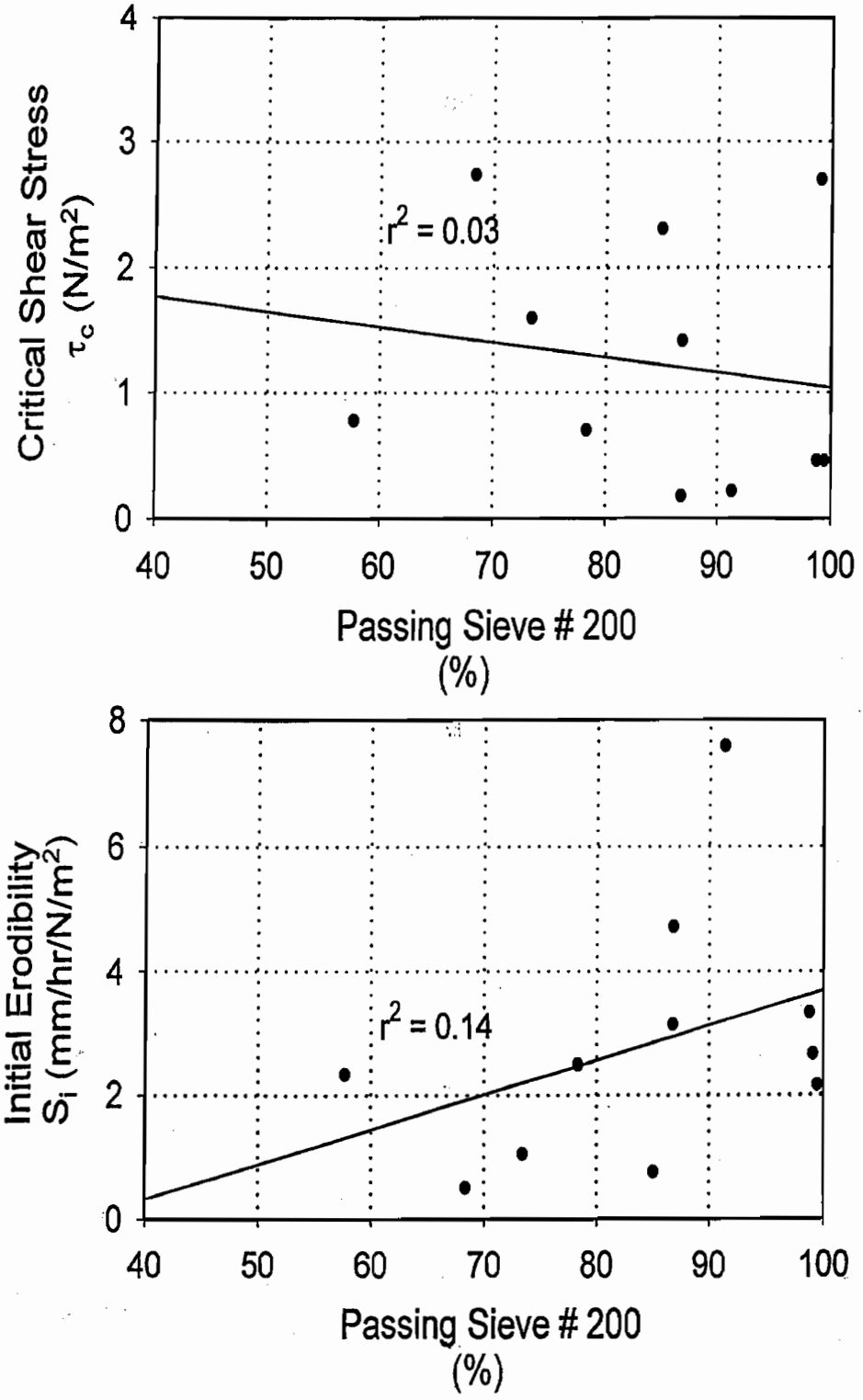

Figure 34. Correlation between Critical Shear Stress, Initial Erodibility, and Percent Passing 200.

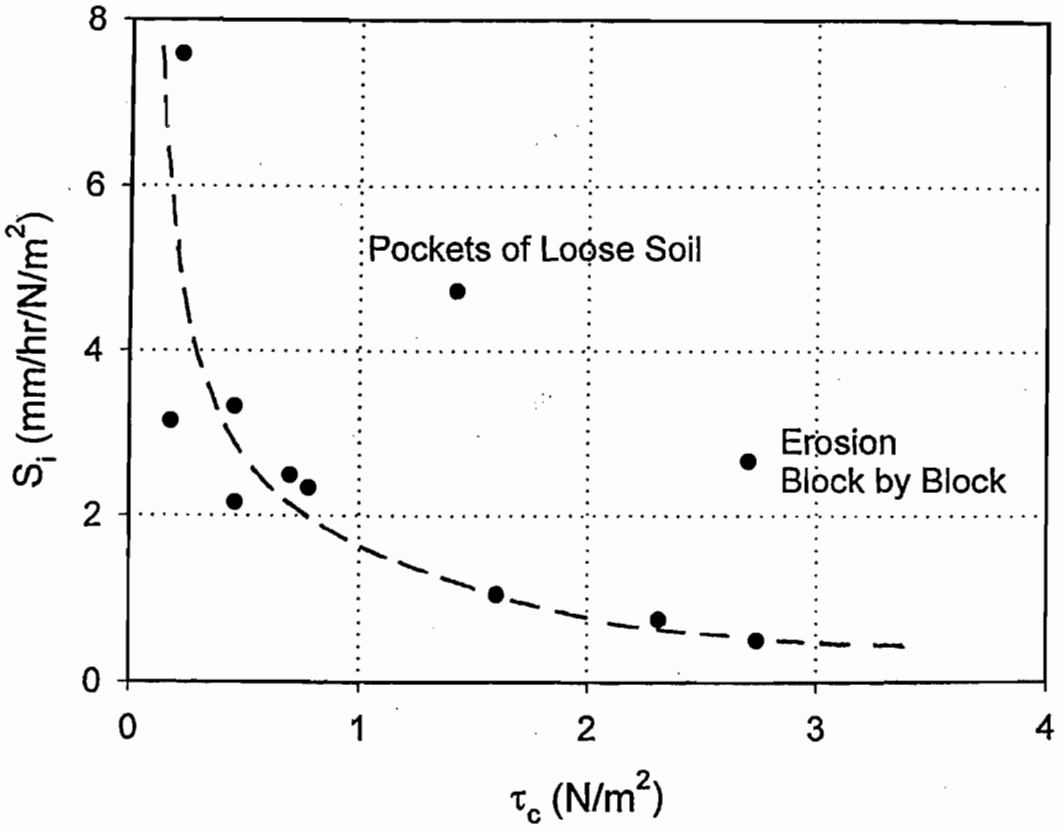

Figure 35. Correlation between Critical Shear Stress and Initial Erodibility.

been described for a constant velocity flow and a uniform soil in Briaud et al. (1999(b)). The process consists of taking soil samples as close as possible to the location of the potential scour holes, running EFA tests to get the $\dot{z}$ versus τ curve, calculating the maximum shear stress τ_{max} around the bridge pier before scour starts, finding the corresponding initial rate of scour $\dot{z}_i$, calculating the maximum depth of scour z_{max}, and using $\dot{z}_i$ and z_{max} as an input to a hyperbolic model describing the scour depth versus time curve. This process was recently extended from a constant velocity to a randomly varying velocity history and from a uniform soil deposit to a randomly layered soil (Kwak et al., 1999). An example of the result for the bent 3 pier of the Navasota River bridge at highway SH7 in Texas is shown on Fig. 36.

2.8 CONCLUSIONS

A new apparatus (EFA) has been developed to measure the erosion function of a soil. This function is the relationship between the erosion rate and the hydraulic shear stress applied.

It gives the critical shear stress corresponding to the initiation of motion and the erosion rate beyond that point. Some correlations are shown between selected erodibility parameters and selected common soil properties for fine-grained soils. This new apparatus is part of a complete procedure to predict the scour depth versus time curve at bridges over water or other erosion processes. An example of use is presented.

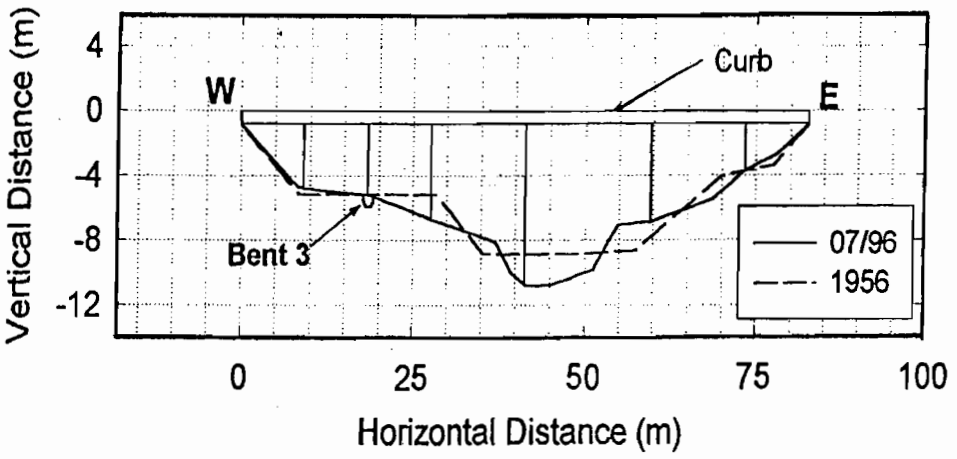

(a)

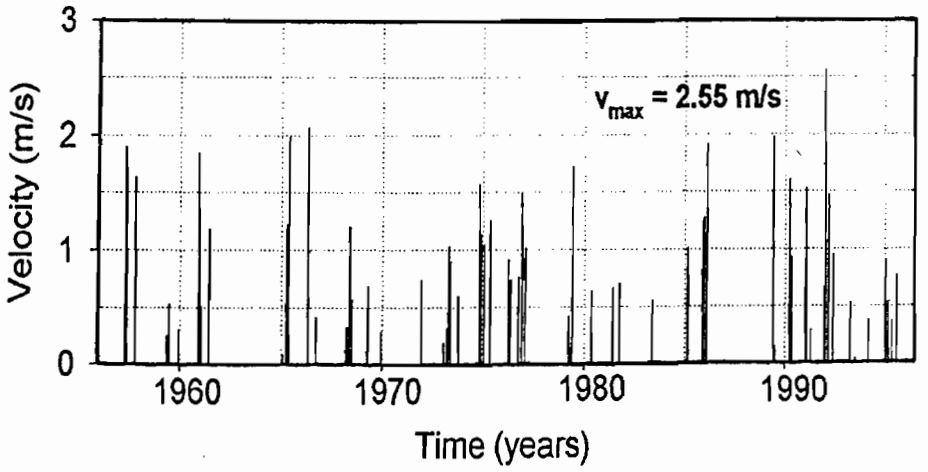

(b)

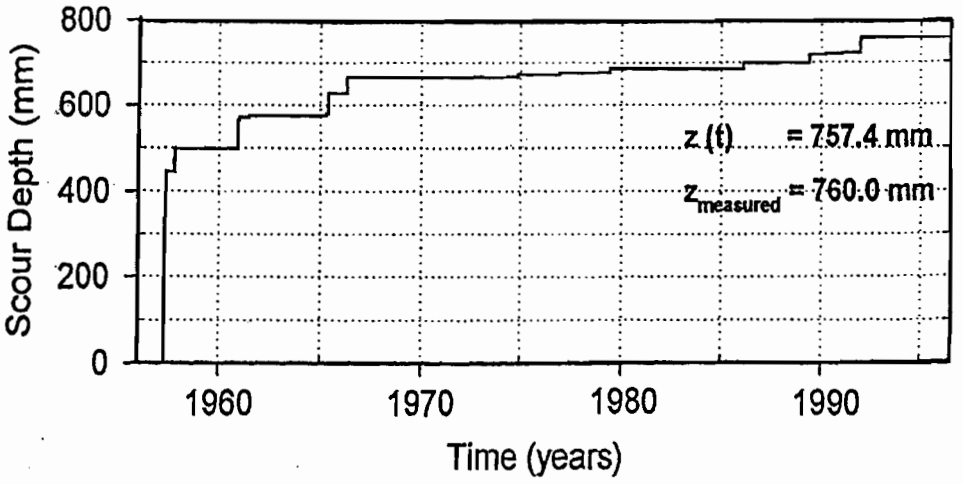

(c)

Figure 36. Example of Use of EFA Results: Navasota River Bridge at Highway SH7.

CHAPTER 3. MULTIFLOOD AND MULTILAYER METHOD FOR SCOUR RATE AT BRIDGE PIERS

3.1 THE SRICOS METHOD

The SRICOS method was proposed in 1999 (Briaud et al., 1999) to predict the scour depth z versus time t curve at a cylindrical bridge pier for a constant velocity flow for a uniform soil and for a water depth larger than two times the pier diameter. It consists of collecting Shelby tube samples near the bridge pier, testing them in the EFA (Erosion Function Apparatus) (Fig. 37) to obtain the erosion rate $\dot{z}$ (mm/hr) versus hydraulic shear stress τ (N/m^2) curve, calculating the maximum hydraulic shear stress τ_{max} around the pier before scour starts, reading the initial erosion rate $\dot{z}_i$ (mm/hr) corresponding to τ_{max} on the $\dot{z}$ versus τ curve, calculating the maximum depth of scour z_{max}, constructing the scour depth z versus time t curve using a hyperbolic model, and reading the scour depth corresponding to the duration of the flood on the z versus t curve.

In the EFA (Briaud et al., 2000), the Shelby tube is placed vertically through a tight fitting hole in the bottom of a pipe with a rectangular cross section. The Shelby tube is kept flush with the bottom of the pipe but the soil sample is pushed out of the Shelby tube by a piston and protrudes 1 mm into the pipe (Fig. 37). Water flows through the pipe at a velocity v and the time t required to erode the 1 mm of soil is recorded. The erosion rate is $\dot{z} = 1/t$ in mm/hr and the hydraulic shear stress τ (N/m^2) imposed by the water on the soil is calculated by using the Moody Chart (Moody, 1944; Briaud et al., 2000):

$$\tau = \frac{1}{8} f \rho v^2 \tag{26}$$

where f is the friction coefficient obtained from the roughness ε/D, ε is the depth of the soil surface asperities taken as $D_{50}/2$, where D_{50} is the soil grain size corresponding to 50 percent passing by weight, D is the hydraulic diameter of the pipe taken as $\frac{4ab}{a+b}$, where a and b are the height and width of the rectangular cross section for the pipe, ρ is the density of water (kg/m^3), and v is the mean flow velocity in the pipe (m/s). The coefficient f is read on the Moody Chart knowing the roughness ε/D and the Reynolds number R_e, which is $\frac{vD}{\upsilon}$ where υ is the water kinematic

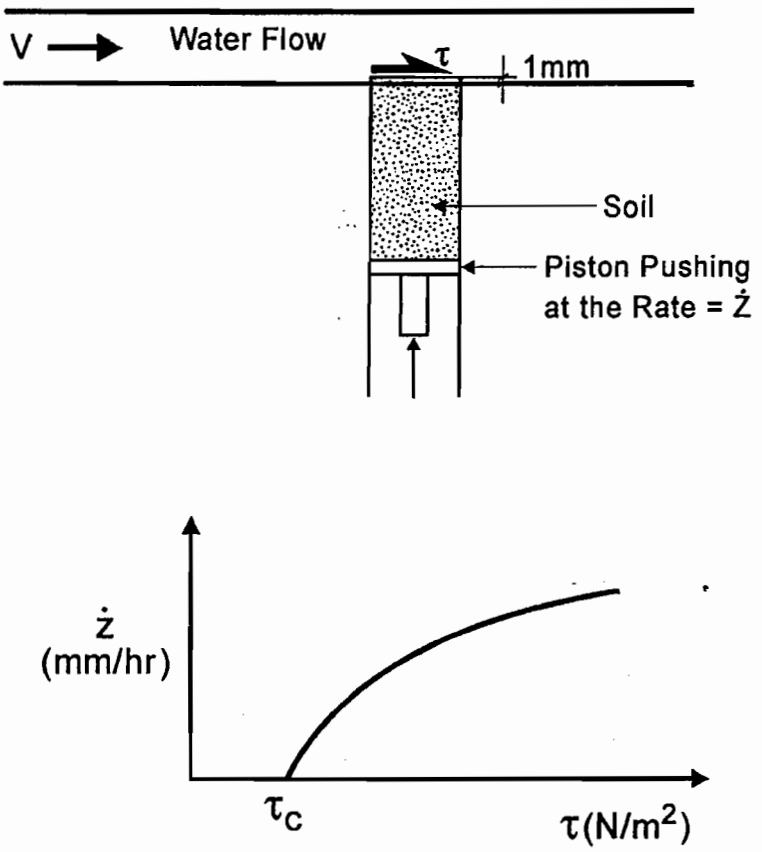

Figure 37. Schematic Diagram and Result of the EFA (Erosion Function Apparatus).

viscosity($10^{-6}\ m^2/s$ at 20∘C). The soil is tested at various velocities and for each velocity a $\dot{z}$ and a τ value are obtained. The complete $\dot{z}$ versus τ curve is obtained in this fashion.

The maximum hydraulic shear stress τ_{max} exerted by the water on the riverbed was obtained by performing a series of three-dimensional numerical simulations of water flowing past a cylindrical pier of diameter B on a flat river bottom and with a large water depth (water depth larger than $2B$). The results of several runs lead to the equation (Briaud et al., 1999):

$$\tau_{max} = 0.094\,\rho\,v^2\left(\frac{1}{\log \mathrm{Re}} - \frac{1}{10}\right) \tag{27}$$

where ρ is the density of water (kg/m³), v is the mean discharge velocity in the river, Re is $\frac{vB}{\upsilon}$ where B is the pier diameter and υ the kinematic viscosity of water $(10^{-6}\ m^2/s \quad at \quad 20^{\circ}C)$. The initial rate of scour $\dot{z}_i$ is read on the $\dot{z}$ versus τ curve from the EFA test at the value of τ_{max}.

The maximum depth of scour z_{max} was obtained by performing a series of model scale flume tests in clay. The results of over 30 experiments lead to the following equation, which was also found to be valid for sand (Briaud et al., 1999):

$$z_{max}(mm) = 0.18\ \mathrm{Re}^{0.635} \tag{28}$$

The equation that describes the shape of the scour depth z versus time t curve is:

$$z = \frac{t}{\frac{1}{\dot{z}_i} + \frac{t}{z_{max}}} \tag{29}$$

where $\dot{z}_i$ and z_{max} have been previously defined. This hyperbolic equation was chosen because it fit well with the curves obtained in the flume tests. Once the duration t of the flood to be simulated is known, the corresponding z value is calculated using Eq. 29 . If $\dot{z}_i$ is large, as it is in clean fine sands, then z is close to z_{max} even for small t values. But if $\dot{z}_i$ is small, as it can be in clays, then z may only be a small fraction of z_{max}. An example of the SRICOS method is shown in Fig. 38.

In the design of the foundation the predicted scour depth z is added to the pile length required to safely carry the foundation load. Assuming that the scour depth will always reach z_{max} during the life of the bridge is uneconomical when the soil scours very slowly. This was the incentive for the development of SRICOS. The method as described in the previous paragraphs is

Problem: *Constant flood velocity = 3 m/s*
Flood duration = 48 hrs
Pier diameter = 2 m
Water depth = 5 m
What is the depth of scour after the flood?

Solution: *SRICOS Method*

1. *Results of EFA tests gave the $\dot{z}$ vs τ curve shown.*
2. *Maximum hydraulic shear stress around the pier is:*

$$\tau_{max} = 0.094\ \rho v^2 \left(\frac{1}{logRe} - \frac{1}{10} \right) = 40\ N/m^2$$

3. *The initial rate of scour $\dot{z}$ is read on the EFA curve at $\tau = \tau_{max}$. $\dot{z}_i = 6$ mm/hr*
4. *The maximum depth of scour z_{max} is:*

$$z_{max} = 0.18\ Re^{0.635} = 3626\ mm$$

5. *The equation for the z(t) curve is:*

$$z = \frac{t}{\frac{1}{\dot{z}_i} + \frac{t}{z_{max}}} = \frac{t(hrs)}{\frac{1}{6} + \frac{t(hrs)}{3626}}$$

6. *Maximum flood lasts 48 hours, therefore $z = 267$ mm or 7.3% of z_{max}*

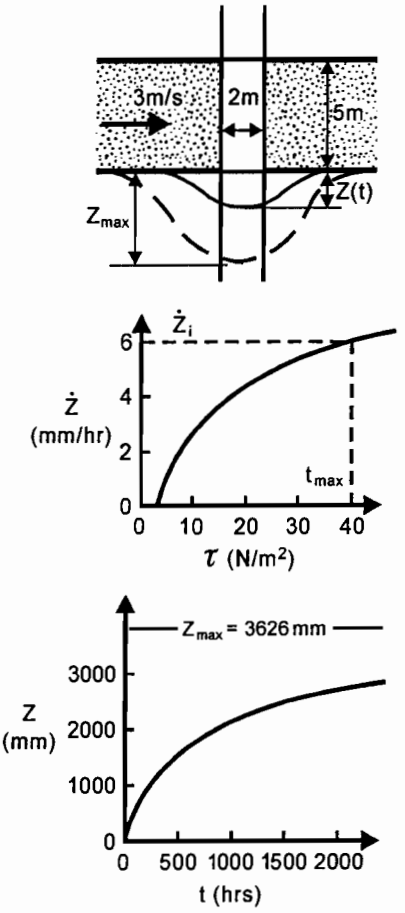

Figure 38. Example of the SRICOS Method.

limited to a constant velocity hydrograph (v = constant), a uniform soil (one $\dot{z}$ versus τ curve), and a relatively deep water depth. In reality, rivers create varying velocity hydrographs and soils are layered. The following describes how SRICOS was extended to include these two features. The case of shallow water flow (water depth over pier diameter < 2) noncircular piers and flow directions different from the pier main axis are not addressed in this article.

3.2 SMALL FLOOD FOLLOWED BY BIG FLOOD

The difference between the constant velocity hydrograph and the true velocity hydrograph is shown on Figures 39a and 39b. In order to investigate the influence of the difference between the two hydrographs on the depth of scour at a bridge pier, the case of a sequence of two different yet constant velocity floods scouring a uniform soil was considered (Fig. 40). Flood 1 has a velocity v_1 and lasts a time t_1 while the subsequent flood 2 has a larger velocity v_2 and lasts a time t_2 . The scour depth z versus time t curve for flood 1 is described by:

$$z = \frac{t}{\frac{1}{\dot{z}_{i1}} + \frac{t}{z_{\max 1}}} \tag{30}$$

For flood 2 the z versus t curve is:

$$z = \frac{t}{\frac{1}{\dot{z}_{i2}} + \frac{t}{z_{\max 2}}} \tag{31}$$

After a time t_1, flood 1 creates a scour depth z_1 given by Eq. 30 (point A on Fig. 40b). This depth z_1 would have been created in a shorter time t_e by flood 2 because v_2 is larger than v_1 (point B on Fig. 40c). This time t_e can be found by setting Eq. 30 with $z = z_1$ and $t = t_1$ equal to Eq. 31 with $z = z_1$ and $t = t_e$.

$$t_e = \frac{t_1}{\frac{\dot{z}_{i2}}{\dot{z}_{i1}} + t_1 \dot{z}_{i2}\left(\frac{1}{z_{\max 1}} - \frac{1}{z_{\max 2}}\right)} \tag{32}$$

When flood 2 starts, even though the scour depth z_1 was due to flood 1 over a time t_1, the situation is equivalent to having had flood 2 for a time t_e. Therefore when flood 2 starts the scour depth

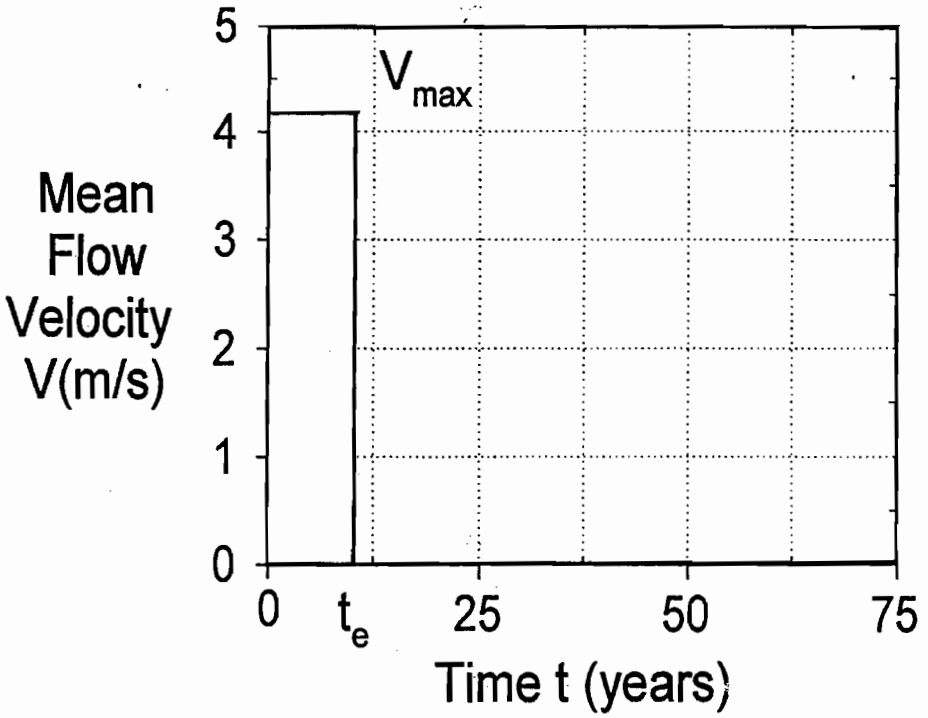

(a)

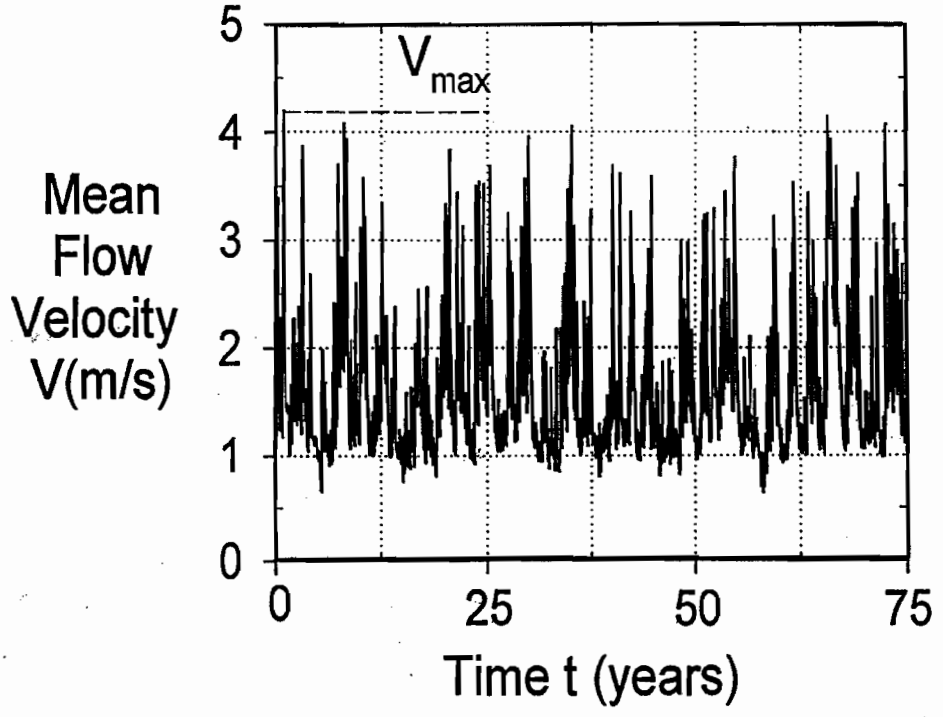

(b)

Figure 39. Velocity Hydrographs: (a) Constant, (b) True Hydrograph.

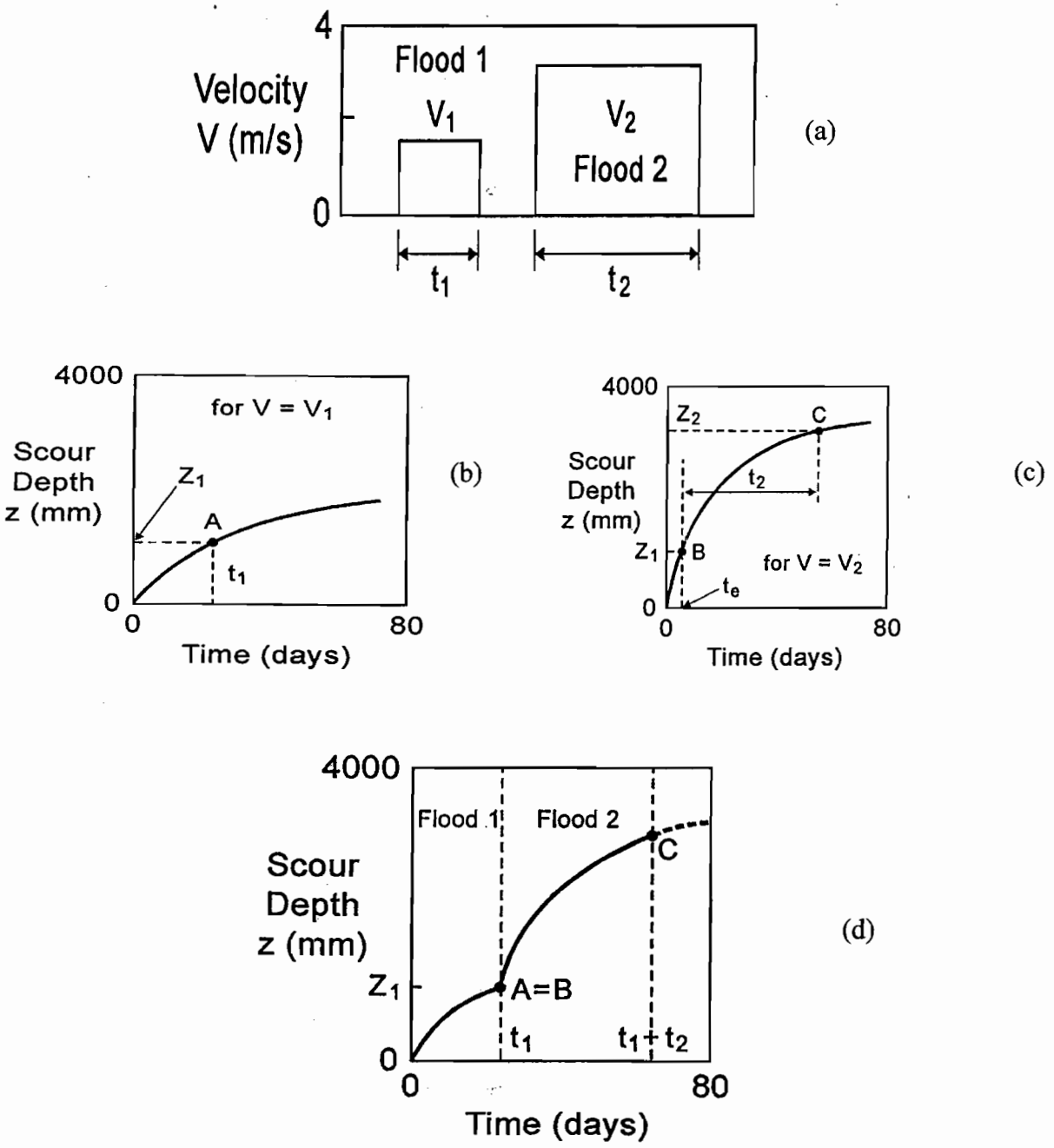

Figure 40. Scour Due to a Sequence of Two Flood Events (Small Flood Followed by Big Flood).

versus time curve proceeds from point B on Fig. 40c until point C after a time t_2. The z versus t curve for the sequence of flood 1 and 2, follows the path OA on the curve for flood 1 then switches to BC on the curve for flood 2. This is shown as the curve OAC on Fig. 40d.

An experiment was conducted to investigate this reasoning. For this experiment, a 25 mm diameter pipe was placed in the middle of a flume. The pipe was pushed through a 150 mm thick deposit of clay made by placing prepared blocks of clay side by side in a tight arrangement. The properties of the clay are listed in Table 8. The water depth was 400 mm and the mean flow velocity was $v_1 = 0.3$ m/s in flood 1 and $v_2 = 0.4$ m/s for flood 2 (Fig. 41a). The first experiment consisted of setting the velocity equal to v_2 for 100 hours and recording the z versus t curve (Fig. 41c). The second experiment consisted of setting the velocity equal to v_1 for 115 hours (Fig. 41b) and then switching to v_2 for 100 hours (Fig. 41d). Also shown on Fig. 41d is the prediction of the portion of the z versus t curve under the velocity v_2 according to the procedure described in Fig. 40. As can be seen, the prediction is very reasonable.

3.3 BIG FLOOD FOLLOWED BY SMALL FLOOD AND GENERAL CASE

Flood 1 has a velocity v_1 and lasts t_1 (Fig. 42a). It is followed by flood 2, which has a velocity v_2 smaller than v_1 and lasts t_2. The scour depth z versus time t curve is given by Eq. 30 for flood 1 and by Eq. 31 for flood 2. After a time t_1, flood 1 creates a scour depth z_1. This depth z_1 is compared with $z_{max\,2}$. If z_1 is larger than $z_{max\,2}$ when flood 2 starts, the scour hole is already larger than it can be with flood 2. Therefore, flood 2 cannot create additional scour and the scour depth versus time curve remains flat during flood 2. If z_1 is smaller than $z_{max\,2}$, then the procedure followed for the case of a small flood followed by a big flood applies and the combined curve is as shown in Fig. 42.

In the general case the velocity hydrograph looks like the one shown in Fig. 39b. The calculations for scour depth are performed by choosing an increment of time Δt and breaking the complete velocity hydrograph into a series of partial flood events each lasting Δt. The first two floods in the hydrograph are handled by using the procedure of Fig. 40 or Fig. 42 depending on the case. Then the process advances by stepping into time and considering a new "flood 2" at each step. The time Δt is typically one day and a velocity hydrograph can be 50 years long. The many

Table 8. Properties of the Porcelain Clay for the Flume Experiment.

1	Liquid Limit, %	34.40
2	Plastic Limit, %	20.25
3	Plasticity Index, %	14.15
4	Specific Gravity	2.61
5	Water Content, %	28.51
6	Mean Diameter D_{50}, (mm)	0.0062
7	Sand Content, %	0.0
8	Silt Content, %	75.00
9	Clay Content, %	25.00
10	Shear Strength, kPa (lab. vane)	12.51
11	CEC, (meq/100 g)	8.30
12	SAR	5.00
13	Ph	6.00
14	Electrical Conductivity, (mmhos/cm)	1.20
15	Unit Weight, (kN/m^3)	18.0

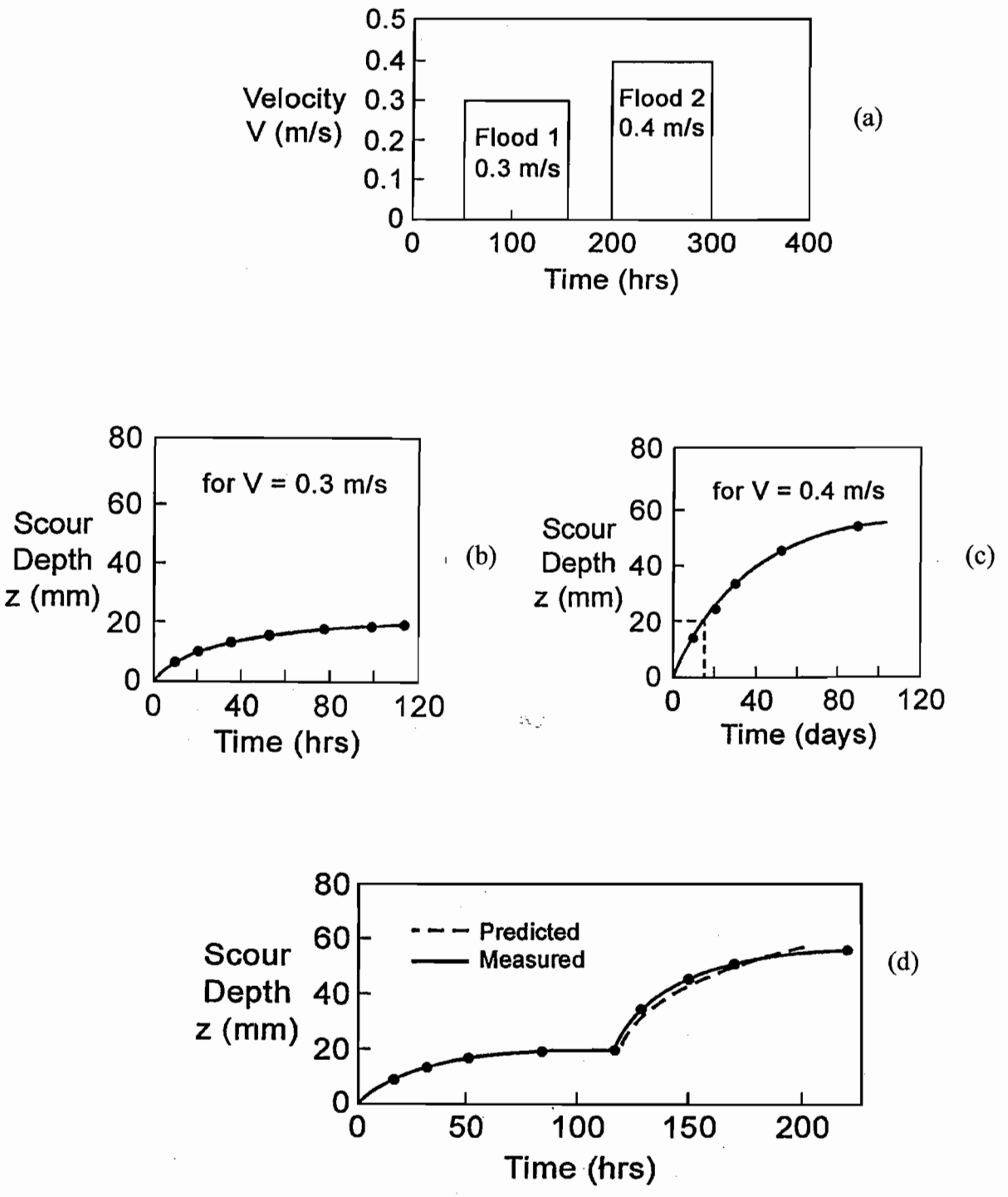

Figure 41. Multiflood Flume Experiment Results.

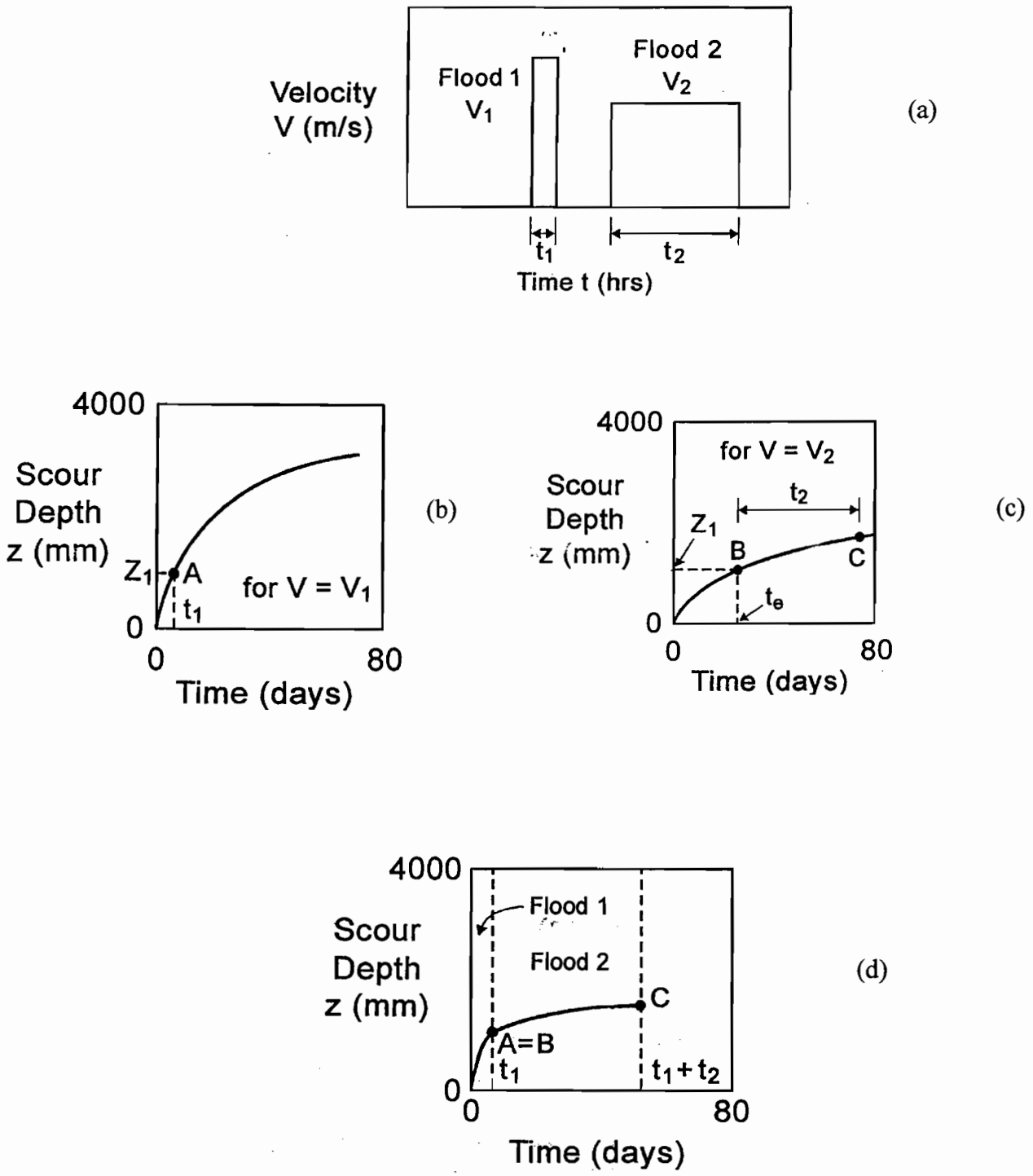

Figure 42. Scour Due to a Sequence of Two Flood Events (Big Flood Followed by Small Flood).

steps of calculations are handled with a computer program called SRICOS. The output of the program is the depth of scour versus time curve over the duration of the velocity hydrograph.

3.4 HARD SOIL LAYER OVER SOFT SOIL LAYER

The original SRICOS method (Briaud et al., 1999) was developed for a uniform soil. In order to investigate the influence of the difference between a uniform soil and a more realistic layered soil on the depth of scour at a bridge pier, the case of a two-layer soil profile scoured by a constant velocity flood was considered (Fig. 43). Layer 1 is hard and Δz_1 thick; layer 2 underlays layer 1 and is softer than layer 1. The scour depth z versus time t curve for layer 1 is given by Eq. 30 (Fig. 43a) and the z versus t curve for layer 2 is given by Eq. 31 (Fig. 43b). If Δz_1 is larger than the maximum depth of scour in layer 1 z_{max1}, then the scour process is contained in layer 1 and does not reach layer 2. If, however, the scour depth reaches Δz_1 (point A on Fig. 43a), layer 2 starts to be eroded. In this case, even though the scour depth Δz_1 was due to the scour of layer 1 over a time t_1 , at that time the situation is equivalent to having had layer 2 scoured over an equivalent time t_e (point B on Fig. 43b). Therefore when layer 2 starts to erode the scour versus depth curve proceeds from point B to point C on Fig. 43b. The combined curve for the two-layer system is OAC on Fig. 43c.

3.5 SOFT SOIL LAYER OVER HARD SOIL LAYER AND GENERAL CASE

Layer 1 is soft and Δz_1 thick; layer 2 underlays layer 1 and is harder than layer 1. The scour depth z versus time t curve for layer 1 is given by Eq. 30 (Fig. 44a) and the z versus t curve for layer 2 is given by Eq. 31 (Fig. 44b). If Δz_1 is larger than the maximum depth of scour in layer 1 z_{max1}, then the scour process is contained in layer 1 and does not reach layer 2. If, however, the scour depth reaches Δz_1 (point A on Fig. 44a) layer 2 starts to erode. In this case, even though the scour depth Δz_1 was due to the scour of layer 1 over a time t_1, at that time the situation is equivalent to having had layer 2 scoured over an equivalent time t_e (Point B on Fig. 44b). Therefore when layer 2 starts to erode the scour versus depth curve proceeds from point B to point C on Fig. 44b. The combined curve for the two-layer system is OAC on Fig. 44c.

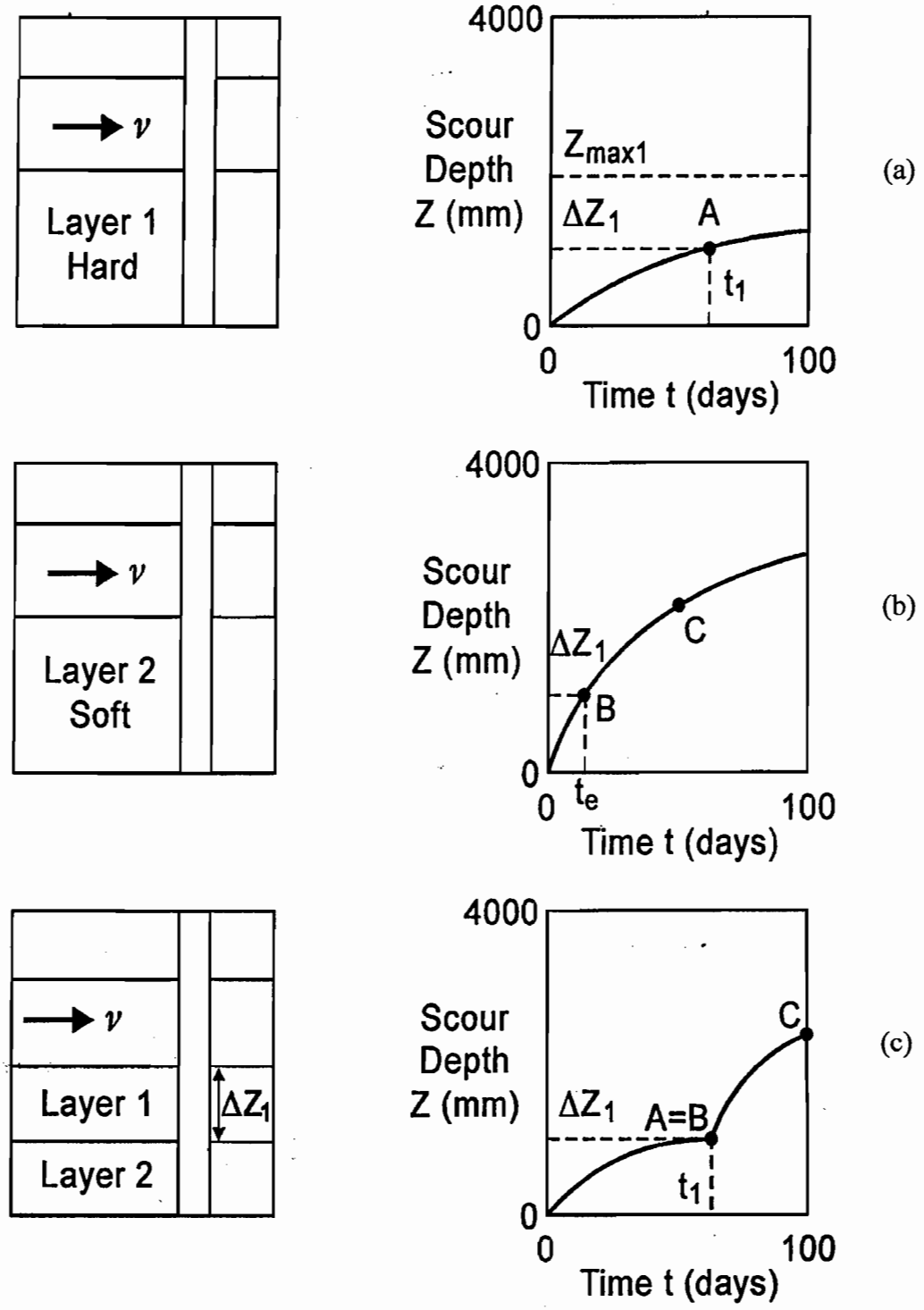

Figure 43. Scour of a Two-Layer Soil (Hard Layer over Soft Layer).

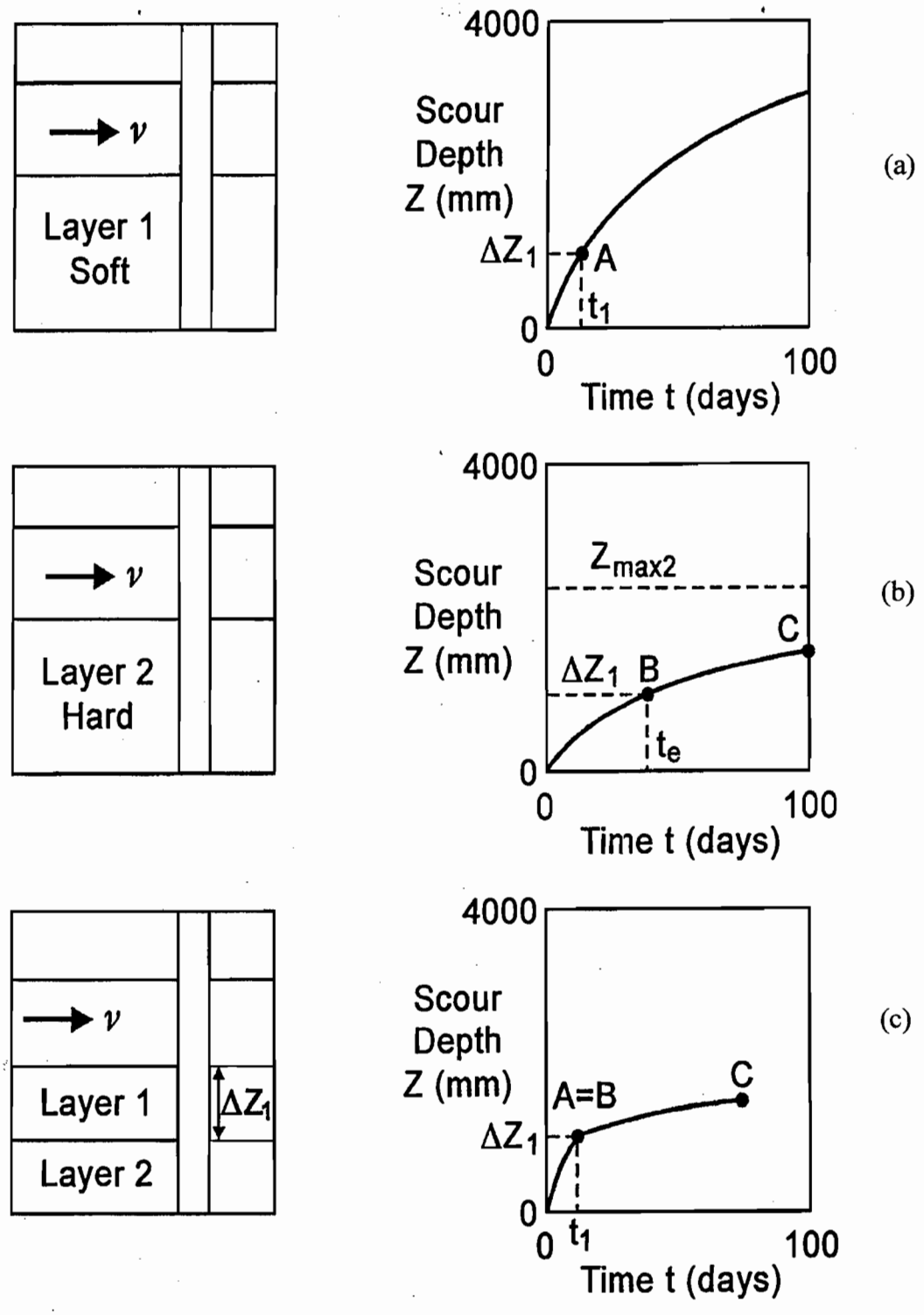

Figure 44. Scour of a Two-Layer Soil (Soft Layer over Hard Layer).

In the general case there may be a series of soil layers with different erosion functions. The computations proceed by stepping forward in time. The time steps are Δt long, the velocity is the one for the corresponding flood event, and the erosion function $(\dot{z}\ vs\ t)$ is the one for the soil layer corresponding to the current scour depth (bottom of the scour hole). When Δt is such that the scour depth proceeds to a new soil layer, the computations follow the process described in Figs. 43 or 44, depending on the case. The calculations are handled by the same SRICOS program as the one mentioned for the velocity hydrograph. The output of the program is the scour depth versus time for the multilayered soil system and for the complete velocity hydrograph.

3.6 EQUIVALENT TIME

The computer program SRICOS is required to predict the scour depth versus time curve as explained in the preceding section. An attempt was made to simplify the method to the point where only hand calculations would be required. The concept of equivalent time was developed for this purpose. By definition the equivalent time t_e is the time required for the maximum velocity in the hydrograph to create the same scour depth as the one created by the complete hydrograph (Fig. 39). The equivalent time t_e was obtained for 55 cases generated from eight bridge sites. For each bridge site soil samples were collected in Shelby tubes and tested in the EFA to obtain the erosion function $\dot{z}$ versus τ; then the hydrograph was collected from the nearest gage station, and the SRICOS program was used to calculate the scour depth. That scour depth was entered in Eq. 29 together with the corresponding $\dot{z}_i$ and $z_{\max}$ to get t_e. The $\dot{z}_i$ value, was obtained from an average $\dot{z}$ versus τ curve within the final scour depth by reading the $\dot{z}$ value which corresponded to $\tau_{\max}$ obtained from Eq. 27. In Eq. 27 the pier diameter B and the maximum velocity $v_{\max}$ found to exist in the hydrograph over the period considered were used. The $z_{\max}$ value was obtained from Eq. 28 while using B and $v_{\max}$ for the pier Reynolds number. The hydrograph at each bridge was also divided in shorter period hydrographs and for each period an equivalent time t_e was calculated. This generated the 55 cases listed in Table 9.

The equivalent time was then correlated to the duration of the hydrograph t_{hydro}, the maximum velocity in the hydrograph $v_{\max}$, and the initial erosion rate $\dot{z}_i$. These quantities are listed in Table 9. A multiple regression on that data gave the following relationship.

Table 9. Equivalent Time t_c and Selected Parameters.

Bridge	$t_{hyd.}$ (years)	v_{max} (m/s)	$\dot{z}_{i,mean}$ (mm/hr)	t_e (hr)
Navasota, Bent 3	5	1.90	8.91	165.40
	10	1.98	8.91	214.08
	15	2.06	8.91	243.60
	20	2.06	8.91	251.02
	25	2.06	8.91	267.66
	30	2.06	8.91	267.93
	35	2.06	8.91	322.35
	41	2.54	8.91	274.05
Navasota, Bent 5	5	3.16	22.39	125.99
	10	3.24	22.39	333.94
	15	3.31	22.39	442.69
	20	3.31	22.39	448.07
	25	3.31	22.39	468.58
	30	3.31	22.39	468.58
	35	3.31	22.39	596.67
	41	3.82	22.39	427.89
Brazos, Bent 3	5	4.20	65.26	540.97
	10	4.20	65.26	543.37
	15	4.20	65.26	595.91
	20	4.20	65.26	595.91
	25	4.20	65.26	595.91
	33	4.20	65.26	812.01
San Jacinto, Bent 43	5	1.73	17.44	271.86
	10	3.07	17.44	196.25
Trinity, Bent 3	5	1.40	50.60	137.74
	10	1.40	50.60	146.29
	15	2.00	50.60	280.21
	17	2.00	50.60	292.96
Trinity, Bent 4	5	3.22	39.82	257.28
	10	3.22	39.82	309.94
	15	4.06	39.82	311.18
	17	4.06	39.82	368.93
San Marcos, Bent 9	5	1.12	61.75	25.42
	10	1.12	61.75	25.78
	15	1.50	61.75	39.97
	20	1.50	61.75	43.47
	25	1.50	61.75	44.84
	30	1.50	61.75	46.55
	35	1.50	61.75	49.85
	40	1.50	61.75	51.66
Sims, Bent 3	3	0.95	2.69	152.84
Bedias 75, Bent 26	5	2.15	127.44	103.53
	10	2.17	127.44	143.49
	15	2.17	127.44	161.32
	20	2.17	127.44	188.14
	25	2.17	127.44	224.44
	30	2.17	127.44	263.28
	35	2.17	127.44	263.28
	40	2.17	127.44	281.80
	45	2.19	127.44	289.03
	20	2.19	127.44	289.03
Bedias 90, Bent 6	5	1.36	44.25	65.36
	10	1.37	44.25	109.04
	15	1.54	44.25	103.68
	18	1.54	44.25	104.26

$$t_e(hrs) = 73\left(t_{hydro}(years)\right)^{0.126}\left(v_{\max}(m/s)\right)^{1.706}\left(\dot{z}_i(mm/hr)\right)^{-0.20} \quad (29)$$

This time t_e can then be used in Eq. 29 to calculate the scour at the end of the hydrograph. A comparison between the scour depth predicted by the Extended-SRICOS method using the complete hydrograph and the Simple SRICOS method using the equivalent time is shown on Fig. 45.

3.7 EXTENDED SRICOS METHOD AND SIMPLE SRICOS METHOD

For final design purposes the Extended SRICOS method (E-SRICOS) is used to predict the scour depth z versus time t over the duration of the design hydrograph. The method proceeds as follows:

1. Calculate the maximum depth of scour $z_{\max}$ for the design velocity by using Eq. 28.
2. Collect samples at the site within the depth $z_{\max}$.
3. Test the samples in the EFA to obtain the erosion functions ($\dot{z}$ versus τ) for the layers involved.
4. Prepare the flow hydrograph for the bridge. This step may consist in downloading the discharge hydrograph from a USGS (United States Geological Survey) gage station near the bridge (Fig. 46). These discharge hydrographs can be found on the Internet at the USGS web site (www.usgs.gov). The discharge hydrograph then needs to be transformed into a velocity hydrograph (Figs. 47, 48, and 49). This transformation is performed by using a program such as HEC-RAS (1997), which makes use of the transversed river bottom profile at the bridge site to link the discharge Q (m^3/s) to the velocity v(m/s) at the anticipated location of the bridge pier.
5. Use the SRICOS program (Kwak et al., 1999) with the following input: the $\dot{z}$ versus τ curves for the various layers involved, the velocity hydrograph v versus t, the pier diameter B, the viscosity of the water υ (typically 10^{-6} m^2/s at 20° C), the density of the water ρ_w (1000 kg/m^3). Note that the water depth y is not an input because at this time the solution is limited to a "deep water" condition. This condition is realized when $y \geq 1.5B$; indeed, beyond this water depth the scour

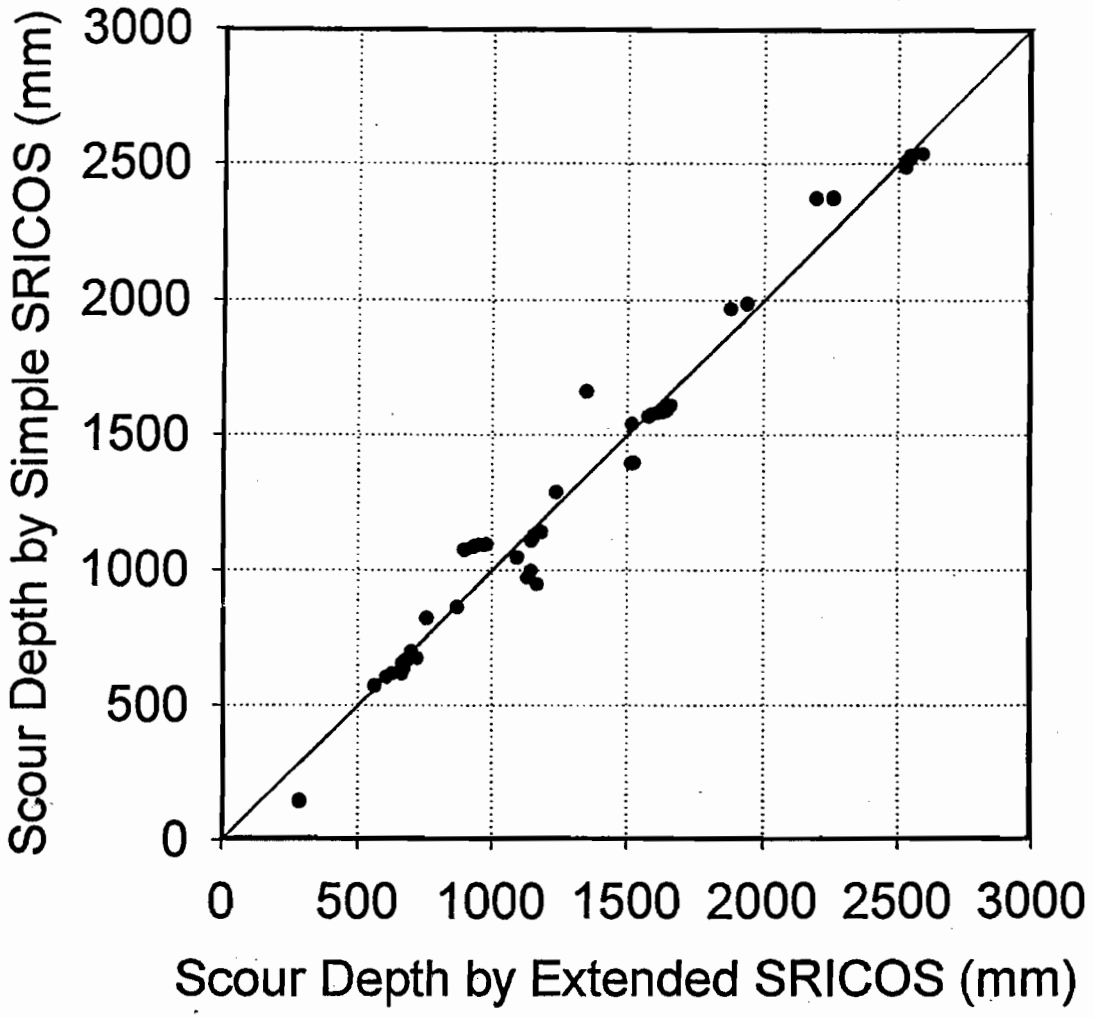

Figure 45. Comparison of Scour Depth Using Extended SRICOS and Simple SRICOS Methods.

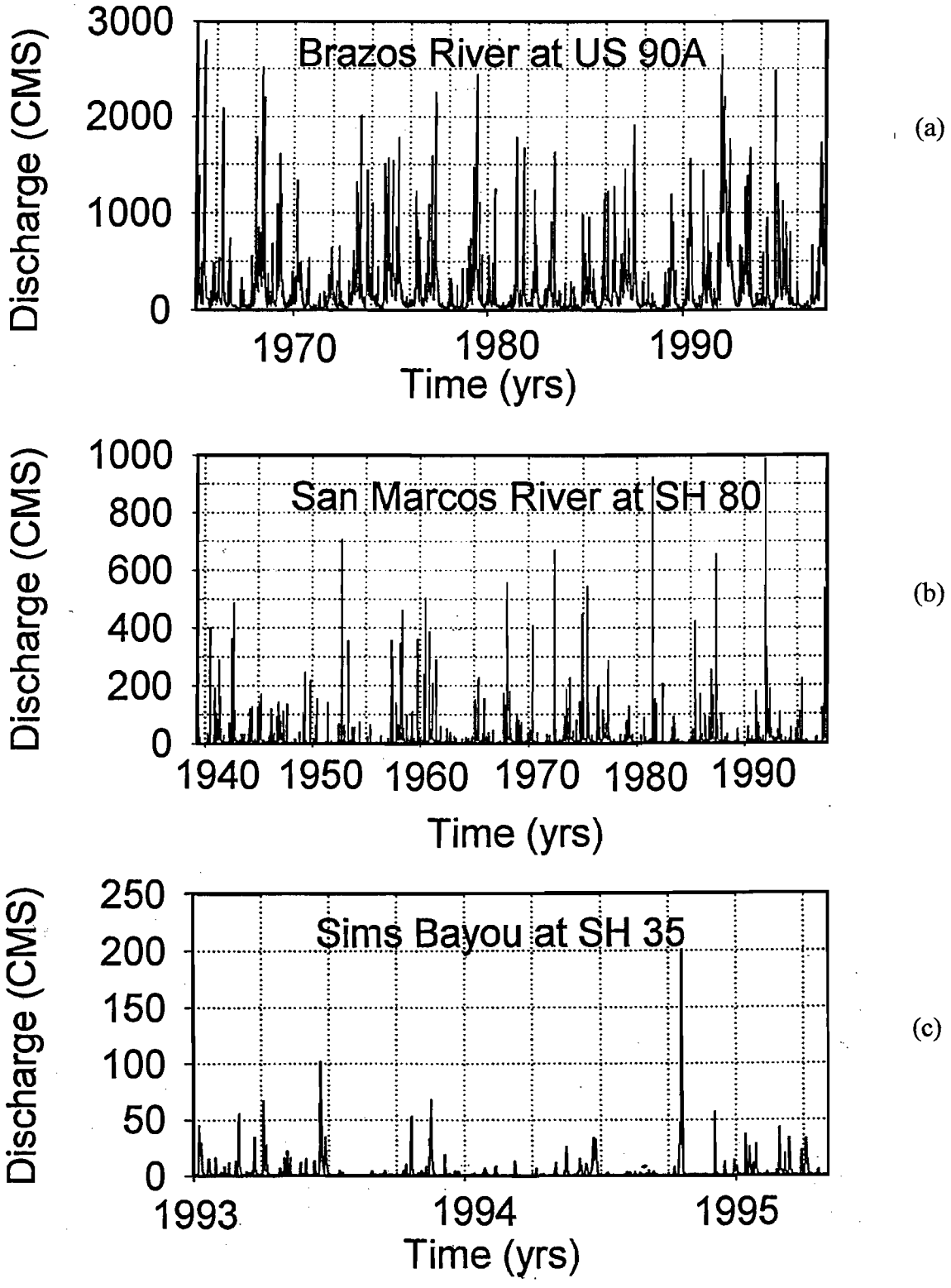

Figure 46. Examples of Discharge Hydrographs: (a) Brazos River at US90A, (b) San Marcos River at SH80, (c) Sims Bayou at SH35.

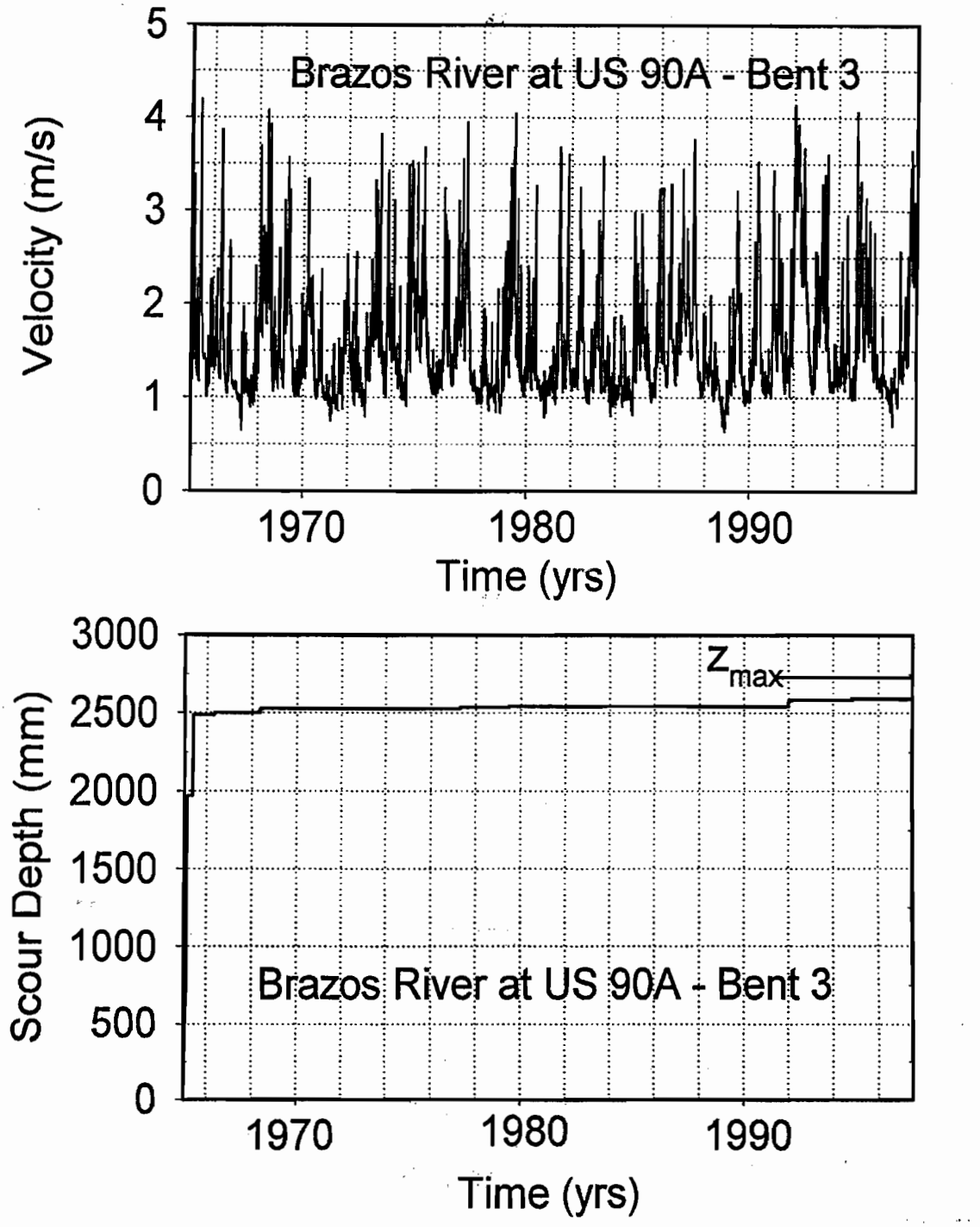

Figure 47. Velocity Hydrograph and Scour Depth versus Time Curve for Bent 3 of the Brazos River Bridge at US90A.

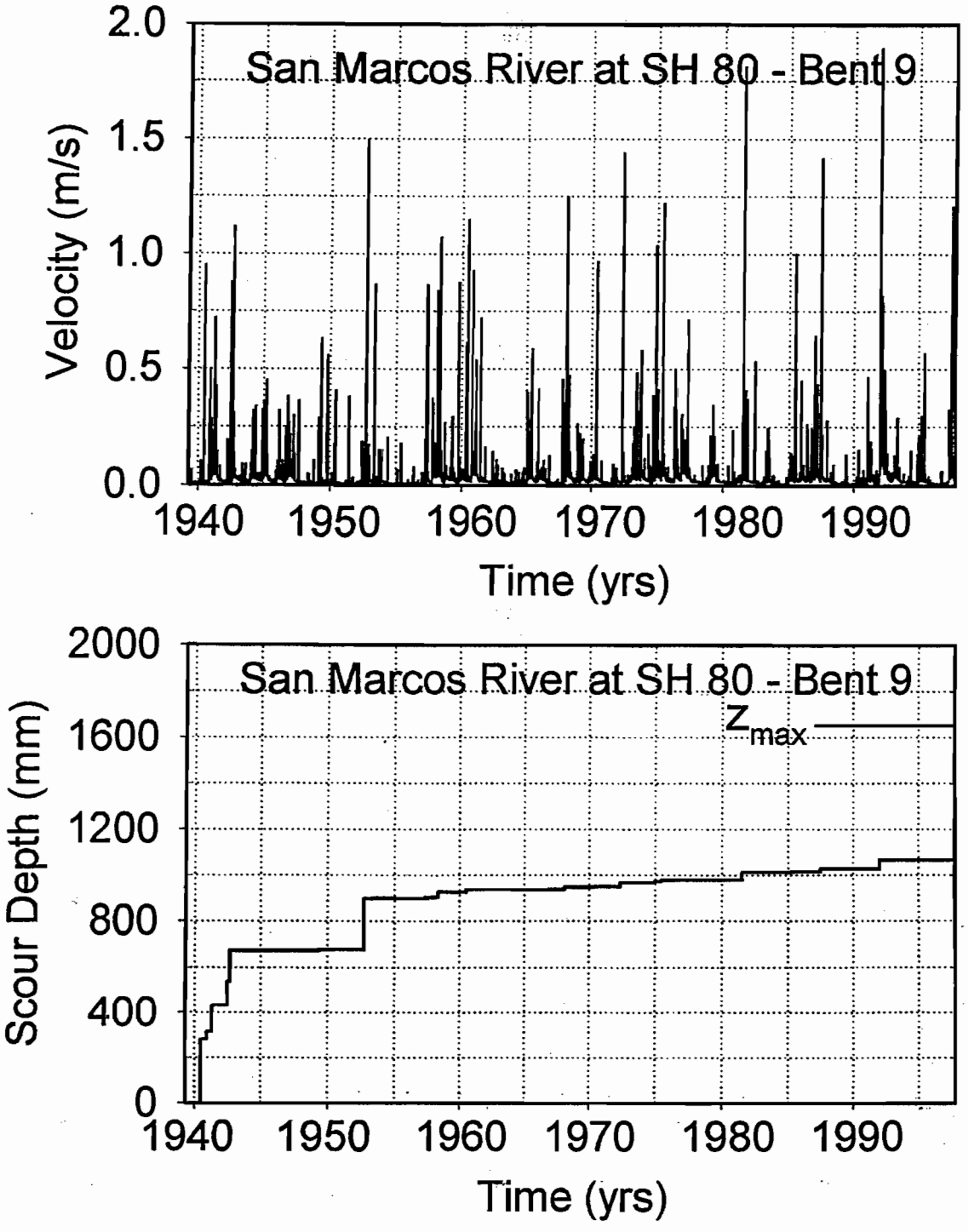

Figure 48. Velocity Hydrograph and Scour Depth versus Time Curve for Bent 3 of the San Marcos River Bridge at SH80.

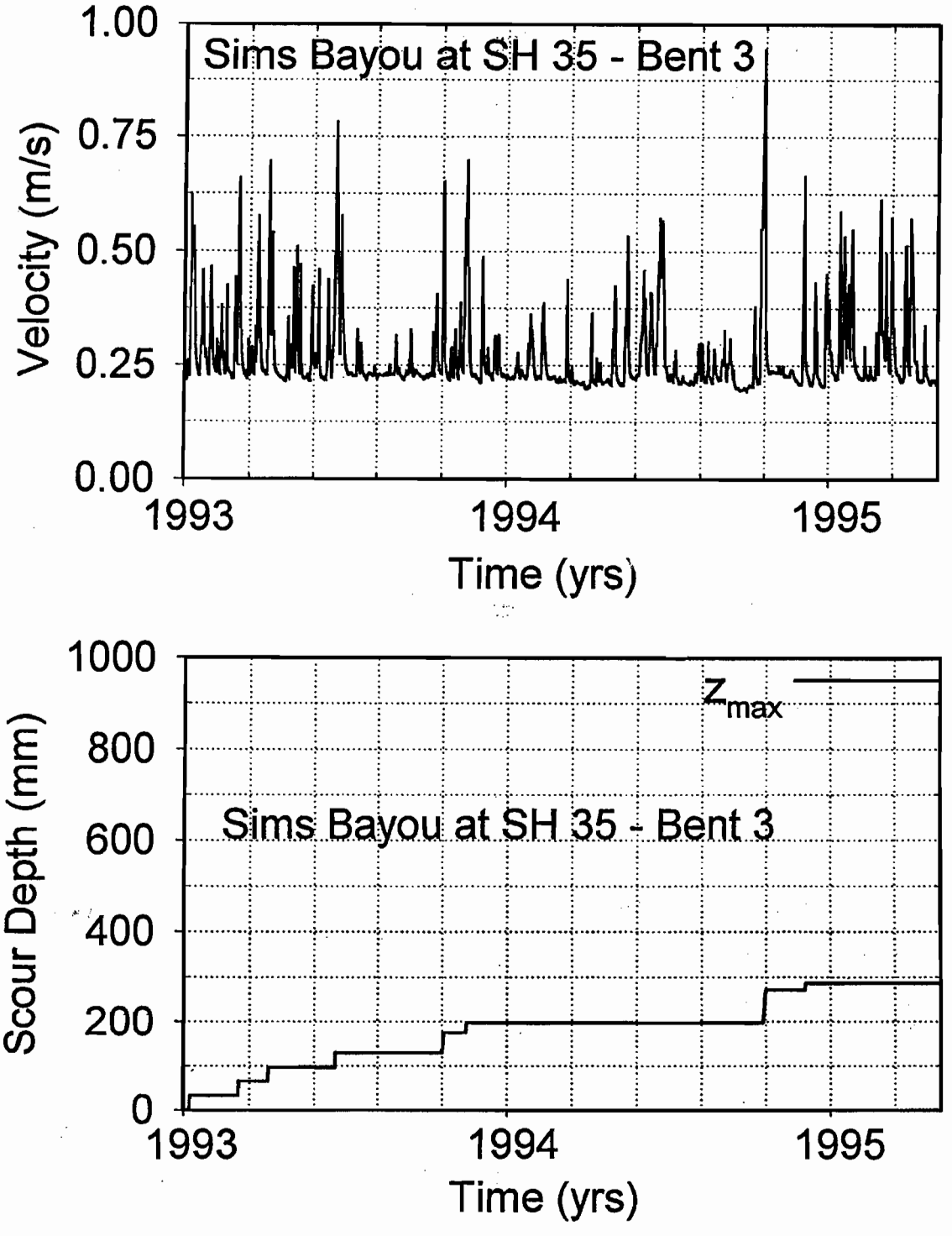

Figure 49. Velocity Hydrograph and Scour Depth versus Time Curve for Bent 3 of the Sims Bayou River Bridge at SH35.

depth becomes independent of the water depth (Melville and Coleman, 1999, p. 197).

6. The SRICOS program steps into time by making use of the original SRICOS method and accumulation algorithms described in Figs. 40, 42, 43, and 44. The usual time step Δt is one day because that is the usual reading frequency of the USGS gages. The duration of the hydrograph can vary from a few days to over 100 years.
7. The output of the program is the depth of scour versus time over the period covered by the hydrograph (Figures 47, 48, and 49).

For predicting the future development of a scour hole at a bridge pier over a design life t_{life}, one can either develop a synthetic hydrograph much like is done in the case of earthquakes or assume that the hydrograph recorded over the last period equal to t_{life} will repeat itself. The time required to perform step 3 is about 8 hours per Shelby tube sample because it takes about 8 points to properly describe the erosion function ($\dot{z}$ versus τ curve) and for each point the water is kept flowing for 1 hour to get a good average $\dot{z}$ value. The time required to perform all other steps, except for step 2, is about 4 hours for someone with experience. In order to reduce these 4 hours to a few minutes a simplified version of SRICOS called S-SRICOS was developed. One must understand that this simplified version is only recommended for preliminary design purposes. If S-SRICOS shows clearly that there is no need for refinement then there is no need for E-SRICOS; if not, one must perform an E-SRICOS analysis.

For preliminary design purposes, the simple SRICOS method (S-SRICOS) can be used. The method proceeds as follows:

1. Calculate the maximum depth of scour z_{max} for the design velocity v_{max} by using Eq. 28. The design velocity is usually the one corresponding to the 100 year flood or the 500 year flood.
2. Collect samples at the site within the depth z_{max}.
3. Test the samples in the EFA to obtain the erosion function ($\dot{z}$ versus τ) for the layers involved.
4. Create a single equivalent erosion function by averaging the erosion functions within the anticipated depth of scour.

5. Calculate the maximum shear stress τ_{max} around the pier before scour starts by using Eq. 27. In Eq. 27 use the pier diameter B and the design velocity v_{max}.

6. Read the erosion rate $\dot{z}_i$ corresponding to τ_{max} on the equivalent erosion function.

7. Calculate the equivalent time t_e for a given design life of the bridge t_{hydro}, for the design velocity v_{max}, and for the $\dot{z}_i$ value of step 6 by using Eq. 33.

8. Knowing t_e, $\dot{z}_i$, and z_{max} calculate the scour depth z at the end of the design life by using Eq. 29 .

An example of such calculations is shown in Fig. 50.

3.8 CASE HISTORIES

In order to evaluate the E-SRICOS and S-SRICOS methods, and after consulting many Texas DOT engineers, after studying many Texas DOT files, and after visiting many bridge sites eight bridges were selected (Table 10). These bridges all satisfied the following requirements: the predominant soil type was fine-grained soils according to existing borings, the river bottom profiles were measured at two dates separated by at least several years, these river bottom profiles indicated anywhere from 0.05 m to 4.57 m of scour, a USGS gaging station existed near the bridge, and drilling access was relatively easy. The bridge locations are shown in Fig. 51.

The Navasota River bridge at SH7 was built in 1956. The main channel bridge has an overall length of 82.8 m and consists of three continuous steel girder main spans with four concrete pan girder approach spans. The foundation type is steel piling down to 5.5 m below the channelbed, which consists of silty and sandy clay down to the bottom of the piling according to existing borings. Between 1956 and 1996 the peak flood took place in 1992 and generated a measured flow of 1600 m^3/s which corresponded to a HEC-RAS calculated mean approach flow velocity of 3.9 *m/s* at bent 5 and 2.6 *m/s* at bent 3. The pier at bent 3 was square with a side equal to 0.36 m while the pier at bent 5 was 0.36 m wide, 8.53 m long, and had a square nose. The angle between the flow direction and the pier main axis was 5° for bent 5. River bottom profiles exist for 1956 and 1996 and show 0.76 m of local scour at bent 3 and 1.8 m of total scour at bent 5. At bent 5 the total scour was made up of 1.41 m of local scour and 0.39 m of contraction scour as explained later.

Problem: *Maximum flood velocity = 3 m/s*
Bridge design life = 75 years
Pier diameter = 2 m
Water depth = 5 m
What is the depth of scour after 75 years?

Solution: *S-SRICOS Method*

1. *Results of EFA tests gave the $\dot{z}$ vs τ curve shown.*
2. *Maximum hydraulic shear stress around the pier is:*

$$\tau_{max} = 0.094\ \rho v^2 \left(\frac{1}{logRe} - \frac{1}{10} \right) = 40\ N/m^2$$

3. *The initial rate of scour $\dot{z}_i$ is read on the EFA curve at $\tau = \tau_{max}$. $\dot{z}_i = 6$ mm/hr*
4. *The maximum depth of scour z_{max} is*

$$z_{max} = 0.18\ Re^{0.635} = 3626\ mm$$

5. *Equivalent time*

$$t_e = 73 \left(t_{hydro}\right)^{0.126} \left(v_{max}\right)^{1.706} \left(\dot{z}_i\right)^{-0.2} = 573\ hrs$$

6. *The equation for the $z(t)$ curve is*

$$z = \frac{t}{\frac{1}{\dot{z}_i} + \frac{t}{z_{max}}} = 1765\ mm \text{ after } 75 \text{ years}$$

$z_{75\ years}$ *is 49% of* z_{max}

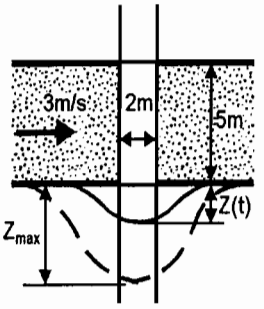

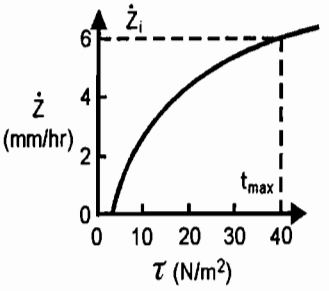

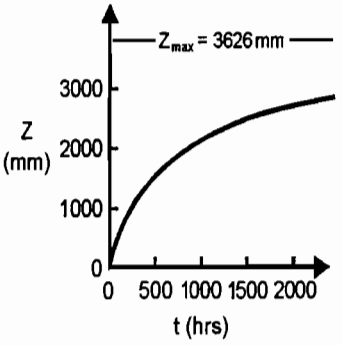

Figure 50. Example of Scour Calculations by the S-SRICOS Method.

Table 10. Full-Scale Bridges as Case Histories.

Bridge	Pier Bent No.	Pier Width (m)	Pier Length (m)	Pier Shape	Skew Angle (°)	River Slope	Manning's Coefficient n	Max. Velocity (m/s)	True Duration of Hydrograph (yrs)
Navasota River at SH 7	3	0.36	0.36	Square	5	0.0010	0.035	2.54	41
Navasota River at SH 7	5	0.36	8.53	Square Nose	5	0.0010	0.035	3.82	41
Brazos River at US 90A	3	0.91	8.53	Round Nose	0	0.0011	0.035	4.20	33
San Jacinto River at US 90	43	0.85	0.85	Square	15	0.0012	0.035	3.07	10
Trinity River at FM 787	3	0.91	7.30	Round Nose	25	0.0011	0.035	2.00	17
Trinity River at FM 787	4	0.91	7.30	Round Nose	25	0.0011	0.035	4.06	17
San Marcos River at SH 80	9	0.91	14.2	Round Nose	0	0.0010	0.035	1.89	60
Sims Bayou at SH 35	3	0.76	0.76	Circular	5	0.0001	0.035	0.95	3
Bedias Creek at US 75	26	0.86	0.86	Square	0	0.0005	0.035	2.19	50
Bedias Creek at SH 90	6	0.38	0.38	Square	5	0.0010	0.035	1.54	18

Bridge	Distance between Pier and Boring (m)	Max. Shear Stress (N/m2)	Initial Erosion Rate (mm/hr)	Equivalent Time (hrs)	Predicted Local Scour (m)		Measured Local Scour (m)	Measured Total Scour (m)	Predicted Max. Local Scour (m)
					E-SRICOS	S-SRICOS			
Navasota River at SH 7	6.5	41.46	8.91	368.8	0.76	0.82	0.76	-	1.10
Navasota River at SH 7	16.1	86.53	22.39	616.0	1.24	1.29	1.41	1.80	1.42
Brazos River at US 90A	55.4	85.86	65.26	568.4	2.59	2.54	2.87	4.43	2.72
San Jacinto River at US 90	146.3	49.62	17.44	373.1	1.30	1.66	1.47	3.17	2.14
Trinity River at FM 787	37.8	22.46	50.60	155.1	1.53	1.40	2.17	4.57	1.70
Trinity River at FM 787	78.4	80.93	39.82	544.6	2.26	2.37	2.17	4.57	2.66
San Marcos River at SH 80	57.3	20.30	61.75	158.4	1.07	1.40	1.27	2.66	1.64
Sims Bayou at SH 35	20.0	26.71	2.69	63.0	0.29	0.14	0.05	-	0.95
Bedias Creek at US 75	33.0	16.31	127.44	172.5	1.66	1.61	1.35	2.13	1.74
Bedias Creek at SH 90	2.9	5.92	44.25	102.8	0.70	0.70	0.61	-	0.83

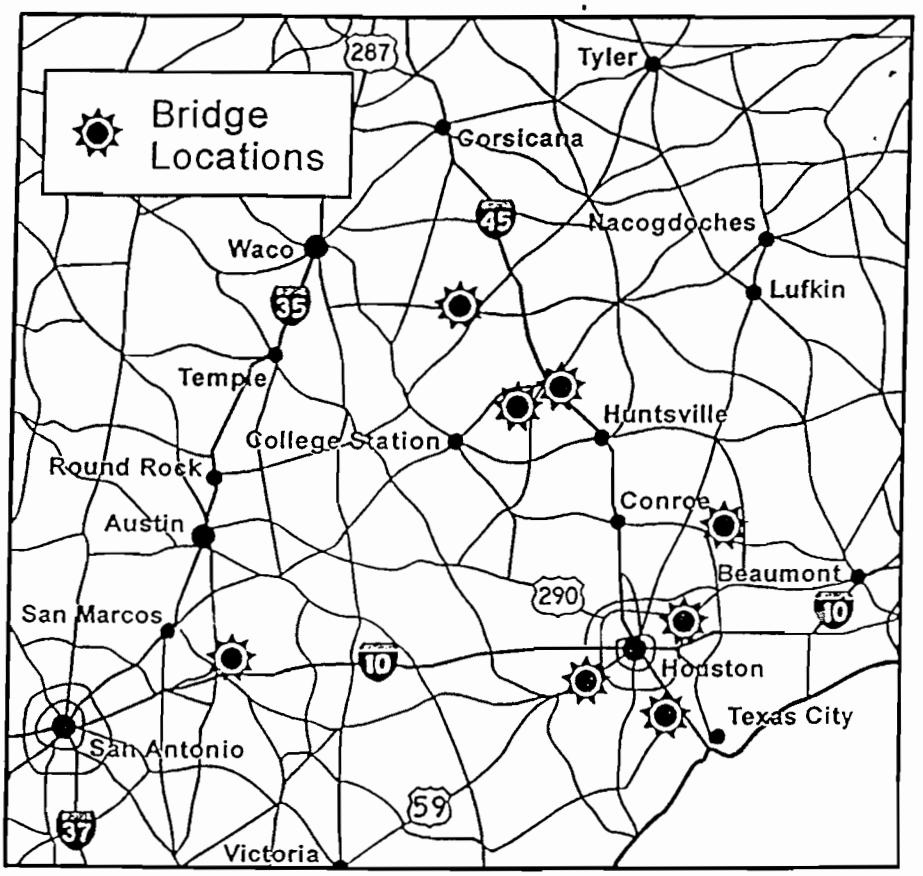

Figure 51. Locations of Case History Bridges.

The Brazos River bridge at US 90A was built in 1965. The bridge has an overall length of 287 m and consists of three continuous steel girder main spans with eight prestressed concrete approach spans. The foundation type is concrete piling penetrating 9.1 m below the channelbed, which consists of sandy clay, clayey sand, and sand down to the bottom of the piling according to existing borings. Between 1965 and 1998, the peak flood occurred in 1966 and generated a measured flow of 2600 m^3/s, which corresponded to a HEC-RAS calculated mean approach velocity of 4.2 *m/s* at bent 3. The pier at bent 3 was 0.91 m wide, 8.53 m long, and had a round nose. The pier was in line with the flow. River bottom profiles exist for 1965 and 1997 and show 4.43 m of total scour at bent 3 made up of 2.87 m of local scour and 1.56 m of combined contraction and general scour as explained later.

The San Jacinto River bridge at US 90 was built in 1988. The bridge is 1472.2 m long and has 48 simple prestressed concrete beam spans and three continuous steel plate girder spans. The foundation type is concrete piling penetrating 24.4 m below the channelbed at bent 43, where the soil consists of clay, silty clay, and sand down to the bottom of the piles according to existing borings. Between 1988 and 1997, the peak flood took place in 1994 and generated a measured flow of 10,000 m^3/s, which corresponded to a HEC-RAS calculated mean approach velocity of 3.1 m/s at bent 43. The pier at bent 43 was square with a side equal to 0.85 m. The angle between the flow direction and the pier main axis was 15°. River bottom profiles exist for 1988 and 1997 and show 3.17 m of total scour at bent 43 made up of 1.47 m of local scour and 1.70 m of combined contraction and general scour as explained later.

The Trinity River bridge at FM 787 was built in 1976. The bridge has three main spans and three approach spans with an overall length of 165.2 m. The foundation type is timber piling and the soil is sandy clay to clayey sand. Between 1976 and 1993, the peak flood took place in 1990 and generated a measured flow of 2950 m^3/s which corresponded to a HEC-RAS calculated mean approach flow velocity of 2.0 m/s at bent 3 and 4.05 m/s at bent 4. The piers at bent 3 and 4 were 0.91 m wide, 7.3 m long, and had a round nose. The angle between the flow direction and the pier main axis was 25°. River bottom profiles exist for 1976 and for 1992 and show 4.57 m of total scour at both bent 3 and 4 made up of 2.17 m of local scour and 2.40 m of contraction and general scour as explained later.

The San Marcos River bridge at SH80 was built in 1939. This 176.2 m long bridge has 11 prestressed concrete spans. The soil tested from the site is a low plasticity clay. Between 1939 and

1998, the peak flood occurred in 1992 and generated a measured flow of 1000 m^3/s which corresponds to a HEC-RAS calculated mean approach flow velocity of 1.9 m/s at bent 9. The pier at bent 9 is 0.91 m wide, 14.2 m long, and has a round nose. The pier is in line with the flow. River bottom profiles exist for 1939 and 1998 and show 2.66 m of total scour at bent 9 made up of 1.27 m of local scour and 1.39 m of contraction and general scour as explained later.

The Sims Bayou bridge at SH35 was built in 1993. This 85.3 m long bridge has five spans. Each bent rests on four drilled concrete shafts. Soil borings indicate mostly clay layers with a significant sand layer about 10 m thick starting at a depth of approximately 4 m. Between 1993 and 1996, the peak flood occurred in 1994 and generated a measure flow of 200 m^3/s which corresponds to a HEC-RAS calculated mean approach flow velocity of 0.93 m/s at bent 3. The pier at bent 3 is circular with a 0.76 m diameter. The angle between the flow direction and the pier main axis was 5°. River bottom profiles exist for 1993 and 1995 and indicate 0.05 m of local scour at bent 3.

The Bedias Creek bridge at US75 was built in 1947. This 271.9 m long bridge has 29 spans and bent 26 is founded on a spread footing. The soil tested from the site varied from low plasticity clay to fine silty sand. Between 1947 and 1996, the peak flood occurred in 1991 and generated a measured flow of 650 m^3/s, which corresponds to a HEC-RAS calculated mean approach flow velocity of 2.15 m/s at bent 26. The pier at bent 26 is square with a side of 0.86 m. The pier is in line with the flow. River bottom profiles exist for 1947 and 1996 and show 2.13 m of total scour at bent 26 made up of 1.35 m of local scour and 0.78 m of contraction and general scour as explained later.

The Bedias Creek bridge at SH90 was built in 1979. This 73.2 m long bridge is founded on 8 m long concrete piles embedded in layers of sandy clay and firm gray clay. Between 1979 and 1996, the peak flood occurred in 1991 and generated a measured flow of 650 m^3/s which corresponds to a HEC-RAS calculated mean approach flow velocity of 1.55 m/s at bent 6. The pier at bent 6 was square with a side of 0.38 m. The angle between the flow direction and the pier main axis was 5°. River bottom profiles exist for 1979 and 1996 and show 0.61 m of local scour at bent 6.

3.9 PREDICTED AND MEASURED LOCAL SCOUR FOR THE EIGHT BRIDGES

For each bridge the E-SRICOS and the S-SRICOS methods were used to predict the local scour at the chosen bridge pier location. One pier was selected for each bridge except for the

Navasota River bridge at SH7 and the Trinity River bridge at FM787 for which two piers were selected. Therefore a total of 10 predictions were made for these eight bridges. These predictions are not Class A predictions since the measured values were known before the prediction process started. However the predictions were not modified once they were obtained.

For each bridge, Shelby tube samples were taken near the bridge pier within a depth at least equal to two pier widths below the pier base. The boring location was chosen to be as close as practically possible to the bridge pier considered. The distance between the pier and the boring varied from 2.9 m to 146.3 m (Table 10). In all instances the boring data available was studied in order to infer the relationship between the soil layers at the pier and at the sampling location. Shelby tube samples to be tested were selected as the most probable representative samples at the bridge pier. These samples were tested in the EFA and yielded erosion functions $\dot{z}$ versus τ. Figs. 52 and 53 are examples of the erosion functions obtained. The samples were also analyzed for common soil properties (Table 11).

For each bridge, the USGS gage data was obtained from the USGS Internet site. This data consisted of a record of discharge Q versus time t over the period of time separating the two river bottom profile observations (Fig. 46). This discharge hydrograph was transformed into a velocity hydrograph by using the program HEC-RAS (1997) and proceeding as follows. The input to HEC-RAS is the bottom profile of the river cross section (obtained from the Texas DOT records), the mean longitudinal slope of the river at the bridge site (obtained from topographic maps, Table 10), and Manning's roughness coefficient (estimated at 0.035 for all cases after Young et al., 1997). For a given discharge Q, HEC-RAS gives the velocity distribution in the river cross section including the mean approach velocity v at the selected pier location. Many runs of HEC-RAS for different values of Q are used to develop a relationship between Q and v. The relationship (regression equation) is then used to transform the Q-t hydrograph into the v-t hydrograph at the selected pier (Figs. 47, 48, and 49).

Then, the program SRICOS (Kwak et al., 1999) was used to predict the scour depth z versus time t curve. For each bridge, the input consisted of the $\dot{z}$ versus τ curves (erosion functions) for each layer at the bridge pier (e.g., Figs. 52 and 53), the v versus t record (velocity hydrograph) (e.g., Figs. 47, 48, and 49), the pier diameter B, the viscosity of the water υ, and the density of the water ρ_w. The output of the program was the scour depth z versus time t curve for

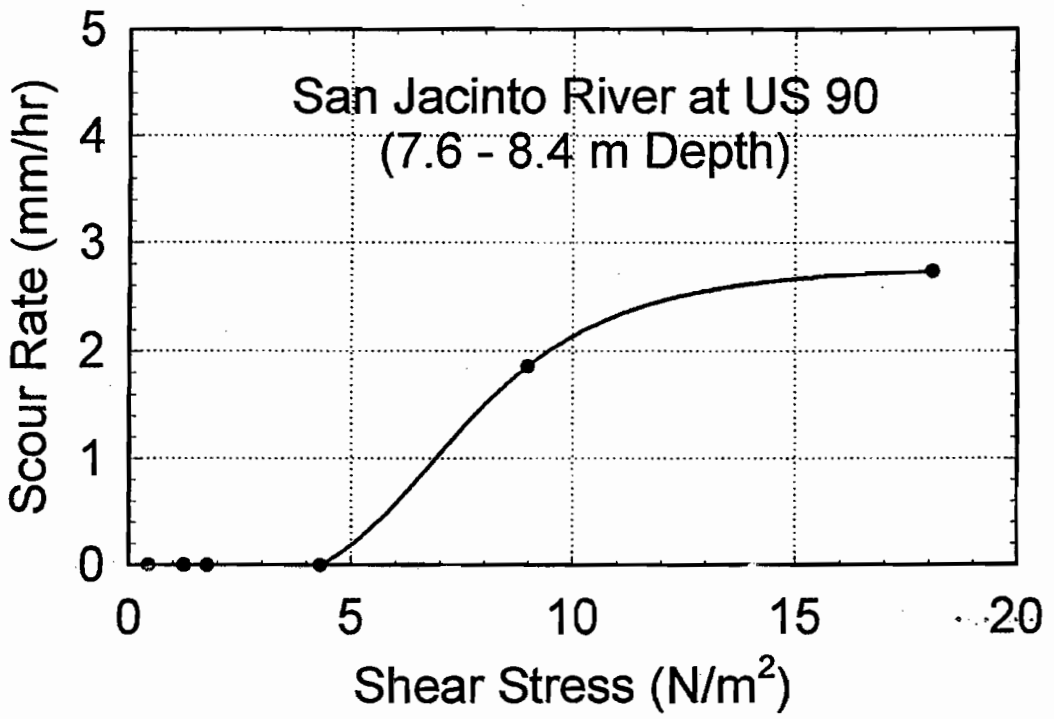

Figure 52. Erosion Function for San Jacinto River Sample (7.6 m to 8.4 m Depth).

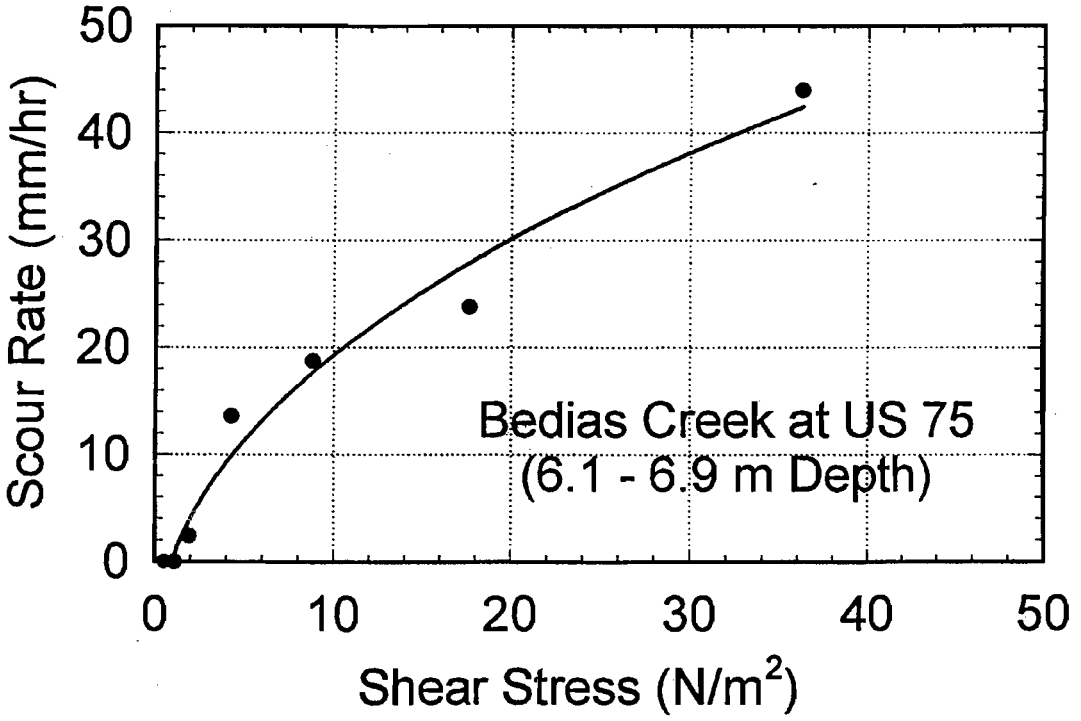

Figure 53. Erosion Function for Bedias Creek River Sample (6.1 m to 6.9 m Depth).

Table 11. Soil Properties at the Bridge Sites.

Soil Properties	Bridge	Navasota		Brazos		San Jacinto		Sims
	Layer No.	1	2	1,2	1,2	3	4	1
	Depth (m)	1.8-2.4	4.9-5.5	13.0-13.7	5.3-6.1	6.9-7.6	7.6-8.4	3.0-3.7
Liquid Limit (%)		27.72	26.42	24.49	22.04	-	37.50	84.16
Plastic Limit (%)		14.29	6.25	9.41	9.09	-	12.71	16.05
Plasticity Index (%)		13.43	20.17	15.08	12.95	-	24.79	68.11
Water Content (%)		19.80	26.60	17.32	151.57	26.88	27.75	25.25
Mean Diameter, D_{50} (mm)		0.125	-	0.265	-	-	-	0.0012
Shear Strength (kPa)		43.10	32.10	45.49	23.94	4.78	21.53	23.00
Unit Weight (kN/m^3)		19.20	18.80	20.20	19.60	16.70	20.80	19.60
% Passing #200 Sieve		26.20	57.70	30.09	50.36	60.71	94.50	99.07

Soil Properties	Bridge	Trinity		San Marcos		Bedias 75		Bedias 90
	Layer No.	1	2	1	2	1	2	1
	Depth (m)	10.7-11.4	13.0-13.7	6.1-6.6	7.0-7.5	6.1-6.9	6.9-7.6	1.5-2.3
Liquid Limit (%)		-	42.24	41.34	40.31	47.86	-	55.08
Plastic Limit (%)		-	8.70	16.67	19.18	13.56	-	15.79
Plasticity Index (%)		-	33.54	24.67	21.13	34.30	-	39.29
Water Content (%)		7.67	22.22	22.00	24.40	18.07	17.50	23.63
Mean Diameter, D_{50} (mm)		6.00	-	-	-	0.048	0.130	0.040
Shear Strength (kPa)		9.57	11.48	27.30	29.67	10.00	32.00	62.00
Unit Weight (kN/m^3)		22.00	22.10	19.60	20.20	20.04	21.30	19.60
% Passing #200 Sieve		11.52	68.40	78.30	73.40	86.81	35.14	91.31

the selected bridge pier (e.g., Figs. 47, 48, and 49) with the predicted local scour depth corresponding to the last value on the curve.

The measured local scour depth was obtained for each case history by analyzing the two bottom profiles of the river cross section (e.g., Figs. 54 and 55). This analysis was necessary to separate the scour components which added to the total scour at the selected pier. The two components were local scour and contraction/general scour. This separation was required because, at this time, SRICOS only predicts the local scour. The contraction/general scour over the period of time separating the two river bottom profiles was calculated as the average scour over the width of the channel. This width was taken as the width corresponding to the mean flow level (width AB on Figs. 54 and 55). Within this width the net area between the two profiles was calculated with scour being positive and aggradation being negative. The net area was then divided by the width AB to obtain an estimate of the mean contraction/general scour. Once this contraction/general scour was obtained it was subtracted from the total scour at the bridge pier to obtain the local scour at the bridge pier. Note that in some instances there was no need to evaluate the contraction/general scour. This is the case of bent 3 for the Navasota Bridge (Fig. 54). Indeed in this case the bent was in the dry at the time of the field visit (floodplain) and the local scour could be measured directly. Fig. 56 shows the comparison between E-SRICOS predicted and measured values of local scour at the bridge piers.

Fig. 56 shows the prediction results for the E-SRICOS method. The S-SRICOS method was performed next. For each bridge pier the maximum depth of scour z_{max} was calculated by using Eq. 28. The velocity used for Eq. 28 was the maximum velocity that occurred during the period of time separating the two river bottom profile observations. Then, at each pier an average erosion function ($\dot{z}$ versus τ curve) within the maximum scour depth was generated. Then, the maximum shear stress τ_{max} around the pier before scour starts was calculated using Eq. 27, and it was assumed that the pier was circular (Table 10). The initial scour rate $\dot{z}_i$ was read on the average erosion function for that pier (Table 10). The equivalent time t_e was calculated using Eq. 33, using t_{hydro} equal to the time separating the two river bottom profile observations and v_{max} equal to the maximum velocity that occurred during t_{hydro} (Table 10). Knowing t_e, $\dot{z}_i$, and z_{max} the scour depth accumulated during the period of t_{hydro} was calculated using Eq. 29. Fig. 57 is a comparison

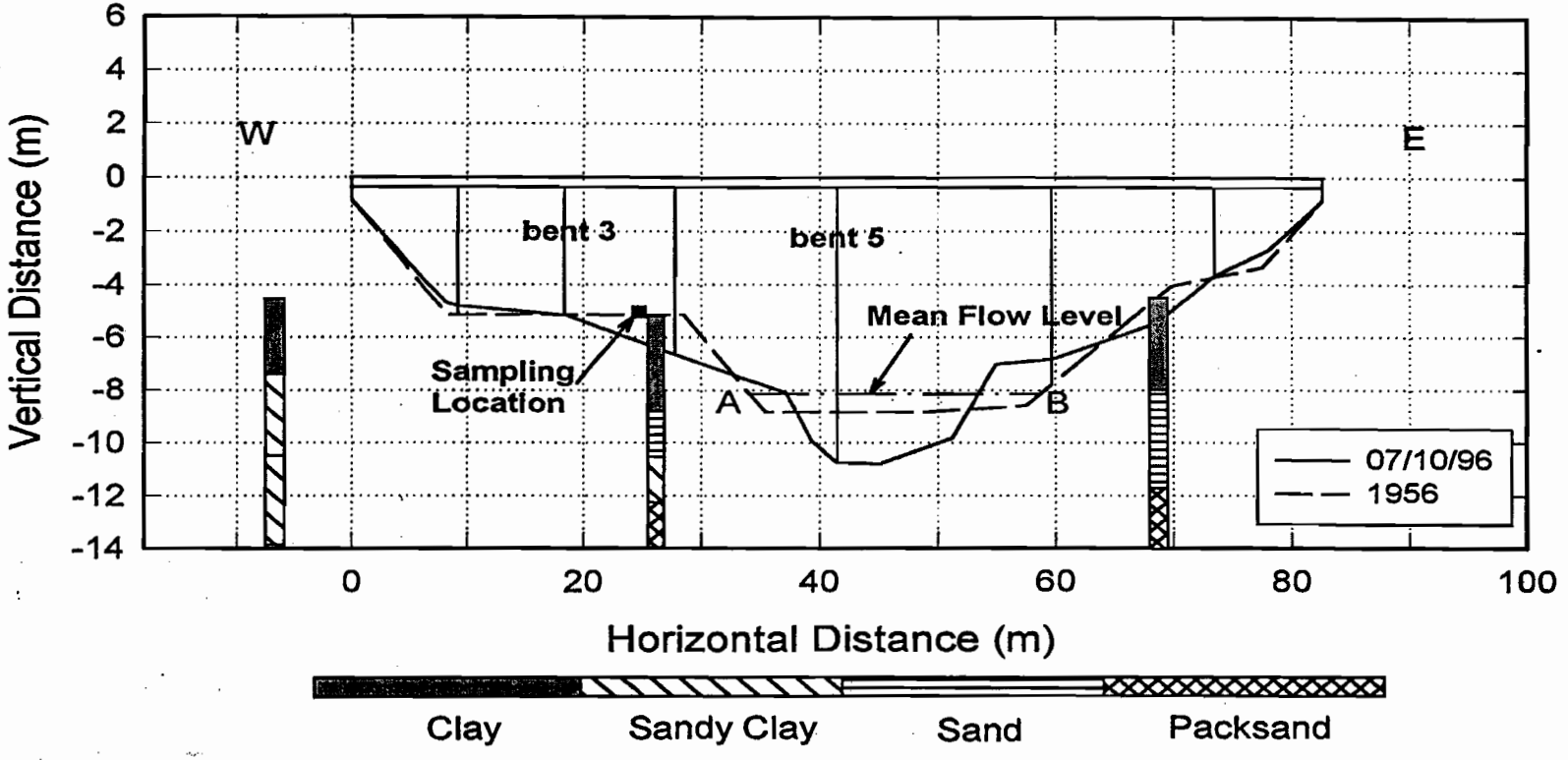

Figure 54. Profiles of Navasota River Bridge at SH7.

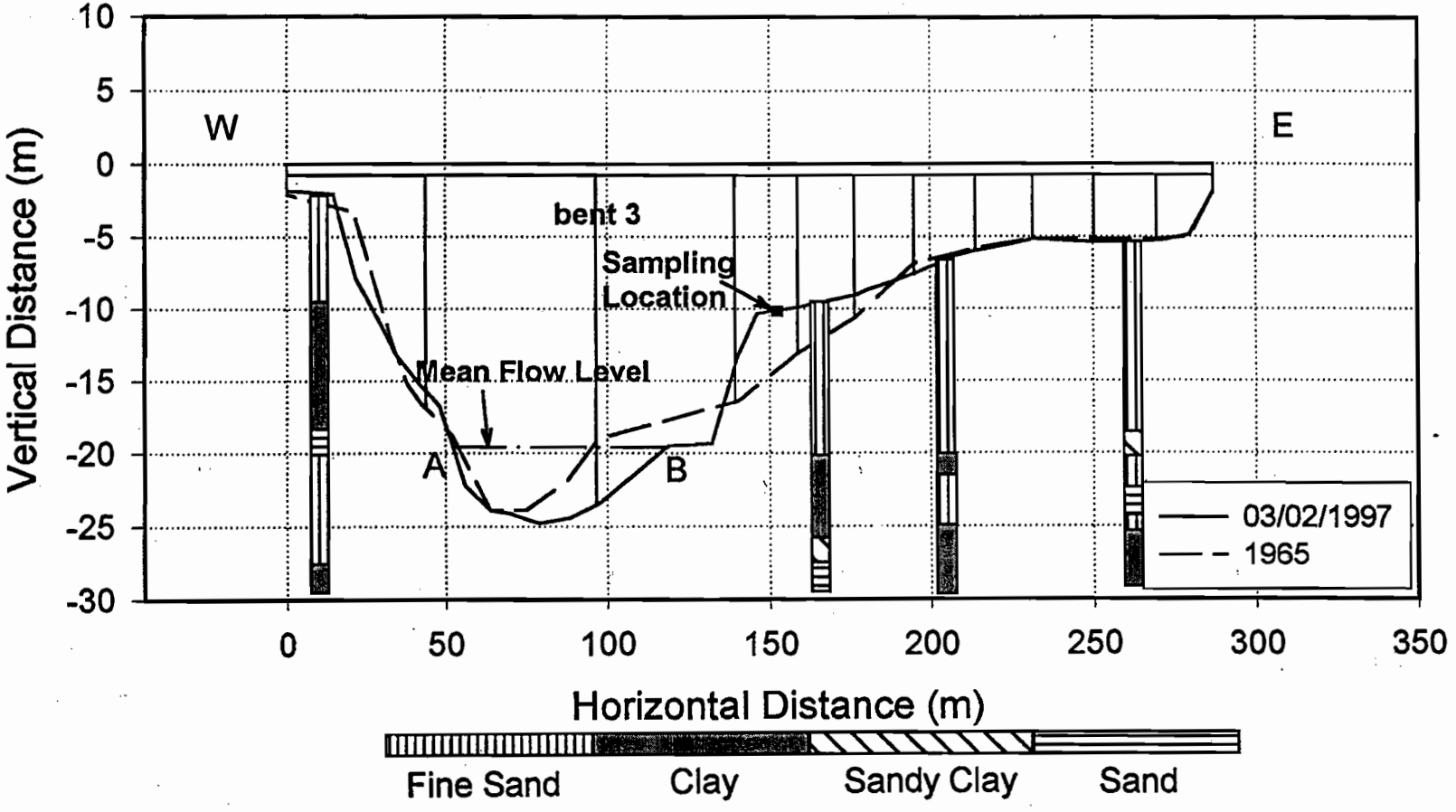

Figure 55. Profiles of Brazos River Bridge at US90A.

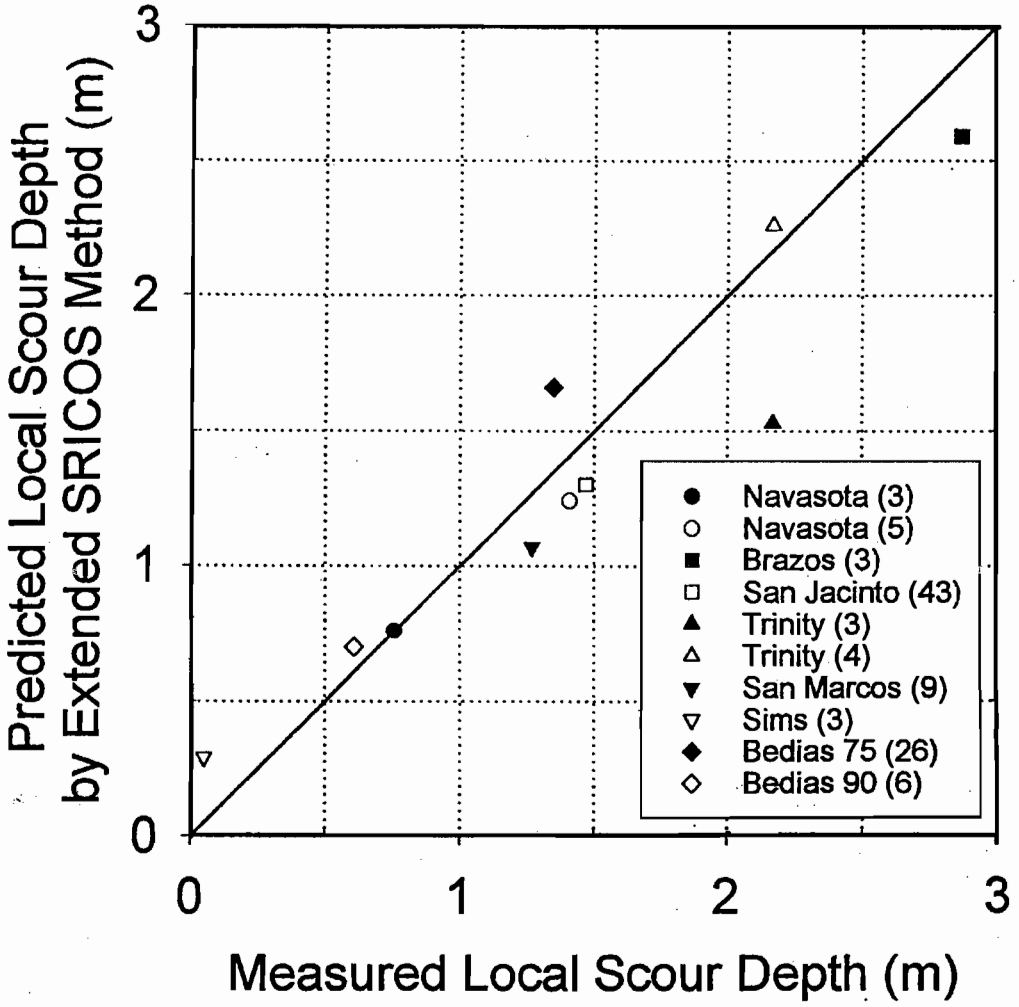

Figure 56. Predicted versus Measured Local Scour for the E-SRICOS Method.

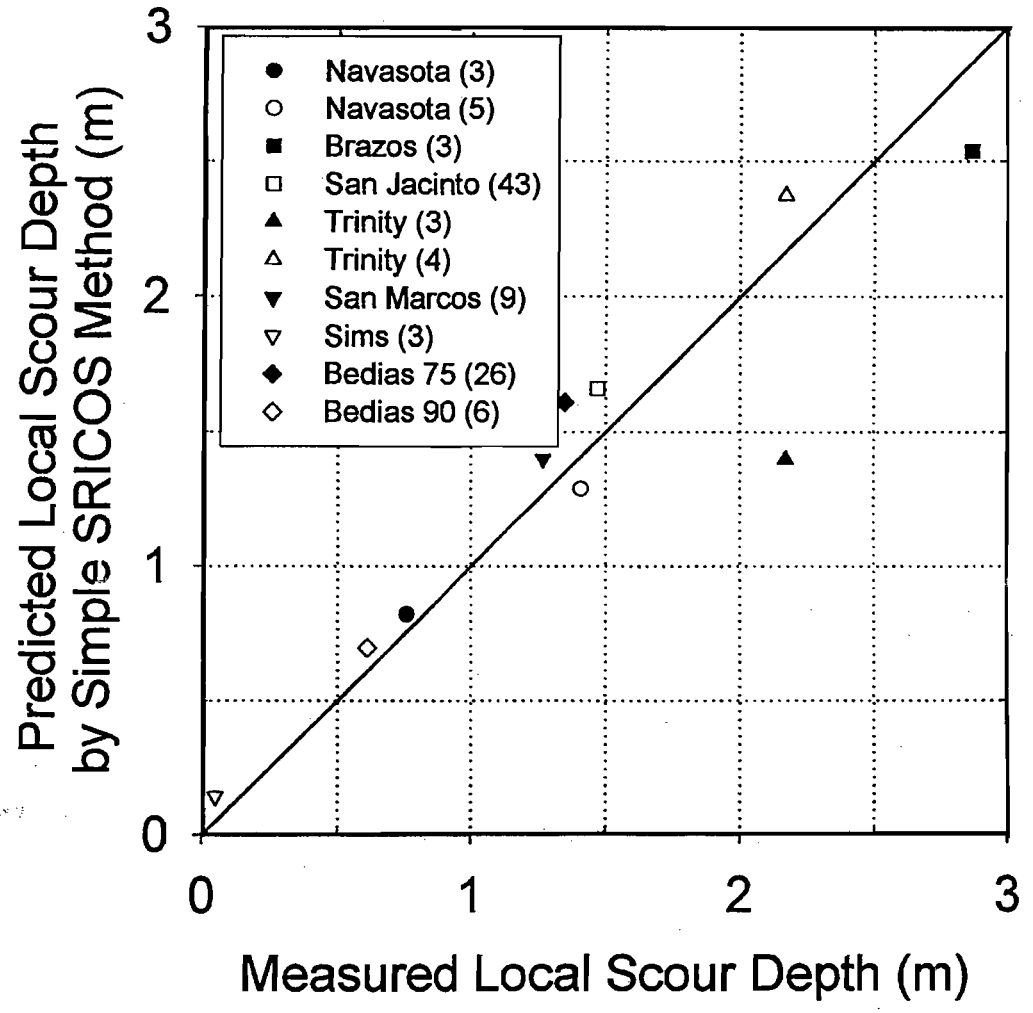

Figure 57. Predicted versus Measured Local Scour for the S-SRICOS Method.

between the measured values of local scour and the predicted values using the S-SRICOS method. All the details of the prediction process can be found in Kwak et al. (1999).

Note that at this time, E-SRICOS and S-SRICOS do not include correction factors for pier shape, skew angle between the flow direction and the pier main axis, and shallow water depth effects. Such factors exist (HEC-18, 1995; Melville and Coleman, 1999) but were derived for sands and not for clays. Research continues to develop such factors for clays.

3.10 CONCLUSIONS

A method is proposed to predict the depth of the local scour hole versus time curve around a bridge pier in a river for a given velocity hydrograph and for a layered soil system. The method is limited at this time to cylindrical piers and water depths larger than two times the pier width. The prediction process makes use of a new flood accumulation principle and a new layer equivalency principle. These are incorporated in a computer program called SRICOS used to generate the scour versus time curve. A simplified version of this method is also proposed and only requires hand calculations. Both methods are evaluated by comparing predicted scour depths and measured scour depths for 10 piers at eight full-scale bridges. Research is continuing to extend this method to other scour problems.

REFERENCES

American Society for Testing and Materials, 1997, *Annual Book of ASTM Standards, Vol. 04.08: Soil and Rock*, Philadelphia, Pennsylvania., USA.

Apperly, L. W., 1968, "Effect of Turbulence on Sediment Entrainment," Ph.D. Dissertation, University of Auckland, Auckland, New Zealand.

Ariathurai, R., and Arulanandan, K., 1978, "Erosion Rates of Cohesive Soils," *Journal of the Hydraulics Division*, Proceedings of the ASCE, Vol. 104, No. HY2, pp. 279-283, ASCE, New York, New York.

Arulanandan, K., 1975, "Fundamental Aspects of Erosion in Cohesive Soils," *Journal of the Hydraulics Division*, Proceedings of the ASCE, Vol. 101, No. HY5, pp. 635-639, ASCE, New York, New York.

Arulanandan, K., Loganathan, P., and Krone, R. B., 1975, "Pore and Eroding Fluid Influence on Surface Erosion of Soil," *Journal of the Geotechnical Engineering Division*, ASCE, Vol. 101, No. GT1, New York, New York, pp. 51-66.

ASTM-D1587, 1999, "Standard Practice for Thin-Walled Tube Geotechnical Sampling of Soils," *Annual Book of ASTM Standards*, Vol. 04.07, pp. 142-144, American Society for Testing and Materials, Philadelphia, Pennsylvania, USA.

ASTM-D4647, 1999, "Standard Test Method for Identification and Classification of Dispersive Clay Soils by the Pinhole Test," *Annual Book of ASTM Standards*, Vol. 04.08, pp. 757-766, American Society for Testing and Materials, Philadelphia, Pennsylvania, USA.

Black, W., De Jongh, J. G. V., Overbeek, J. Th., and Sparnaay, M. J., 1960, *Transactions of the Faraday Society*, London, Vol. 56, p. 1597.

Briaud, J. L., Chen, H. C., Nurtjahyo, P., Kwak, K., and Han, S. W., 1999(a), "Bridge Scour in Cohesive Materials," Interim Report on NCHRP Project 24-15, NCHRP, Washington, D.C., pp. 149 + App.

Briaud, J. L., Ting, F. C. K., Chen, H. C., Gudavalli, R., Perugu, S., and Wei, G., 1999(b), "SRICOS: Prediction of Scour Rate in Cohesive Soils at Bridge Piers," *Journal of Geotechnical and Geoenvironmental Engineer*, Vol. 125, No. 4, April 1999, pp. 237-246, American Society of Civil Engineers, Reston, Virginia, USA.

Briaud, J. L., Ting, F. C. K., Chen, H. C., Perugu, S., Han, S. W., and Kwak, K., 2000, "The Erosion Function Apparatus for Scour Rate Predictions," proposed in Sept. 1999 for publication in the *Journal of Geotechnical and Geoenvironmental Engineering*, American Society of Civil Engineers, Reston, Virginia, USA.

Chen, H. C., Chen, M., and Huang, E. T., 1996, "Chimera-RANS Simulations of Unsteady 3D Flows Induced by Ship and Structure Interactions," Flow Modeling and Turbulence Measurements VI, edited by C. J. Chen, C. Shih, J. Lienau, and R. J. Kung, pp. 373-380, A. A. Balkema Publishers, Rotterdam, Netherlands.

Chen, H. C., and Patel, V. C., 1988, "Near-Wall Turbulence Models for Complex Flows Including Separation," *AIAA Journal*, Vol. 26, No. 6, pp. 641-648.

Christensen, B. A., September 1965, "Discussion of the Article by Partheniades, E.," January 1965, Erosion and Deposition of Cohesive Soils, *Journal of Hydraulic Division*, Proceedings of the ASCE, Vol. 91, No. HY5, pp. 301-308.

Dunn, I. S., 1959, "Tractive Resistance of Cohesive Channels," *Journal of Soil Mechanics and Foundations Division,* Vol. 85, No. SM3, Proceedings Paper No. 2062, pp. 1-24, ASCE, New York, New York.

Einstein, H. A., and El-Samni, E. S. A., 1949, "Hydrodynamic Forces on a Rough Wall," *Review of Modern Physics*, Vol. 21, pp. 520-524.

Enger, P. F., Smerdon, E. T., and Masch, F. D., Task Committee on Erosion of Cohesive Soils, July 1968, "Erosion of Cohesive Soils," *Journal of the Hydraulics Division*, Proceedings of the ASCE, Vol. 94, No. HY4, pp. 1017-1049.

Gudavalli, R., Ting, F., Briaud, J.-L., Chen, H. C., Perugu, S., and Wei, G., 1997, "Flume Tests to Study Scour Rate of Cohesive Soils," Research Report to the Texas DOT, Department of Civil Engineering, Texas A&M University, College Station, Texas.

HEC-18, 1995, Hydraulic Engineering Circular No. 18 authored by Richardson, E. V., and Davis, S. R., Report No. FHWA-IP-90-017, Federal Highway Administration, Washington, D.C.

HEC-RAS, 1997, Hydrologic Engineering Center-River Analysis System, User's Manual, Version 2.0, U.S. Army Corps of Engineers, Davis, California.

Hydrotechnical Construction, Moscow, May 1936 as quoted in Raudkivi, A. J., 1976, *Loose Boundary Hydraulics*, p. 276, Pergamon Press, New York, New York.

Kelly, E. K., and Gularte, R. C., 1981, "Erosion Resistance of Cohesive Soils," *Journal of the Hydraulics Division*, Proceedings of the ASCE, Vol. 107, No. HY10, pp. 1211-1224, ASCE, New York, New York.

Kwak, K., Briaud, J. L., Chen, C. H., Han, S. W., and Ting, F. C. K., 2000, "The SRICOS Method for Predicting Local Scour at Bridge Piers," Research Report to the Texas Department of Transportation on Project 2937, Civil Engineering, Texas A&M Univeristy, College Station, Texas, USA.

Kwak, K., Briaud, J. L., Chen, H. C., Ting, F. C. K., and Han, S. W., 1999, "Generalized SRICOS Method and Verification for Prediction of Scour Depth Versus Time at Bridge Piers," Research Report to the Texas DOT, Department of Civil Engineering, Texas A&M University, College Station, Texas, USA.

Lagasse, P. F., Schall, J. D., Johnson, F., Richardson, E. V., and Chang, F., 1995, "Stream Stability at Highway Structures," Federal Highway Administration Report No. FHWA-IP-90-014 (HEC 20), Washington, D.C., pp. 144.

Landers, M. N., and Mueller, D. S., 1996, "Channel Scour at Bridges in the United States," Federal Highway Administration Report No. FHWA-RD-95-184, Washington, D.C., p. 140.

Laursen, E. M., 1962, "Scour at Bridge Crossings," *Transactions of the ASCE*, Vol. 127, Part 1, No. 3294, pp. 166-209, ASCE, New York, New York.

Lee, S. C., and Mehta, A. J., 1994, "Cohesive Sediment Erosion," Dredging Research Program, Contract Report DRP-94-6, pp. 83, University of Florida, Gainsville, Florida, USA.

Lyle, W. M., and Smerdon, E. T., 1965, "Relation of Compaction and Other Soil Properties to Erosion and Resistance of Soils," *Transaction of the American Society of Agricultural Engineers*, Vol. 8, No. 3.

Melville, B. W., and Coleman, S. E., 1999, "Bridge Scour," Water Resource Publications, LLC, Highlands Ranch, Colorado, USA, p. 551.

Mitchell, J. K., 1993, *Fundamentals of Soil Behavior*, 2nd Edition, John Wiley and Sons, Inc., New York, New York, p. 422.

Moody, L. F., 1994, "Friction Factors for Pipe Flow," *Transaction of the American Society of Mechanical Engineers,* American Society of Mechanical Engineers, College Station, TX, USA. Vol. 66.

Munson, B. R., Young, D. F., and Okiishi, T. H., 1990, *Fundamentals of Fluid Mechanics*, John Wiley and Sons, Inc., New York, New York, p. 843.

National Bridge Inventory, 1997, Bridge Management Branch, Federal Highway Administration, Washington, D.C.

Pagan-Ortiz, J. E., 1998, "Status of Scour Evaluation of Bridges Over Waterways in the United States," *Proceedings of the ASCE Conference on Water Resources Engineering 98*, ASCW, Reston, Virginia, pp. 2-4

Parola, A., 1997, "Research Needs: Scour at Bridge Foundations," NCHRP Report, Project 24.8, Transportation Research Board, Washington, D.C.

Perugu, S., Briaud, J. L., Ting, F., Chen, H. C., Gudavalli, R, and Wei, G., 1999, "Erosion Function Apparatus to Study Scour Rate of Cohesive Soils," Research Report to the Texas DOT, Department of Civil Engineering, Texas A&M University, College Station, Texas.

Philogene, B., and Briaud, J. L., 1996, "Scour of Cohesive Soils: A Literature Review," Research Report to the Texas DOT, Civil Engineering, Texas A&M University, College Station, Texas.

Richardson, E. V., and Davis, S. R., 1995, "Evaluating Scour at Bridges," Federal Highway Administration Report No. FHWA-IP-90-017 (HEC 18), Washington, D.C., p. 204.

Rohan, K., Lefebvre, G., Douville, S., and Milette, J. P., 1986, "A New Technique to Evaluate Erosivity of Cohesive Material," *Geotechnical Testing Journal*, GTJODJ, Vol. 9, No. 2, June 1986, pp. 87-92, American Society for Testing and Materials, Philadelphia, Pennsylvania, USA.

Shaikh, A., Ruff, J. F., and Abt, S. R., March 1988, "Erosion Rate of Compacted Na - Montmorillonite Soils," *Journal of Geotechnical Engineering*, ASCE, Vol. 114, No. 3, pp. 296-305, New York, New York.

Shen, H. W., Schneider, V. R., and Karaki, S., 1969, "Local Scour Around Bridge Piers," *Journal of the Hydraulics Division*, ASCE, Vol. 95, No. HY6, pp. 1919-1940, ASCE, New York, New York.

Shields, A., 1936, "Anwendung der Aehnlichkeits-Mechanik und der Turbulenzforschung auf die Geschiebebewegung," Preussische Versuchsanstalt für Wasserbau und Schiffbau, Berlin.

Shirole, A. M., and Holt, R. C., 1991, "Planning for a Comprehensive Bridge Safety Assurance Program," *Transportation Research Record No. 1290*, pp. 137-142, Washington, D.C.

Smerdon, E. T., and Beasley, R. P., 1959, "Tractive Force Theory Applied to Stability of Open Channels in Cohesive Soils," Research Bulletin No. 715, Agricultural Experiment Station, University of Missouri, Columbia, Missouri.

Vanoni, V. A. (editor), 1975, "Sedimentation Engineering," *ASCE Manuals and Reports on Engineering Practice*, No. 54, ASCE, Reston, Virginia, p. 745.

Wei, G., Chen, H. C., Ting, F., Briaud, J. L., Gudavalli, R., and Perugu, S., 1997, "Numerical Simulation to Study Scour Rate in Cohesive Soils," Research Report to the Texas DOT, Department of Civil Engineering, Texas A&M University, College Station, Texas, USA.

White, C. M., 1940, "The Equilibrium of Grains on the Bed of a Stream," *Proceedings Royal Society of London*, Series A, No. 958, Vol. 174, February 1940, pp. 322-338.

Young, D. F., Munson, B. R., and Okisshi, T. H., 1997, *A Brief Introduction to Fluid Mechanics*, John Wiley & Sons, New York, New York, USA.

APPENDIX

USER'S MANUAL OF SRICOS PROGRAM

INTRODUCTION

The SRICOS program was developed to predict the scour depth z versus time t around a bridge pier founded in clay. This program includes all the procedures in the SRICOS method, re needed to calculate the variation of a pier scour depth as a function of time, as well as how to handle a multi-layered soil and multi-flood system. In order to run the SRICOS program, the necessary data sets are as follows.

1. EFA results, for each soil layer (scour rate $\dot{z}$ versus the hydraulic shear stress τ),
2. Hydrologic data such as a discharge hydrograph or a velocity history,
3. Pier width, and
4. Soil stratigraphy around the bridge pier.

The program SRICOS was written in Fortran 90 by using Fortran PowerStation 4.0.

STARTING SRICOS PROGRAM

The SRICOS program should be executed from the directory occupied by the program's files by typing 'SRICOS' at the DOS prompt or double-clicking 'SRICOS.EXE' in the Windows® environment. The SRICOS program is a user friendly, interactive code that guides the user through a step by step data input procedure except velocity or discharge data. Generally, the number of velocity or discharge data could be at least several thousands if the duration of a scour analysis is several years of daily data. The velocity or discharge data should be prepared in the format of an ASCII file or a text document before running the program.

STEPS OF DATA INPUT

After starting the program, the logo of SRICOS shows up, and then data input procedures are as follows.

- *UNIT OF INPUT DATA – SI UNIT (1) OR ENGLISH UNIT (2)*

- User decides the unit of input data. Press (1) to use SI unit or (2) to use English unit.

- *UNIT OF OUTPUT DATA – SI UNIT (1) OR ENGLISH UNIT (2)*

- User decides the unit of output data. Press (1) to use SI unit or (2) to use English unit.

- *FIRST DATE OF ANALYSIS – FORMAT (MM/DD/YYYY)*

- Input the first date of analysis, for example, 01-01-1999.

- *LAST DATE OF ANALYSIS – FORMAT (MM/DD/YYYY)*

- Input the last date of analysis, for example, 12-31-1999.

- *THE NUMBER OF INPUT (HYDROLOGIC) DATA AS INTEGER*

- Input the number of discharges or velocities as an integer number for the duration of the analysis.

  These hydrologic data basically have the same time step.

- *PIER DIAMETER AS REAL – UNIT [(M) OR (FT)]*

- Input the diameter of the pier as a real number in meters if the unit of input data is SI unit, or in feet if the unit of input data is English unit.

- *CORRECTION FACTOR K1 FOR PIER SHAPE AS REAL*

- Input the correction factor K_1 for the pier shape as shown in Table A.1.

- *CORRECTION FACTOR FOR K2 FOR ATTACK ANGLE OF FLOW AS REAL*

- Input the correction factor K_2 for the attack angle of flow as shown in Table A.2.

- *TIME STEP, dt AS REAL – UNIT [hrs]*

- Input the time step in hours as a real number.

- *TYPE OF INPUT (HYDROLOGIC) DATA – DISCHARGE (1) OR VELOCITY (2)*

- User decides the type of hydrologic data. In actual calculation of this program, the velocity data are used. If user has velocity data, press '2'. Otherwise, if user has no velocity data but discharge data, press '1' to use discharge data, several sub-procedures are necessary to transform the discharge data to velocity data. User should decide the regression equation for the relationship between velocity and discharge, or sufficient points representing the relationship.

- *HOW TO TRANSFORM DISCHARGE DATA TO VELOCITY DATA*
  - *DEFINED BY USER -(0)*
  - *REGRESSION EQUATION – (1-20)*

- If user finds the same type of regression equation as the regression equations included in this program (shown in the next section) select it and press the number of the equation.

- *COEFFICIENTS OF REGRESSION EQUATION AS REAL*

  (VELOCITY VS. DISCHARGE)

  - *FORMAT (A B C)*

- Input the coefficients as directed on screen. There are three coefficients in this example.
- Otherwise, user should press '0', and then, input the values of points representing the relationship between velocity data and discharge data.

- *THE NUMBER OF REGRESSION POINTS AS INTEGER*

  - *FOR TRANSFORMING DISCHARGE DATA TO VELOCITY DATA*

- Input the number of regression points representing the relationship between velocity data and discharge data.

- *VALUES OF REGRESSION POINTS AS REAL*

  - *FOR TRANSFORMING DISCHARGE DATA TO VELOCITY DATA*
  - *FORMAT [DISCHARGE (I) VELOCITY (I)]*
  - *UNIT [(CMS) OR (CFS) (m/s) OR (ft/s)]*

- Input the values of regression points (discharge or velocity) as real numbers. If the unit of input data is SI unit, the units of discharge and velocity are (CMS) and (m/s), respectively. Otherwise, they are (CFS) and (ft/s).

  For example, if the unit system of input data is SI unit and the number of points is three,

5.0 0.2

50.0 0.8

100.0 1.2

The values of the first column represent discharges and the unit is (CMS). Similarly the values of the second column represent velocities and the unit is (m/s).

- *THE NUMBER OF LAYERS AS INTEGER*

- Input the number of soil layers as an integer number.

- *PROPERTIES OF 1st LAYER*
  - *FORMAT [THICKNESS CRITICAL SHEAR STRESS]*
  - *UNIT [(m) OR (ft) (N/m^2)]*
- Input thickness of the layer and the critical shear stress. User should repeat this input as many times as the number of layers.

- *HOW TO ESTIMATE INITIAL SCOUR RATE –1ST LAYER*
  - *DEFINED BY USER -(0)*
  - *REGRESSION EQUATION -(1-20)*
- Input the regression equation for the relationship between the scour rate $\dot{z}$ and the hydraulic shear stresses τ, which is the result of EFA test. Basically, this is the same procedure as the step above, '*HOW TO TRANSFORM DISCHARGE DATA TO VELOCITY DATA*'.

- *FILE NAME OF INPUT*

- Input the file name of hydrologic data such as discharges or velocities. This file should be in the directory occupied by the program files.

- *FILE NAME OF CALCULATION RESULT ONLY*

- Input a file name for calculation result only. This file would include the results such as time t, velocity v, shear stress τ, maximum scour depth z_{max}, and scour depth z for each time step.

- *FILE NAME OF OUTPUT*

- Input a file name for output.

REGRESSION EQUATION USED IN SRICOS PROGRAM

- Sigmoid

- 3 Parameters

$$y = \frac{a}{1 + e^{-\left(\frac{x-b}{c}\right)}} \tag{1}$$

- 4 Parameters

$$y = a + \frac{b}{1 + e^{-\left(\frac{x-c}{d}\right)}} \tag{2}$$

- 5 Parameters

$$y = a + \frac{b}{\left[1 + e^{-\left(\frac{x-c}{d}\right)}\right]^e} \tag{3}$$

- Logistic

- 3 Parameters

$$y = \frac{a}{1 + \left(\frac{x}{b}\right)^c} \tag{4}$$

- 4 Parameters

$$y = a + \frac{b}{1 + \left(\frac{x}{c}\right)^d} \tag{5}$$

- Hyberbola

- Single Rectangular, 2 Parameters

$$y = \frac{ax}{b+x} \tag{6}$$

- Single Rectangular I, 3 Parameters

$$y = a + \frac{bx}{c+x} \tag{7}$$

- Single Rectangular II, 3 Parameters

$$y = \frac{ax}{b+x} + cx \tag{8}$$

- Double Rectangular, 4 Parameters

$$y = \frac{ax}{b+x} + \frac{cx}{d+x} \tag{9}$$

- Double Rectangular, 5 Parameters

$$y = \frac{ax}{b+x} + \frac{cx}{d+x} + ex \tag{10}$$

- Modified Hyberbola I, 2 Parameters

$$y = \frac{ax}{1+bx} \tag{11}$$

- Modified Hyperbola II, 2 Parameters

$$y = \frac{x}{a+bx} \tag{12}$$

- Modified Hyperbola III, 4 Parameters

$$y = a - \frac{b}{(1+cx)^{1/d}} \tag{13}$$

- Exponential Rise to Maximum

- Single, 2 Parameters

$$y=a(1-e^{-bx}) \tag{14}$$

- Single, 2 Parameters

$$y=a+b(1-e^{-cx}) \tag{15}$$

- Double, 4 Parameters

$$y=a(1-e^{-bx})+c(1-e^{-dx}) \tag{16}$$

- Double, 5 Parameters

$$y=a+b(1-e^{-cx})+d(1-e^{-ex}) \tag{17}$$

- Simple Exponent, 2 Parameters

$$Y=a(1-b^{x}) \tag{18}$$

• Sigmoid – Hill

- 3 Parameters

$$y = \frac{ax^{b}}{c^{b}+x^{b}} \tag{19}$$

- 4 Parameters

$$y = a + \frac{bx^{c}}{d^{c}+x^{c}} \tag{20}$$

Table A.1 Correction Factor K_1 for Pier Nose Shape

Shape of Pier Nose	K_1
Square Nose	1.1
Round Nose	1.0
Circular Cylinder	1.0
Sharp Nose	0.9
Group of Cylinders	1.0

Table A.2 Correction Factor K_2 for Angle of Attack

Angle	L/a=4	L/a=8	L/a=12
0	1.0	1.0	1.0
15	1.5	2.0	2.5
30	2.0	2.75	3.5
45	2.3	3.3	4.3
90	2.5	3.9	5.0